CONSTITUTIVE MODELS OF SHAPE MEMORY ALLOYS AND THEIR IMPLEMENTATION TO FINITE ELEMENTS

by

Mete Yurtoğlu

B.S., Mechanical Engineering, Boğaziçi University, 2008

B.S., Physics, Boğaziçi University, 2008

Submitted to the Institute for Graduate Studies in
Science and Engineering in partial fulfillment of
the requirements for the degree of
Master of Science

Graduate Program in Mechanical Engineering

Boğaziçi University

2012

CONSTITUTIVE MODELS OF SHAPE MEMORY ALLOYS AND THEIR IMPLEMENTATION TO FINITE ELEMENTS

APPROVED BY:

Prof. Günay Anlaş (Thesis Supervisor)	.....
Prof. Gülay Altay	.....
Assist. Prof. C. Can Aydıner	.....

DATE OF APPROVAL: 01.03.2012

ACKNOWLEDGEMENTS

I would like to express my gratitude to my thesis supervisor, Professor Günay Anlaş for his support and encouragement during this study. It has been an honor to work under his guidance. I would like to thank Assist. Prof. Can Aydıner for his helpful comments and encouraging discussions and Prof. Gülay Altay for her interest and review of the thesis.

I would like to thank my friends Alpay, Selçuk, Sertan, and Sevgi for their assistance and helpful discussions on the subject.

Finally, I want to thank my mother, my father, and my dear wife, Başak, who did all they could so that I could "live out this undying dream."

ABSTRACT

CONSTITUTIVE MODELS OF SHAPE MEMORY ALLOYS AND THEIR IMPLEMENTATION TO FINITE ELEMENTS

The aim of this work is to study existing constitutive models for shape-memory alloys and to implement them to finite elements. Fracture behavior in Mode-I and mixed-mode is studied and, for this purpose, a 2-D edge cracked shape-memory alloy plate is discretized and UMAT interface of Abaqus, with different constitutive models is used. Phase transformation stress distributions around the crack tip are studied in detail for different amounts of loadings, and crack lengths. Results are tabulated and plotted to show the differences between different models. The effect of stress induced phase transformation is also studied.

ÖZET

ŞEKİL HAFIZALI ALAŞIMLARIN BÜNYE MODELLERİ VE SONLU ELEMANLAR YÖNTEMİNE UYARLANMASI

Bu çalışmanın amacı, şekil hafızalı alaşımlar için literatürde mevcut olan bünye modellerinin incelenmesi ve bu modellerin sonlu elemanlar yönetmine uyarlanmasıdır. Mode-I ve mixed-mode kırılma davranışının incelenmesi amacıyla kenar çatlaklı bir şekil hafızalı alaşım levha 2 boyutlu olarak modellenmiştir ve Abaqus yazılımının UMAT arayüzünde farklı modeller ile simule edilmiştir. Çatlak ucu etrafında faz dönüşümü gerilme dagılımları farklı yüklemeler ve çatlak uzunlukları için ayrıntılı olarak incelenmiştir. Sonuçlar tablolarla gösterilmiş ve modeller arasındaki farkları göstermek için sonuç resimleri çizdirilmiştir. Strese bağlı faz dönüşüm etkisi de incelenmiştir.

TABLE OF CONTENTS

ACKNOWLEDGEMENTS . . . iii
ABSTRACT . . . iv
ÖZET . . . v
LIST OF FIGURES . . . viii
LIST OF TABLES . . . xii
LIST OF SYMBOLS . . . xiii
LIST OF ACRONYMS/ABBREVIATIONS . . . xvi
1. INTRODUCTION . . . 1
1.1. Shape Memory Alloys . . . 1
1.1.1. Superelasticity and Shape Memory Effect . . . 1
1.1.2. A Brief History of SMA . . . 3
1.1.3. Applications of SMAs . . . 3
1.1.4. Physical Mechanism of Superelasticity and Shape Memory Effect 3
1.2. Literature Survey . . . 6
2. THEORY . . . 14
2.1. Thermodynamical Fundamentals . . . 14
2.1.1. First and Second Laws . . . 14
2.1.1.1. First Law . . . 14
2.1.1.2. Second Law - Clausius-Duhem Inequality . . . 16
2.1.1.3. Dissipation Inequality . . . 18
2.1.2. Thermodynamic Potentials . . . 18
2.2. Use of Thermodynamic Fundamentals in SMA Modeling . . . 24
2.2.1. Thermodynamical Fundamentals in Tanaka *et al.*'s Model . . . 25
3. CONSTITUTIVE MODELING FOR SMAs . . . 28
3.1. Tanaka *et al.* . . . 28
3.2. Liang and Rogers . . . 32
3.3. Brinson . . . 35
3.4. Lagoudas *et al.* . . . 41
3.5. Leclercq and Lexcellent . . . 46

3.6. Auricchio *et al.* 48
4. COMPUTATIONAL ANALYSIS OF EDGE CRACKED SMA SPECIMEN . 54
4.1. Stress Distributions for Mode-I Loading 59
4.2. Mode-I Crack Martensite Fraction 63
4.3. Mixed-mode Loading 72
4.4. Fracture Toughness in Mode-I 77
5. CONCLUSIONS 81
APPENDIX A: SOME BACKGROUND FORMULATIONS 84
A.1. The equality of $\dot{u}_{i,j}\sigma_{ij}$ and $\dot{\epsilon}_{ij}\sigma_{ij}$ 84
REFERENCES 86

LIST OF FIGURES

Figure 1.1. The so called superelastic behavior in SMA. 2

Figure 1.2. Shape Memory Effect in a stress-strain-temperature space and the respective microstructures of a typical NiTi SMA material. 2

Figure 1.3. Four phase transformation temperatures shown on temperature axis. 4

Figure 1.4. Lattice shapes and deformation mechanisms of shape memory alloys under different inputs. 5

Figure 1.5. Idealized stress-strain diagram showing Superelasticity Effect for T $> A_f$. 5

Figure 1.6. A simple sketch of the dead loading scheme applied by Muller. . . 8

Figure 1.7. Stress-Strain Curves derived by Patoor *et al.* for a single Al crystal at different isothermal cases (Curve 1 at T=–34℃) and (Curve 2 at T=18℃). 10

Figure 3.1. Martensite fraction vs. Uniaxial stress in forward transformation. 31

Figure 3.2. Martensite fraction vs. Uniaxial stress in reverse transformation. . 32

Figure 3.3. Martensite fraction vs. temperature curves in stress-free state. . . 33

Figure 3.4. Evolutions of phase transition stresses with respect to temperature traced by Liang and Rogers using experimental data. 35

Figure 3.5. Evolutions of phase transition stresses with respect to temperature traced by Brinson using experimental data by Dye. 37

Figure 3.6. Different phases and their relations. 47

Figure 3.7. Comparison of different schemes for the evolution of elastic modulus. 50

Figure 3.8. 1D Uniaxial Tension Test. 51

Figure 4.1. Mode-I loaded edge-cracked specimen (W = 100 mm, H = 200 mm, a = 25 mm). 55

Figure 4.2. Symmetry simplification of edge-cracked specimen. 55

Figure 4.3. Mixed-mode loaded specimen (W = 100 mm, H = 200 mm, a = 46.2 mm, b = 40 mm, $\alpha = 30°$). 56

Figure 4.4. Mesh configuration of the edge-cracked specimen with the crack 25mm away from the edge. 57

Figure 4.5. Comparison of uniaxial stress vs. strain diagrams of four different constitutive models used. 59

Figure 4.6. σ_{yy} vs. distance from crack tip, a/W = 0.25, σ = 100 MPa. 60

Figure 4.7. σ_{yy} vs. distance from crack tip, a/W = 0.25 and σ = 100 MPa with close-ups at about (a) 5 mm (b) 25 mm away from the crack. 61

Figure 4.8. σ_{yy} vs. distance from crack tip for different applied loads, σ, using Auricchio's model. 62

Figure 4.9. σ_{yy} vs. distance from crack tip for different applied loads, σ, using Tanaka's model. 62

Figure 4.10. σ_{yy} vs. distance from crack tip, a/W = 0.35 and σ = 100 MPa. . . 63

Figure 4.11. Martensite fraction distribution, a/W = 0.4 and σ = 150 MPa Auricchio's model used (M signifying the fully martensitic zone, M+A signifying the transformation zone, A signifying the fully austenitic zones). 64

Figure 4.12. Martensite fraction distribution of specimen with a/W = 0.4 and σ = 150 MPa using Tanaka's model. 65

Figure 4.13. Martensite fraction contours obtained using four different models, a/W = 0.4 and σ =150 MPa (Fully martensite inside the red contours, fully austenite outside the blue contours). 66

Figure 4.14. Close-up of martensite fraction contours for four different models shown in Figure 4.13 (Fully martensite inside the red contours). . 67

Figure 4.15. Martensite fraction contours of four different models, a/W = 0.35 and σ = 125 MPa (Fully martensite inside the red contours, fully austenite outside the blue contours). 69

Figure 4.16. Close-up of martensite fraction contours for four different models shown in Figure 4.15 (Fully martensite inside the red contours). . 70

Figure 4.17. Martensite fraction contours using Lagoudas' model with a/W = 0.4 and three different loadings (Fully martensite inside the red contours, fully austenite outside the blue contours). 71

Figure 4.18. Close-up of martensite fraction contours shown in figure 4.17 (Fully martensite inside the red contours). 72

Figure 4.19. The extent of martensite transformation zones under mixed-mode loading, $\sigma = 190$ MPa (Fully austenite outside blue contours). . . 73

Figure 4.20. Close-up of superimposed martensite fraction contours shown in Figure 4.19 (Fully martensite inside red contours). 74

Figure 4.21. Von Mises stress distribution around the crack tip under mixed-mode loading. 75

Figure 4.22. Martensite fraction distributions, a/W = 0.4 and b/W = 0.4 for mode-I and mixed-mode loadings respectively. 76

Figure 4.23. Node release scheme. 78

LIST OF TABLES

Table 3.1. Theoretical SMA specimen properties used for Tanaka's formulations. 31

Table 4.1. Nitinol properties. 54

Table 4.2. Comparison of approximate martensite areas, a/W = 0.4. 68

Table 4.3. Comparison of energy release rates. 79

Table 4.4. Comparison of stress intensity factors. 80

LIST OF SYMBOLS

A_f	Austenitic transformation end temperature
A_s	Austenitic transformation start temperature
b_i	Body force per unit volume vector
c	Specific heat
C_{ijkl}	Compliance tensor
D	Dissipation
E	1D elastic modulus
E_A	Elastic modulus of austenite phase
E_{ijkl}	Elastic modulus tensor
E_{kin}	Kinetic energy
E_{KL}	Elastic modulus tensor in Voigt notation
E_M	Elastic modulus of martensite phase
F_L	Landau Free Energy
F^n	n^{th} degree Landau Free energy term
G	Gibbs free energy
J	Invariant
K_{ij}	Piola Kirchoff stress tensor
L_{ij}	Green (Lagrangian) strain tensor
M_f	Martensitic transformation end temperature
M_s	Martensitic transformation start temperature
n_i	Unit vector normal to boundary surface
p	Pressure
p_{ext}	External pressure
q	Heat flux vector
Q	Heat input to the system
s	Specific entropy
S	Entropy of the system
T	Temperature

T_0	Reference temperature
T_{surr}	Temperature of the surroundings
u	Specific internal energy
u_i	Displacement vector
U	Internal energy
W	Work input to the system
Y	Threshold value of phase transformation
z	Martensite fraction
z_0	Reference martensite fraction
z_{ij}	Martensite fraction tensor
z_T	Temperature induced (self-accommodating) martensite fraction
z_σ	Stress induced (oriented) martensite fraction
α_A	Coefficient of thermal expansion for austenite
α_{ij}	Second order thermal expansion tensor
α_M	Coefficient of thermal expansion for martensite
Γ	Transformation coefficient
$\Delta\psi$	Interaction energy
ϵ_{ij}^e	Elastic strain tensor
ϵ_{ij}^{ie}	Inelastic strain tensor
ϵ_{ij}	Strain tensor
ϵ_{ij}^{th}	Thermal strain tensor
ϵ_{ij}^{tr}	Transformation strain tensor
ϵ_K	Strain tensor in Voigt notation
ϵ_L	Maximum transformation strain
ϵ_L^V	Maximum volumetric transformation strain
ϵ_{ij}^p	Plastic strain tensor
ζ_n	N-element set of internal variables
Θ_{ij}	Thermoelastic modulus tensor
θ	Heat supply per unit time

Λ_{ij}	Transformation tensor determining the transformation strain direction
ν_A	Poisson ratio for austenite
ν_M	Poisson ratio for martensite
π	General thermodynamic force
ρ	Density
$\rho\Delta s^A$	Stress influence coefficient of austenite
$\rho\Delta s^M$	Stress influence coefficient of martensite
$(\partial\sigma/\partial T)_L$	Rate of change of stress w.r.t. temperature in loading
$(\partial\sigma/\partial T)_U$	Rate of change of stress w.r.t. temperature in unloading
σ_{Af}	Martensite to austenite transformation end stress
σ_{As}	Martensite to austenite transformation start stress
σ_{ij}	Stress tensor
σ_K	Stress tensor in Voigt notation
σ_{Mf}	Austenite to martensite transformation end stress
σ_{Ms}	Austenite to martensite transformation start stress
ψ	Helmholtz free energy
Ω_{ij}	Transformation modulus tensor

LIST OF ACRONYMS/ABBREVIATIONS

1D	One Dimensional
2D	Two Dimensional
3D	Three Dimensional
MT	Martensite Transformation
NiTi	Nickel-Titanium
NOL	Naval Ordnance Laboratory
PE	Pseudoelasticity
SE	Superelasticity
SIF	Stress Intensity Factor
SIM	Stress Induced Martensite
SMA	Shape-Memory Alloy
SME	Shape-Memory Effect
TWSME	Two-Way Shape Memory Effect

1. INTRODUCTION

1.1. Shape Memory Alloys

1.1.1. Superelasticity and Shape Memory Effect

Shape-memory alloys (SMA) are generally defined as "materials with an intrinsic ability to remember their initial configuration". This memory shows itself at the macroscopic level mainly in two unusual behaviors, the superelasticity (SE) and the shape-memory effect (SME) [1]. For the isothermal case, where temperature is kept constant, the stress-strain graph of an alloy showing superelastic -also called pseudoelastic- behavior is shown in Figure 1.1. This behavior can be described as undergoing large deformations compared to other conventional engineering materials without any residual deformations. In Figure 1.1, a hysteresis loop can be seen. This hysteresis loop arises from phase transformation, and the result of this hysteresis is heat dissipation. However, as mentioned above, this is the isothermal case; thus, for the above condition to occur, it is assumed that ambient temperature is kept constant and the loading is done slowly, so that the difference between material temperature and the surroundings disappears, and the dissipated heat does not change the temperature of the material. For the non-isothermal case, the behavior of an SMA can be seen on a stress-temperature-strain space in Figure 1.2. Alloy's micromechanical properties can change under loading and, it can even be reverted back to its initial form by heating. This phenomenon is not the main objective of this thesis and is not investigated in this work. Superelasticity is the main point of interest in this work. "When shape memory alloys are plastically deformed at one temperature, they have the ability to completely recover their original shape upon temperature rise" [2] which is named *shape-memory effect*. *Superelasticity*, on the other hand, indicates the material's ability to undergo large deformations, up to 10-15% strains, without showing notable permanent deformations [3].

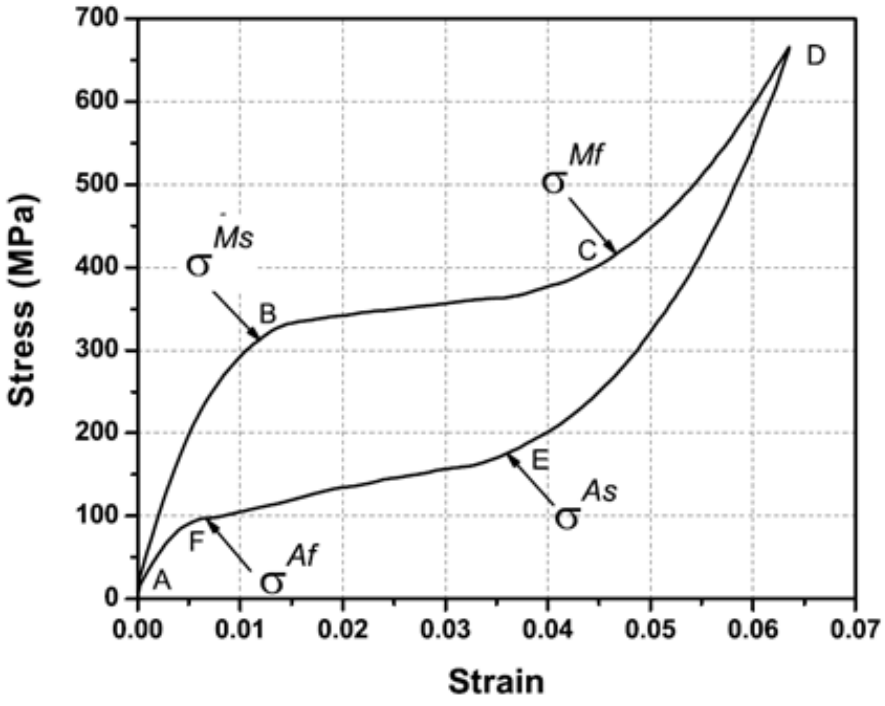


Figure 1.1. The so called superelastic behavior in SMA [3].

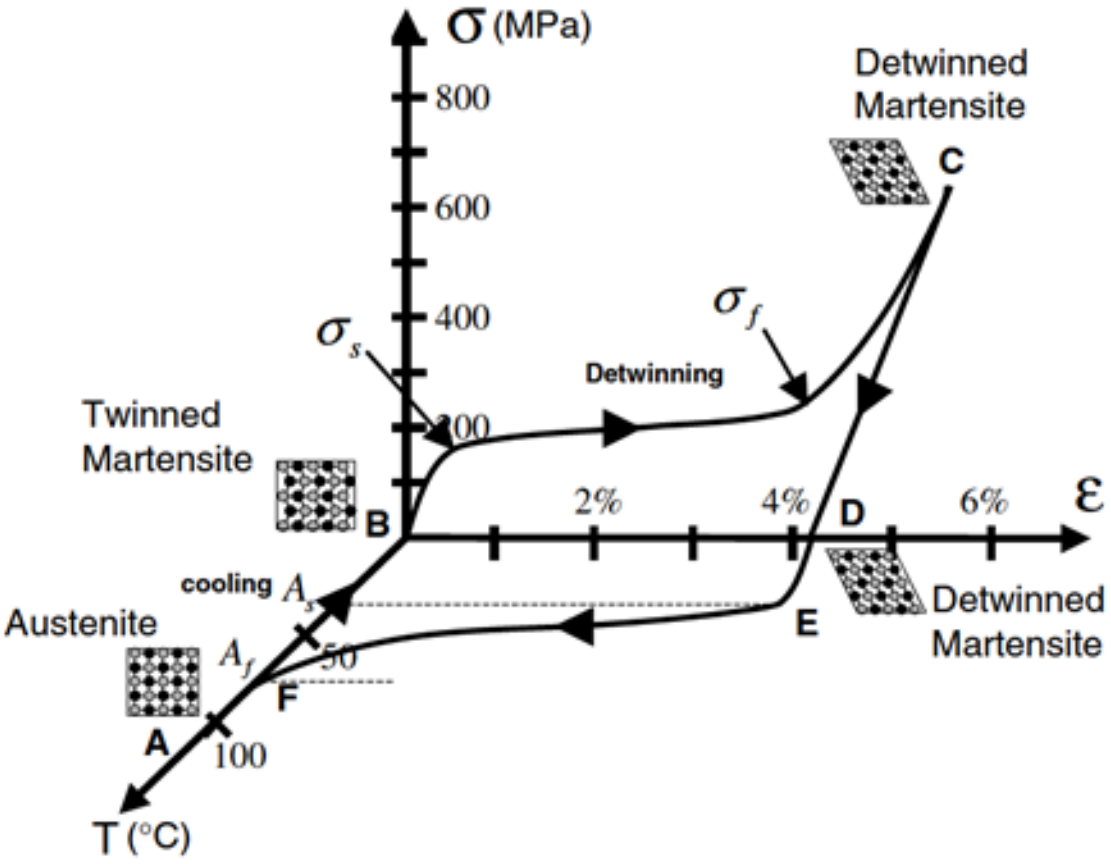


Figure 1.2. Shape Memory Effect in a stress-strain-temperature space and the respective microstructures of a typical NiTi SMA material [3].

1.1.2. A Brief History of SMA

In 1962 the shape memory phenomenon came into worldwide attention with the announcement of a shape-memory alloy Nickel Titanium (NiTi), Nitinol. [2]. The inventors W. J. Buehler and R. Wiley named the alloy "NITINOL". The name comes from the chemical symbol "NiTi" followed by "NOL", the acronym for Naval Ordnance Laboratory, the prior designation of the Naval Surface Weapons Center. With the demand for its properties, the NITINOL technology community prepared a manual [4].

1.1.3. Applications of SMAs

Nickel Titanium alloys have many properties that are useful in a wide variety of areas. Since recoverable strains of up to 8% can be obtained in NiTi alloys over a relatively narrow temperature range, and since by constraining NiTi alloys stresses of up to 700 MPa can be generated [5], these two extremes of 8% strain with little or no force generation, and 700 MPa stress, provide a broad envelope to design components with different strain outputs. Although not all of them commercially successful, it is estimated that there are over 10000 patents based on SMA's. In addition to SME, where strain is recovered upon heating, the SE can also be used in designs, where the material undergoes a transformation cycle with no external temperature change, simply by loading above A_f (Austenite finish temperature which is explained below). Shape-memory alloys are the basis for innovative applications, ranging from devices used in orthodontia (arch-wires) to self-expanding microstructures for the treatment of organ occlusions (stents) or ranging from coupling devices to micro-actuators [1].

1.1.4. Physical Mechanism of Superelasticity and Shape Memory Effect

Although not the main topic in this thesis, it is useful to introduce micromechanics for better understanding of superelasticity and shape memory effect.

> "Shape-memory alloys present reversible martensitic phase transformations, that is, solid-solid diffusionless transformations between a crystallographically

more-ordered phase, the austenite, and a crystallographically less-ordered phase, the martensite. Typically, the austenite is stable at lower stresses and at higher temperatures, while the martensite is stable at higher stresses and at lower temperatures" [1].

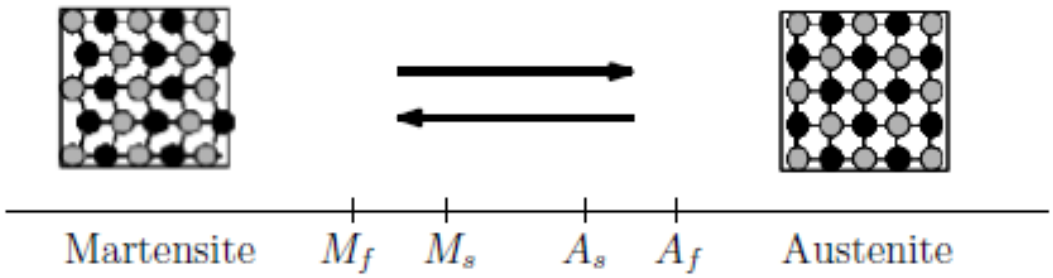


Figure 1.3. Four phase transformation temperatures shown on temperature axis [6].

The phase transformation (from austenite to martensite or vice versa) is typically marked by four transition temperatures, named as Martensite start, M_s, Martensite finish, M_f, Austenite start, A_s, and Austenite finish, A_f. The ordering between these temperatures under constant stress is as follows; $M_f < M_s < A_s < A_f$ [7]. These four temperatures are given in Figure 1.3 with the microstructural shapes of austenite and martensite phases as the result of diffusionless transformation. From this figure, it can be seen that a change in temperature within $M_s < \mathrm{T} < A_s$ range does not lead to a phase change, and, also, within $M_f < \mathrm{T} < A_f$ range, both the martensite and austenite phases may coexist [7]. The phase transformation may take place with temperature, with temperature and loading simultaneously (SME) or with loading only keeping temperature constant (SE) [7]. Resulting deformation mechanisms and their lattice structures are shown in Figure 1.4. The effect of loading at a constant temperature above Austenite finish temperature, A_f, (the superelasticity effect) can be seen in Figure 1.5. From 1980 up to now, constitutive modeling of shape memory alloys has been a subject of active research. In general, the models developed can be categorized as micro, micro-macro or macro models according to the length-scale of the theory. Micro models describe phenomena occurring at micro-scale level, such as nucleation, interface motion, twin growth, etc [1]. Micro-models, generally, do not consider martensitic volume and austenitic volume fractions as internal variables, but as consequences of interface motion. However, most models deal with a single interface to limit

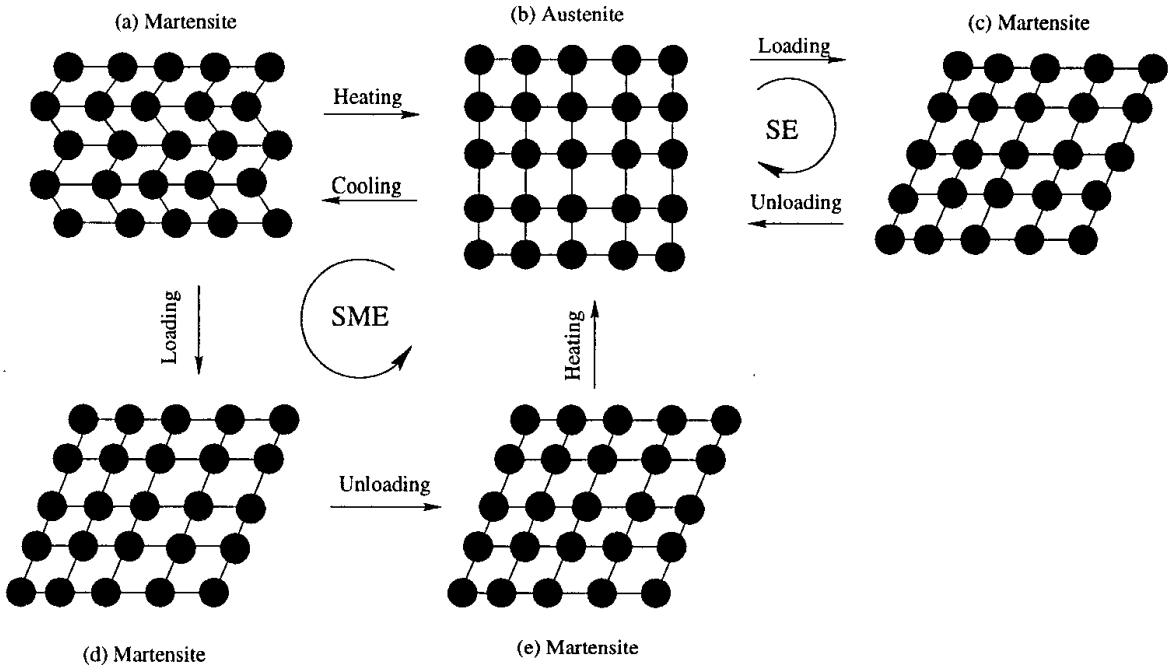


Figure 1.4. Lattice shapes and deformation mechanisms of shape memory alloys under different inputs [8].

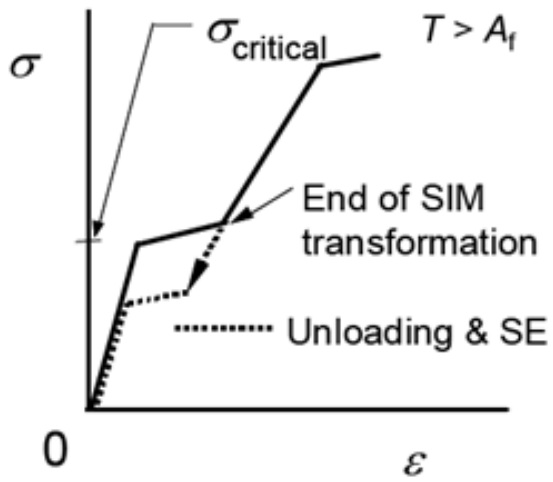


Figure 1.5. Idealized stress-strain diagram showing Superelasticity Effect for T $> A_f$ [7].

complexity and actual real transition processes are typically characterized with a very high number of nucleation sites. Therefore, a micro-level approach is not suitable for modeling phenomenological behavior. Micro-macro studies combine micromechanics and continuum mechanics to derive constitutive laws for the material. Although they provide good predictions of the materials behavior,this is in expense of time-consuming computations [9]. In phenomenological or macro approaches the average material behavior is studied through macroscopic variables. They are suitable for continuum-level numerical methods (such as finite elements). As mentioned before, although the SE was observed in the 50s and the SME was observed in the 60s, research based on the phenomenological constitutive modeling of SMAs started in the 80s. Initial experimental investigations are mostly based on simple stress states due to the complexity of the occurring phenomena [1]. As a natural consequence, the initial modeling efforts were mostly directed toward the development of simple one-dimensional (1D) constitutive equations.

1.2. Literature Survey

Currently, the level achieved in SMA production technologies, together with a deeper knowledge of the micro and macro-scale phenomena, has created the possibility of performing complex experimental investigations, such as combined tension/torsion or general non-proportional loading tests. As a result, researchers have also moved toward the development of more sophisticated and accurate constitutive models [1].

Before starting this work, different approaches were classified, and from the available literature, macro-level models dealing with macroscopic quantities such as stress and strain were picked. According to Auricchio [1], macro-level models are mostly derived using thermodynamics' principles with input parameters coming from experiments.

To name a few models; first of all, Tanaka *et al.*, in 1982 and 1986 [10, 11], studied constitutive behavior of shape memory alloys, using Free Energy concepts and martensite fraction evolution. For the hardening during transformation, an exponen-

tial hardening rule is used but material properties (e.g., elastic modulus) are assumed to remain constant during phase transformation [3, 11]. Second, Liang and Rogers, in 1990, proposed another 1D model, using Helmholtz Free Energy concepts, similar to Tanaka *et al.*'s work, but this time using a cosine hardening rule for the hardening during phase transformation. Later, in 1992, they extended it to a three-dimensional (3D) model [12, 13]. Lagoudas and Boyd developed another model in 1996 [14, 15]. In this model, a potential function is defined using Gibbs Free Energy concept and the variables of the potential function are stress, temperature, and, volumetric martensite fraction. In their paper named "A General Macroscopic Description of the Thermomecanical Behavior of Shape Memory Alloys", Leclercq and Lexcellent proposed a model based on Helmholtz Free Energy and used classical plasticity concepts in explaining the phase transformation surfaces [16]. A.C. Souza *et al.* in 1998 based their model on Generalized Standard Materials approach where internal variables are defined to describe the phase transformation process [17]. They proposed a 3D phenomenological model of SMAs. In addition to Generalized Standard Materials, a potential is defined via Helmholtz Free Energy and from this potential 4 constitutive relations are found, giving mean stress, deviatoric stress, transformation stress and, entropy density. Potential function is a function of linear strain, deviatoric strain, transformation strain and, of temperature (notice that since Helmholtz Energy is used, strain is an internal variable in contrast to Lagoudas and Boyd's Gibbs Free Energy model where stress is an internal variable).

In formulating the macroscopic model, the choice between Gibbs Free Energy and Helmholtz Free Energy them depends on the selection of the independent variable of the thermodynamic potential function. If stress is desired to be the independent variable, Gibbs Free Energy is chosen whereas if strain is elected, Helmholtz Free Energy is chosen. Starting from this point and expanding on it, different models employ different principles. The goal of this study is to distinguish these differences and identify their advantages/disadvantages.

Following up on this brief summary, in the rest of this section, academic literature on SMA modeling is presented, chronologically but not in an exhaustive manner in

order to outline the progression of the field.

Delaey *et al.*, in 1974, published a three part work over SE and SME associated with martensitic transformations [18–20]. This work, mostly presents experimental data, e.g., the stress-strain curves of superelastic behavior. Only Part 3 involves some theory. In this part, using free enthalpy change, the transformation is quantified but no thermodynamical framework involving the second law or Clausius-Duhem inequality is given. Their model is mostly limited to explaining their experimental data.

Muller's article, published in 1979 is the first article to present the phenomenon of pseudoelasticity in the case of a rod under tension [21]. A simple sketch reproduced from his paper can be seen in Figure 1.6, where D is the large elastic displacement created by the load P under 20°. Over test cases like this, methods from statistical

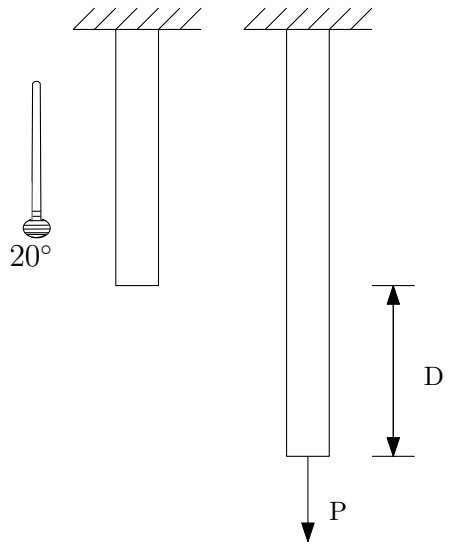


Figure 1.6. A simple sketch of the dead loading scheme applied by Muller.

physics are employed and load-displacement curves of shape-memory alloys are produced. This approach, describes the pseudoelastic behavior phenomenologically and, the thermodynamic nature of pseudoelasticity or the microscopic interactions are not investigated.

Falk's work published in 1982 can also be given as one of the earliest examples in the modeling of SMAs [22, 23]. In his work, Falk refers to the early study by Delaey

et al. mentioned above [18]. Both of these models are based on 1D phenomenological behavior of shape memory alloys and they state SME and SE are result of martensitic phase transformation. However, Falk does not take martensitic volume fraction as a variable in his model only considering strain and temperature as independent variables. Falk's work in 1982 adds strain rate to these variables in order to improve the free energy model used, namely the Landau Free Energy and, reflects the effect of strain rates. A theory used for formulating phase transitions with thermodynamic arguments is Ginzburg-Landau theory. Using it to derive Landau Free Energy with a Taylor Expansion is an important step for these earlier models [24]. The Landau free energy obtained is given by:

$$F_L(\epsilon, T) = \epsilon^6 - \epsilon^4 + (T + 1/4)\epsilon^2 \tag{1.1}$$

where, F_L is the Landau Free Energy, ϵ is the strain and, T is the temperature.

Achenbach and Muller's 1982 study [25] presents a 1D model of SMAs. They try to trace load vs. displacement curves of SMA by using a variant of Landau Free Energy, namely, Devonshire-Landau Free Energy. The reason for employing this concept is the similarity between SME and the behavior of SMAs to the behavior of ferroelectric bodies which were previously modeled with this form of free energy. They mention that, polarization vs. electric field curves of ferroelectric bodies are similar to load vs. displacement curves of SMAs. Using this free energy concept, potential wells are shown and methods of statistical physics/mechanics are employed to probabilistically calculate the tendencies of transformation occurrences. Although not thermodynamically very advanced, this paper is notable in the effort to write evolution equations of martensitic and austenitic fractions inside the SMA material. This work has been elaborated in another work by Achenbach *et al.* in 1986 [26]. Once again, though this model does not simulate the SMA behavior in thermodynamically sound manner. It rather employs statistical methods and succeeds to trace the load vs. displacement curves of SMAs.

Tanaka and Nagaki in their 1982 paper, based their description of SMA materials on a thermomechanical framework [10]. They used Large Strains and theorized a 3D

incremental model. Then, Tanaka *et al.* in their paper dated 1986, reverted back to 1D modeling, but added new elements to SMA modeling [11]. The model included martensitic fraction and proposed a rule of mixtures which gives the elastic modulus at any moment before, during and after the transformation. Second, Clausius–Duhem inequality is used to derive the constitutive equations and the kinetics of transformation. The inequality is used in the following form, which will be investigated in Chapter 2:

$$\rho\dot{s} - \rho\frac{\theta}{T} + \left(\frac{q_i}{T}\right)_{,i} \geq 0 \tag{1.2}$$

where ρ is the density, s is the entropy, θ is the heat supply term, T is the temperature, and, q_i is the heat flux vector. One shortcoming of this model is that the materials properties are assumed to remain constant always, which is not true. Since this model is one of the most important ones and since it is used in Chapter 4, a more detailed investigation can be found in Chapter 3

Patoor *et al.* their work dated 1987, carry a micromechanics based approach [27, 28]. Using Gibbs free energy to define the transformation and the flow rule, they model single crystal behavior (Figure 1.7). Transition from single crystal to polycrystalline behavior is established by averaging the results of single crystal model.

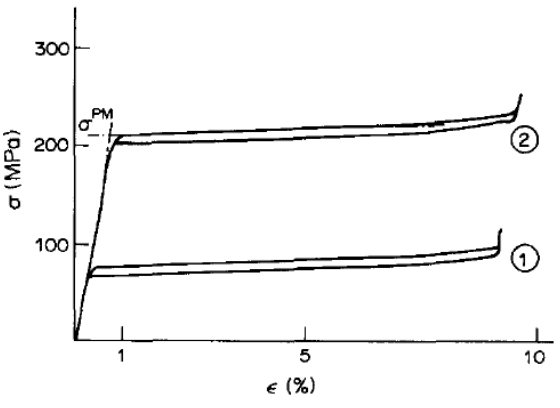


Figure 1.7. Stress-Strain Curves derived by Patoor *et al.* for a single Al crystal at different isothermal cases (Curve 1 at T=–34°C) and (Curve 2 at T=18°C) [27].

Falk and Konopka's work published in 1990, utilizing Falk's former principles derived from Landau Theory; extends the scope of free energy function to three di-

mensional case [29]. Internal variables are not used, hence, martensite fraction is not taken into account. Starting from a microscopic point of view and considering only the homogeneous case (one-phase single crystals) the energy function is written for 3D depending on temperature and strain. In three dimensions, Equation 1.1 becomes:

$$F = \sum_{i=1}^{3} F_i^2 J_i^2 + \sum_{i=1}^{5} F_i^4 J_i^4 + \sum_{i=1}^{2} F_i^6 J_i^6 \tag{1.3}$$

where, J_i^n are the strain invariants in the Strain space defined in their article and, F^n are the nth degree Landau Free energy terms. This way, the stress-strain relation can be found by partial differentiation of the free energy with respect to strain. The elastic moduli are defined again in Voigt notation as:

$$E_{KL} = \partial^2 F / \partial \epsilon_K \partial \epsilon_L \tag{1.4}$$

Liang and Rogers also did one-dimensional modeling of shape memory materials [12]. The main novelties of their work is the usage of Helmholtz Free Energy and the hardening rule. In their work, the martensite fraction's evolution is a cosine function. Building on this cosine hardening function concept, different cases for SMA wires or fibers are investigated in the rest of their work. Liang and Rogers claim that, with this hardening function, their SMA model captures the SMA behavior more accurately. This model, of which some elements is used in Chapter 4, is investigated in more detail in Chapter 3.

Berveiller *et al.*, in their work, in 1991 [30], do micromechanical constitutive modeling of SMAs. By summation, they indicate that the macroscopic rate forms can be obtained. In those summations, thermodynamic forces on interfaces must also be taken into account.

Abeyaratne and Knowles (1993) [31], also studied 1D modeling using Helmholtz free energy as Liang and Rogers' work. They did not, however, make use martensite

fraction, instead; stress is only a function of strain and temperature in their model. This work investigates the microscale nucleation phenomenon in detail which is out of the scope of this thesis. However for researchers working in microscale modeling of SMAs, this work is one of the milestones.

For those who study models devised from micromechanical principles in 1990s, some other works by Lindgaard [32], by Raniecki *et al.* [33], by Sun and Hwang [34,35], by Raniecki and Lexcellent [36], by Entemeyer *et al.* [37], by Patoor *et al.* [38], by Goo and Lexcellent [39], and, by Huang and Brinson [40] can be listed chronologically.

Brinson, her work dated 1993, continues with Tanaka *et al.*'s and Liang and Rogers' discussions, and, uses the same concepts and methodologies. But contrary to them, she divides martensite fraction into two as z_σ and z_T, stress induced martensite fraction and temperature induced martensite fraction respectively. This way, she extends the usability of Liang and Rogers' constitutive model to a broader temperature scope. She also uses variable elastic and transformation tensors in the final form of her constitutive law. For more details and derivations about this model, see Chapter 3.

Leclerq and Lexcellent, in their work published in 1996, extend this concept of stress induced and temperature induced martensite fractions to 3D [16]. Instead of solely taking the martensite fraction as a single variable, two variables related to martensite fraction, namely, volume fraction of self-accommodating (pure thermal effect) and oriented (stress-induced) product-phase are taken into account. Helmholtz free energy, valid in the total range of phase transition is defined with interaction terms. Kinetic equations for internal variables are written. These equations satisfy the thermodynamical rules. This work is able to model complete thermomechanical loadings, including non-isothermal ones. The volume fraction of self-accommodating martensite is given as z_σ and the oriented volume fraction as z_T. It should be noted that this is similar to Brinson's approach of temperature induced and stress induced martensite fractions approach in her 1993 work. For both phases, the free energy is the same and they can both exist at the same time in a sample. Also, the strain is decomposed into

two parts as:

$$\epsilon = \epsilon^e + \epsilon^{tr} \tag{1.5}$$

where ϵ^e is the elastic strain, and ϵ^{tr} is the transformation strain. Small strains assumption, different than the work of Tanaka's, Liang and Rogers' and Brinson's is made. In addition to that, thermal dilation is ignored since it is negligible compared to the elastic and transformation strains. This model, since one of the most important, is investigated throughly in Chapter 3.

Auricchio and Sacco, in their 1997 work on a 1D model able to simulate the superelastic behavior of shape memory alloys [41]. Martensite fraction is used and for martensite fraction, evolutionary equations in rate form are proposed. For the evolution of elastic modulus, E, different methodologies such as Voigt scheme, Reuss scheme, and Mori-Tanaka scheme with elliptical or spherical inclusions are considered. Reuss and Mori-Tanaka schemes are chosen, since experimentally Reuss scheme is realized best experimentally and since Mori-Tanaka scheme represents a feasible upper bound. In proceeding from elastic moduli, in order to devise uniaxial stress-strain behavior, 1D plasticity methods are used. The model can be distinguished from most of the other models by the lack of free energy concepts thermodynamical principles. A more detailed investigation of this model can be seen in Chapter 3 among others by Auricchio *et al.* [42, 43].

Also, some recent models devised from micromechanical principles, which are not studied in this thesis, such as, Bernardini [44], by Govindjee and Miehe [45], by Brocca *et al.* [46], by Hall and Govindjee [47], by Levitas and Preston [48], by Nae *et al.* [49], by Ikeda *et al.* [50], by Jung *et al.* [51], by Idesman *et al.* [52], by Patoor *et al.* [53] are worth mentioning.

2. THEORY

2.1. Thermodynamical Fundamentals

Most of the SMA models are based on thermodynamic functions and here a brief review of thermodynamics is provided.

2.1.1. First and Second Laws

The explanations here will closely follow the book, *The Mechanics of Constitutive Modeling* [54].

2.1.1.1. First Law. First law of thermodynamics, which is the principle of conservation of energy, states that infinitesimal change in internal energy is given by,

$$dE_{kin} + dU = \delta Q + \delta W, \tag{2.1}$$

where, E_{kin} is the kinetic energy, U is the internal energy, W is the work done on the system, and Q is the heat input to the system.

It can also be written in the following global form [54],

$$\dot{E}_{kin} + \dot{U} = \frac{\delta Q}{dt} + \frac{\delta W}{dt}, \tag{2.2}$$

where, kinetic energy in rate form is,

$$\dot{E}_{kin} = \int_V \rho \dot{u}_i \ddot{u}_i dV \tag{2.3}$$

where, u_i is the displacement. Internal energy written in terms of specific internal

energy, u, is,

$$U = \int_V \rho u dV \tag{2.4}$$

Heat input rate is,

$$\frac{\delta Q}{dt} = \int_V \theta dV - \int_S q_i n_i dS \tag{2.5}$$

where θ is the heat generation per unit time and unit volume, q_i is the heat flux vector and, n_i is the unit vector normal to boundary and outward.

Work rate is,

$$\frac{\delta W}{dt} = \int_S \dot{u}_i t_i dS + \int_V \dot{u}_i b_i dV \tag{2.6}$$

where t_i the traction acting on the surface S and, b_i is the body force per unit volume acting on the volume V.

With the help of Gauss' divergence theorem; Equation 2.5 and 2.6 can be rewritten as,

$$\frac{\delta Q}{dt} = \int_V \theta dV - \int_V q_{i,i} dV \tag{2.7}$$

and,

$$\frac{\delta W}{dt} = \int_V (\dot{u}_i \sigma_{ij})_{,j} dV + \int_V \dot{u}_i b_i dV \tag{2.8}$$

inserting Equation 2.3, 2.4, 2.7, and 2.8 into Equation 2.2, one obtains [54],

$$\int_V [\dot{u}_i(\rho \ddot{u}_i - \sigma_{ij,j} - b_i) + \rho \dot{u} - \dot{u}_{i,j}\sigma_{ij} - \theta + q_{i,i}] dV = 0 \tag{2.9}$$

Also, inserting Cauchy's equation of motion,

$$\sigma_{ij,j} + b_i = \rho \ddot{u}_i \tag{2.10}$$

into, Equation 2.9 results in the following simplified form,

$$\int_V (\rho \dot{u} - \dot{\epsilon}_{ij}\sigma_{ij} - \theta + q_{i,i}) dV = 0 \tag{2.11}$$

In transition from Equation 2.9 to Equation 2.11, the fact that $\dot{u}_{i,j}\sigma_{ij} = \dot{\epsilon}_{ij}\sigma_{ij}$ is used. This is proved in the Appendix A.

Finally, the local form of the first law is obtained as,

$$\rho \dot{u} = \dot{\epsilon}_{ij}\sigma_{ij} + \theta - q_{i,i} \tag{2.12}$$

which holds at every point in the body.

2.1.1.2. Second Law - Clausius-Duhem Inequality. Clausius inequality states that,

$$dS = \frac{\delta Q}{T} \tag{2.13}$$

for reversible processes, and,

$$dS > \frac{\delta Q}{T} \tag{2.14}$$

for irreversible processes, where T is the temperature and S is the entropy of the system.

If s is defined as the specific entropy per unit mass; the following relation can be

given,

$$S = \int_V \rho s dV \tag{2.15}$$

on the other hand, dividing Clausius inequality by dt, one obtains,

$$\dot{S} \geq \frac{1}{T}\frac{\delta Q}{dt} \tag{2.16}$$

which holds for isothermal and homogeneous systems.

For a body within which temperature is nonuniform, the following form of second law can be stated as;

$$\dot{S} \geq \int_V \frac{\theta}{T} dV - \int_S \frac{q_i}{T} n_i dS \tag{2.17}$$

which is also called the global form of Clausius–Duhem inequality [54].

By applying the divergence theorem on the right hand side of the Equation 2.17,

$$\int_S \frac{q_i}{T} n_i dS = \int_V (\frac{q_i}{T})_{,i} dV \tag{2.18}$$

and, inserting Equation 2.15 and 2.18 into 2.17 while considering ρ constant, one obtains,

$$\int_V [\rho \dot{s} - \frac{\theta}{T} + (\frac{q_i}{T})_{,i}] dV \geq 0 \tag{2.19}$$

and consequently,

$$\rho \dot{s} - \frac{\theta}{T} + \frac{q_{i,i}}{T} - \frac{q_i T_{,i}}{T^2} \geq 0 \tag{2.20}$$

which is the local form of Clausius–Duhem inequality. Only when Clausius–Duhem inequality is satisfied by the constitutive model, the model is thermodynamically admissible [54].

2.1.1.3. Dissipation Inequality. Combining First and Second Laws, namely, Equation 2.12 and 2.20, gives,

$$D \equiv T\rho\dot{s} - \rho\dot{u} + \dot{\epsilon}_{ij}\sigma_{ij} - \frac{q_i T_{,i}}{T} \geq 0 \tag{2.21}$$

namely, the dissipation inequality where D is called the dissipation.

Again, as in Equation 2.20, any constitutive model that fulfills Equation 2.21, fulfills all the thermodynamical requirements [54].

2.1.2. Thermodynamic Potentials

In deriving constitutive equations, thermodynamic potentials are needed. A thermodynamic potential is a function that defines the thermodynamic state of a system as a function of system's state variables. All thermodynamic potentials are scalar-valued functions, at least twice differentiable with respect to the state variables [55]. In thermoelasticity, typically, four types of potentials are defined. These are the internal energy, u, the enthalpy, h, the Helmholtz free energy, ψ, and the Gibbs free energy, G. These quantities are specific, i.e., they are all defined per unit mass [56]. Among these four, internal energy, u, and enthalpy, h, will not be adequate for accurate representation of thermoelastic effects. This stems from the fact that the state variables of internal energy are strain and entropy and the state variables of enthalpy are stress and entropy where entropy is not experimentally controlled [54]. Thus, the choice has to be done between the Helmholtz and the Gibbs free energies. As explained below, both can be chosen in the constitutive modeling of shape-memory alloys.

Assuming constant kinetic energy in Equation 2.1 yields:

$$dU = \delta Q + \delta W, \tag{2.22}$$

Combining Clausius inequality from Equation 2.14 and 2.22, assuming the work to be done only by the external pressure, p_{ext}, and, temperature to be the temperature of the surroundings, T_{surr}; the following criterion for spontaneous occurrence is obtained [57]:

$$dU + p_{ext}dV - T_{surr}dS < 0 \tag{2.23}$$

Assuming constant volume V and temperature $T = T_{surr}$, Equation 2.23 yields:

$$dU - TdS < 0 \tag{2.24}$$

Or, when both terms are written inside the same parenthesis,

$$d(U - TS) < 0 \tag{2.25}$$

From (2.25), $\psi = U - TS$ is obtained, where ψ is the *Helmholtz free energy*, which is defined as the work obtainable from a closed thermodynamic system with its conditions given above as constant temperature and volume.

This free energy can also be written in the specific energy form as [3, 58];

$$\psi = u - Ts \tag{2.26}$$

where u is the specific internal energy and s is the specific entropy.

Going back to our global form and considering another case, where $T = T_{surr}$

and $p = p_{ext}$ are constant, (2.23) yields the following relation:

$$dU + pdV - TdS < 0 \tag{2.27}$$

Or, when all the terms are written inside the same parenthesis:

$$d(U + pV - TS) < 0 \tag{2.28}$$

From (2.28), $G = U + pV - TS$ is obtained, where G is the *Gibbs free energy*, which is defined as the work obtainable from a system at constant temperature and pressure.

Written in terms of Helmholtz free energy, it is,

$$G = \psi + pV \tag{2.29}$$

Or it can also be written in the specific energy form as [3, 58];

$$G = \psi - \frac{1}{\rho}\sigma_{ij}\epsilon_{ij} = u - Ts - \frac{1}{\rho}\sigma_{ij}\epsilon_{ij} \tag{2.30}$$

Now, with three thermodynamical potentials obtained; specific internal energy, Helmholtz free energy, and, Gibbs free energy; u, ψ and, G respectively, knowledge of one will bring the knowledge of all state variables. In order to prove this; first, total differential forms of the potential must be obtained;

$$du = Tds + \frac{1}{\rho}\sigma_{ij}d\epsilon_{ij} \tag{2.31}$$

from (2.12) when heat supply θ is equal to zero and since,

$$-q_{i,i} = T\dot{s} \tag{2.32}$$

Likewise, for Helmholtz free energy, differentiating (2.26) and inserting (2.31) into it,

we obtain;

$$\begin{aligned} d\psi = &= du - Tds - sdT \\ &= Tds + \frac{1}{\rho}\sigma_{ij}d\epsilon_{ij} - Tds - sdT \\ &= \frac{1}{\rho}\sigma_{ij}d\epsilon_{ij} - sdT \end{aligned} \tag{2.33}$$

which is the total differential form of Helmholtz free energy.

Also, for Gibbs free energy, differentiating (2.30) and inserting (2.31) into it, we obtain;

$$\begin{aligned} dG = &= du - Tds - sdT - \frac{1}{\rho}\sigma_{ij}d\epsilon_{ij} - \frac{1}{\rho}d\sigma_{ij}\epsilon_{ij} \\ &= Tds + \frac{1}{\rho}\sigma_{ij}d\epsilon_{ij} - Tds - sdT - \frac{1}{\rho}\sigma_{ij}d\epsilon_{ij} - \frac{1}{\rho}d\sigma_{ij}\epsilon_{ij} \\ &= -sdT - \frac{1}{\rho}d\sigma_{ij}\epsilon_{ij} \end{aligned} \tag{2.34}$$

which is the total differential form of Gibbs free energy. From (2.31), (2.33) and, (2.34), following relations can be obtained;

$$\frac{\partial u}{\partial s} = T \qquad \rho\frac{\partial u}{\partial \epsilon_{ij}} = \sigma_{ij} \tag{2.35}$$

$$\frac{\partial \psi}{\partial T} = -s \qquad \rho\frac{\partial \psi}{\partial \epsilon_{ij}} = \sigma_{ij} \tag{2.36}$$

$$\frac{\partial G}{\partial T} = -s \qquad \rho\frac{\partial G}{\partial \sigma_{ij}} = -\epsilon_{ij} \tag{2.37}$$

Also, from (2.33) and, (2.34); it can be seen that during an isothermal process, complementary work on the body increases Gibbs free energy while decreasing the Helmholtz free energy [58]. This shows the duality between these two potentials.

In the modeling of shape-memory alloys, Helmholtz and Gibbs free energies are frequently used, since compared to the internal energy approach, they are more useful

in modeling thermoelasticity instead of elasticity where internal energy is used. The choice between Helmholtz and Gibbs potentials depends on the selection of control variables. As it can be seen from (2.33) and, (2.34) or from (2.36) and (2.37); for Helmholtz free energy, ψ, control variables are, temperature, T, and strain, ϵ_{ij}. For Gibbs free energy, G, control variables are, temperature, T, and stress, σ_{ij}. Since most experiments are done with strain control methods, most publications reflect this in the usage of Helmholtz free energy with only a few exceptions. Since they are complementary energies, although the control variables are different, there should be no difference in their results.

Since Helmholtz free energy is a function of strain, ϵ_{ij} and temperature, T, i.e. $\psi = \psi(T, \epsilon_{ij})$, doing Taylor expansion on it around the reference state where $T = T_0$ and $\epsilon_{ij} = 0$, one obtains,

$$\begin{aligned}\psi(T,\epsilon_{ij}) = \psi_0 + (\frac{\partial\psi}{\partial\epsilon_{ij}})_0\epsilon_{ij} + (\frac{\partial\psi}{\partial T})_0(T-T_0) + \frac{1}{2}\epsilon_{ij}(\frac{\partial^2\psi}{\partial\epsilon_{ij}\partial\epsilon_{kl}})_0\epsilon_{kl} \\ + \frac{1}{2}(\frac{\partial^2\psi}{\partial T^2})_0(T-T_0)^2 + (\frac{\partial^2\psi}{\partial T\partial\epsilon_{ij}})_0(T-T_0)\epsilon_{ij}\end{aligned} \tag{2.38}$$

where the subscript 0 means "at the reference state" and where $(\quad)_0$ means the entity inside the parenthesis is evaluated at the reference state.

Since the stress can be obtained from the Helmholtz free energy by using the relation (2.36), and since we have the second order Taylor expansion of Helmholtz potential, combining these two yields the stress, σ_{ij}, as;

$$\sigma_{ij} = \rho\frac{\partial\psi}{\partial\epsilon_{ij}} = \rho(\frac{\partial\psi}{\partial\epsilon_{ij}})_0 + \rho(\frac{\partial^2\psi}{\partial\epsilon_{ij}\partial\epsilon_{kl}})_0\epsilon_{kl} + \rho(\frac{\partial^2\psi}{\partial T\partial\epsilon_{ij}})_0(T-T_0) \tag{2.39}$$

Assuming that at the reference state no stresses exist, the term, $(\partial\psi/\partial\epsilon_{ij})_0$ becomes zero and (2.39) reduces to [54]:

$$\sigma_{ij} = D_{ijkl}\epsilon_{kl} - \beta_{ij}(T-T_0) \tag{2.40}$$

where D_{ijkl} is defined as:

$$D_{ijkl} = \rho(\frac{\partial^2 \psi}{\partial \epsilon_{ij} \partial \epsilon_{kl}})_0 \tag{2.41}$$

and β_{ij} is defined as:

$$\beta_{ij} = -\rho(\frac{\partial^2 \psi}{\partial T \partial \epsilon_{ij}})_0 \tag{2.42}$$

Here, we can introduce α_{ij},

$$D_{ijkl}\alpha_{kl} = \beta_{ij} \tag{2.43}$$

Also, introducing $C_{ijkl} \equiv D^{-1}_{ijkl}$

$$\alpha_{ij} = C_{ijkl}\beta_{kl} \tag{2.44}$$

Thus, combining (2.40) and (2.44) yields

$$\sigma_{ij} = D_{ijkl}(\epsilon_{kl} - \epsilon^{th}_{kl}) \tag{2.45}$$

Where, ϵ^{th}_{kl} is the thermal strain tensor, defined as;

$$\epsilon^{th}_{kl} = \alpha_{ij}(T - T_0) \tag{2.46}$$

For inelastic materials; the strain tensor is decomposed into different parts. Typically [54]:

$$\epsilon_{ij} = \epsilon^{e}_{ij} + \epsilon^{ie}_{ij} + \epsilon^{th}_{ij} \tag{2.47}$$

where, ϵ^{e}_{ij} is the elastic strain, ϵ^{ie}_{ij} is the inelastic strain, and ϵ^{th}_{ij} is the thermal strain tensor.

In the SMA literature, Machado and Lagoudas [3, 56] propose the following decomposition:

$$\epsilon_{ij} = \epsilon_{ij}^{th} + \epsilon_{ij}^{in} \tag{2.48}$$

where, ϵ_{ij}^{th} is the thermoelastic strain and ϵ_{ij}^{in} is the inelastic strain. In this approach, the thermal strain tensor is inside the elastic strain term and it is named the thermoelastic strain.

Also, for SMA, it is assumed that the inelastic strain tensor is the strain associated with only the transformation strain:

$$\epsilon_{ij}^{in} = \epsilon_{ij}^{tr} \tag{2.49}$$

where ϵ_{ij}^{tr} is the transformation strain. Further detailed discussion on the individual SMA modeling approaches and variable choices will be investigated in more detail in Chapter 3.

2.2. Use of Thermodynamic Fundamentals in SMA Modeling

As explained in Section 2.1, in modeling materials, Helmholtz free energy function, $\psi = \psi(T, \epsilon_{ij})$, and, Gibbs free energy functions, $G = G(T, \sigma_{ij})$, can be used in modeling linear materials. However, the state of nonlinear materials cannot be determined only by controllable and/or measurable variables like temperature and strain, which are generally called *external variables* [55]. Hence by including additional variables, the thermodynamic state of inelastic materials can be determined. Named *internal variables* or *hidden variables*, these are unobservable state variables which describe the dissipative effects in nonlinear materials. Used in inelastic constitutive modeling [59, 60], Helmholtz free energy and Gibbs free energy respectively take the following forms; $\psi = \psi(T, \epsilon_{ij}, \zeta_n)$, $G = G(T, \sigma_{ij}, \zeta_n)$, where ζ_n denotes the n-element set of internal variables. For SMA modeling, there are different approaches

for introducing internal variables. These will be discussed in detail in Chapter 3, but in order to illustrate a general case, the first constitutive model studied in Chapter 3, namely Tanaka's model is studied in this section to show the usage of thermodynamical fundamentals in SMA modeling.

2.2.1. Thermodynamical Fundamentals in Tanaka *et al.*'s Model

Tanaka claims that [11], the SMA phenomena can be described fully by using the following set of variables:

$$\mathbf{j} = (L_{ij}, T, z) \tag{2.50}$$

where, L_{ij} is the Green strain (Tanaka considers large deformations), T is the temperature, and, z is the variable representing the extent of transformation, namely, the martensite fraction. This is an example of internal variable ζ that was mentioned in the previous section. Rewriting Helmholtz free energy as:

$$\psi(L_{ij}, T, z) = u - Ts \tag{2.51}$$

its time derivative gives in terms of $\dot{u}$:

$$\dot{u} = T\dot{s} + s\dot{T} + \psi_L \dot{L}_{ij} + \psi_T \dot{T} + \psi_z \dot{z} \tag{2.52}$$

where ψ_L, ψ_T, and, ψ_z are derivatives of Helmholtz free energy with respect to Green strain, to temperature, and to martensite fraction respectively.

Combining First law given in Equation 2.12 with the Clausius-Duhem inequality given in Equation 2.20 and writing it in the reference configuration gives:

$$\rho_0 \dot{s} - \frac{(\rho_0 \dot{u} + q_{i,i} - \dot{L}_{ij} K_{ij})}{T} + \frac{q_{i,i}}{T} - \frac{q_i T_{,i}}{T^2} \geq 0 \tag{2.53}$$

which simplifies to:

$$\rho_0 \dot{s} - \frac{\rho_0 \dot{u}}{T} + \frac{\dot{L}_{ij} K_{ij}}{T} - \frac{q_i T_{,i}}{T^2} \geq 0 \tag{2.54}$$

Now, instead of $\dot{u}$, using differential form of internal energy obtained in Equation 2.52, Equation 2.54 becomes:

$$\rho_0 \dot{s} - \frac{\rho_0 (T\dot{s} + s\dot{T} + \psi_L \dot{L}_{ij} + \psi_T \dot{T} + \psi_z \dot{z})}{T} + \frac{\dot{L}_{ij} K_{ij}}{T} - \frac{q_i T_{,i}}{T^2} \geq 0 \tag{2.55}$$

which, after multiplication of both sides by T, simplifies to:

$$-\rho_0 \left(s\dot{T} + \psi_L \dot{L}_{ij} + \psi_T \dot{T} + \psi_z \dot{z}\right) + \dot{L}_{ij} K_{ij} - \frac{q_i T_{,i}}{T} \geq 0 \tag{2.56}$$

Equation 2.56 can be rewritten by grouping the variables as:

$$(K_{ij} - \rho_0 \psi_L)\dot{L}_{ij} - \rho_0 (s + \psi_T) - \rho_0 \psi_z \dot{z} - \frac{q_i T_{,i}}{T} \geq 0 \tag{2.57}$$

For Equation 2.56 to hold, the following conditions are imposed:

$$\begin{aligned} K_{ij} &= \rho_0 \psi_L, \\ s &= -\psi_T, \end{aligned} \tag{2.58}$$

and,

$$-\psi_z \dot{z} - \frac{q_i T_{,i}}{\rho_0 T} \geq 0 \tag{2.59}$$

From conditions in Equation 2.58, stress can be obtained in rate form by taking the time differential as:

$$\dot{K}_{ij} = \rho_0 (\psi_{LL} \dot{L}_{ij} + \psi_{LT} \dot{T} + \psi_{Lz} \dot{z}) \tag{2.60}$$

which can also be written as follows:

$$\dot{K}_{ij} = E_{ijkl}\dot{L}_{kl} + \Theta_{ij}\dot{T} + \Omega_{ij}\dot{z} \tag{2.61}$$

where $\dot{K}_{ij}$ is the incremental second Piola Kirchoff stress tensor, $E_{ijkl} = \rho_0\,\psi_{LL}$ is the elastic modulus tensor, L_{ij} is the Green strain tensor, $\Theta_{ij} = \rho_0\,\psi_{LT}$ is the thermoelastic modulus tensor, T is the temperature, z is the martensite fraction, ρ_0 is the reference configuration density, and $\Omega_{ij} = \rho_0\,\psi_{Lz}$ is the transformation tensor.

Again, from conditions in Equation 2.58, entropy can also be obtained in rate form by taking the time differential as:

$$\dot{s} = -\psi_{TL}\dot{L}_{ij} - \psi_{TT}\dot{T} - \psi_{Tz}\dot{z} \tag{2.62}$$

which can also be written as follows:

$$\dot{s} = -\frac{1}{\rho_0}\Theta_{ij}\dot{L}_{ij} + \frac{1}{\rho_0}c\dot{T} + \Gamma\dot{z}, \tag{2.63}$$

where s is the entropy, $c = -\rho_0\psi_{TT}$ is the specific heat and $\Gamma = -\rho_0\psi_{Tz}$ is the transformation coefficient.

3. CONSTITUTIVE MODELING FOR SMAs

In this chapter, the models which are going to be used in the solution of the crack problem in Chapter 4 will be investigated. In addition to those models, a few of others which are not directly used in this study but have influenced the ones in use, are also detailed.

3.1. Tanaka *et al.*

In 1982, Tanaka and Nagaki based their description of SMA materials on a thermomechanical framework [10]. The basis of the model was derived in Chapter 2 to exemplify the derivation of SMA constitutive relations with thermodynamic principles. The discussion here follow from the final result there:

$$\begin{aligned} \dot{K}_{ij} &= E_{ijkl}\dot{L}_{kl} + \Theta_{ij}\dot{T} + \Omega_{ij}\dot{z}, \\ \dot{s} &= -\frac{1}{\rho_0}\Theta_{ij}\dot{L}_{ij} + \frac{1}{\rho_0}c\dot{T} + \Gamma\dot{z}, \end{aligned} \tag{3.1}$$

where K_{ij} is the second Piola Kirchoff stress tensor, E_{ijkl} is the elastic modulus tensor, L_{ij} is the Green strain tensor, Θ_{ij} is the thermoelastic modulus tensor, T is the temperature, z is the martensite fraction, s is the entropy, ρ_0 is the density, c is the specific heat, Ω_{ij} is the transformation tensor and Γ is the transformation coefficient derived by the differentials of energy potential.

The transformation kinetics which describe the evolution of martensite fraction, z, is not included in Tanaka and Nagaki's 1982 paper but later investigated by Tanaka *et al.* in a 1986 paper [11]. The model proposed in this paper is 1D and is based on uniaxial stress-strain. The work can be distinguished by a couple of novel ideas. First of all, it includes martensitic volume fraction's evolution. With the help of this fraction, elastic modulus at any moment before, during and after the transformation

is derived by applying the rule of mixtures, i.e.

$$E = E_A + (E_M - E_A)z \tag{3.2}$$

where, E is the elastic modulus of SMA with the martensite fraction, z. E_A is the full austenite elastic modulus ($z = 0$), and, E_M is the full martensite elastic modulus ($z = 1$).

The evolution of martensitic volume fraction, using Koistinen and Marburger's transformation kinetics for iron-carbon alloys and pure steels [61, 62] is adopted in Tanaka's work. Accordingly, for forward transformation (from austenite to martensite), z is given by:

$$z = 1 - exp\Big[a_M(M_s - T) + b_M\sigma\Big] \tag{3.3}$$

where, σ is the uniaxial stress, and, T is current temperature. a_M and b_M are material constants in terms of transition temperatures, M_s, M_f, A_s, and, A_f, which are martensite transformation start temperature, martensite transformation finish temperature, austenite transformation start temperature, and, austenite transformation finish temperature, respectively. The formula giving a_M is as follows:

$$a_M = -\frac{4.605}{M_s - M_f} \tag{3.4}$$

and, the relation giving b_M is:

$$b_M = a_M/1.5 \tag{3.5}$$

For reverse transformation (from martensite to austenite), on the other hand, the relation is:

$$1 - z = 1 - exp\Big[a_A(A_s - T) + b_A\sigma\Big] \tag{3.6}$$

which can be rewritten as:

$$z = exp\Big[a_A(A_s - T) + b_A\sigma\Big] \tag{3.7}$$

where, analogous to Equation 3.3, a_A and b_A are material constants in terms of transition temperatures M_s, M_f, A_s, and, A_f:

$$a_A = \frac{4.605}{A_f - A_s}, \tag{3.8}$$

$$b_A = a_A/1.5 \tag{3.9}$$

Tanaka *et al.*, with these martensite fraction functions given in Equation 3.3 and 3.6, provide the exponential relation used in finite elements, giving the relation between the martensite fraction and the temperature and stress.

As an example and verification of these martensite fraction relations, a theoretical SMA specimen with the specifications given in Table 3.1 under constant temperature of T = 20°C is simulated for uniaxial stress between 70.5 MPa to 100 MPa. The resulting forward transformation martensite fraction vs. stress diagram is shown in Figure 3.1. For the resulting reverse transformation by the relaxing of the specimen, the resulting diagram is shown in Figure 3.2. It should be noted that both of these curves have exponential nature, which is expected since Tanaka's martensite fraction relation is an exponential function.

Table 3.1. Theoretical SMA specimen properties used for Tanaka's formulations.

Property	Value
a_M $(^\circ C^{-1})$	-0.658
b_M (MPa^{-1})	-0.439
a_A $(^\circ C^{-1})$	0.419
b_A (MPa^{-1})	0.279
M_s (°C)	-27
A_s (°C)	-25
$\rho\Delta s^M$ (MPa/K)	-0.35

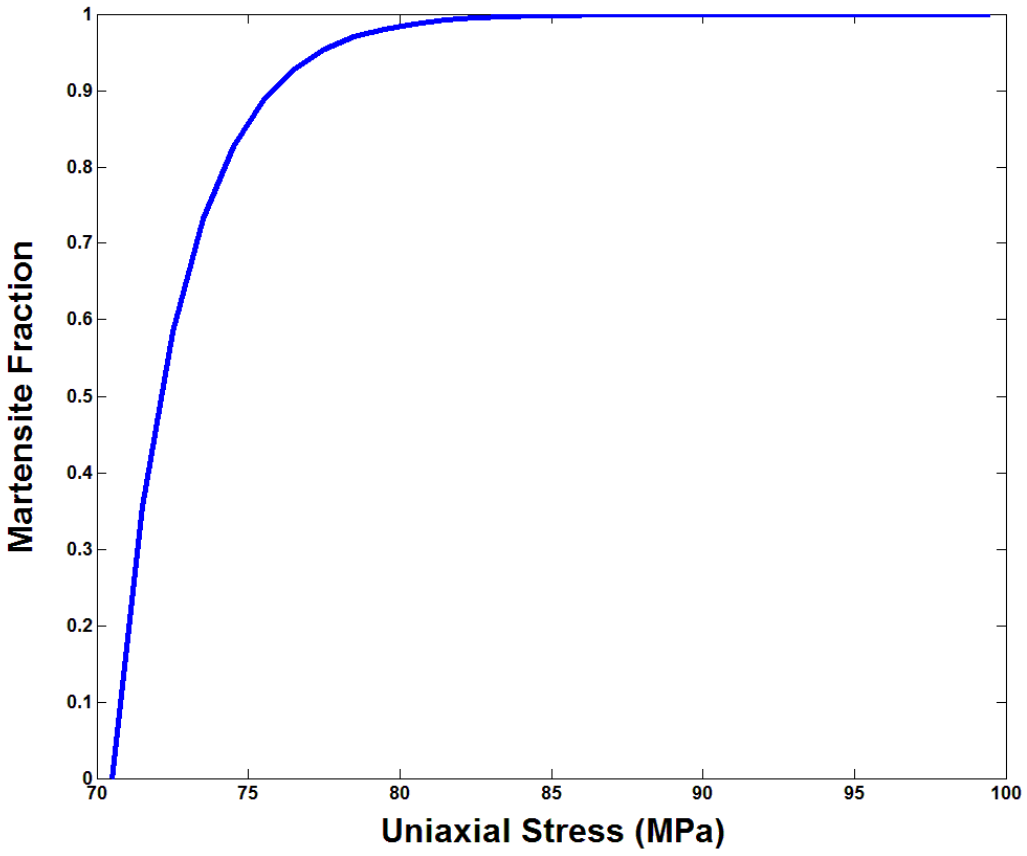


Figure 3.1. Martensite fraction vs. Uniaxial stress in forward transformation.

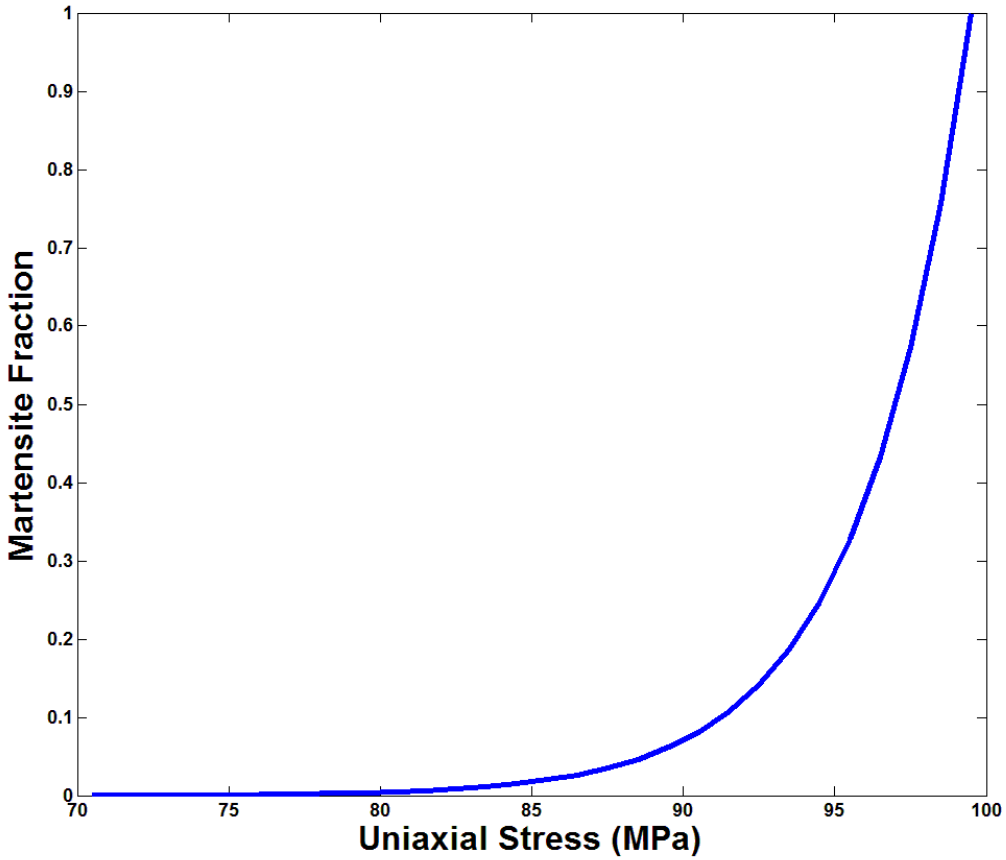


Figure 3.2. Martensite fraction vs. Uniaxial stress in reverse transformation.

3.2. Liang and Rogers

In 1990, Liang and Rogers published their work on one-dimensional modeling of shape memory materials [12]. In this work, which stems from Liang's PhD thesis [63] a brief review of Muller's [21] and Tanaka's [10,11] models are done. Tanaka's rate form given in Equation 3.1 is again reiterated in 1D as:

$$\dot{K} = \frac{\partial K}{\partial L}\dot{L} + \frac{\partial K}{\partial T}\dot{T} + \frac{\partial K}{\partial z}\dot{z} = E\dot{L} + \Theta\dot{T} + \Omega\dot{z} \tag{3.10}$$

where K is the Piola-Kirchoff stress, L is the Green strain, E is the Young's modulus, Θ is the thermoelastic modulus, T is the temperature, z is the martensite fraction, Ω is transformation modulus, all in 1D.

From this rate form, Liang and Rogers, obtain what they call the unified constitutive relation by integrating Equation 3.10 with respect to time. The relation obtained is as follows:

$$K - K_0 = E(L - L_0) + \Theta(T - T_0) + \Omega(z - z_0) \tag{3.11}$$

where the subscript "0" means that the variable with it is at initial conditions. Here, the material properties are assumed constant.

Also, different from Tanaka's, the martensite fraction's evolution is given by a different set of functions, using a cosine function to describe the martensite vs. temperature (z vs. T) behavior. As it can be seen in Figure 3.3, the experimentally obtained relation between the martensite fraction and temperature in stress-free case can be approximated by a cosine function. For forward transformation, z is given by:

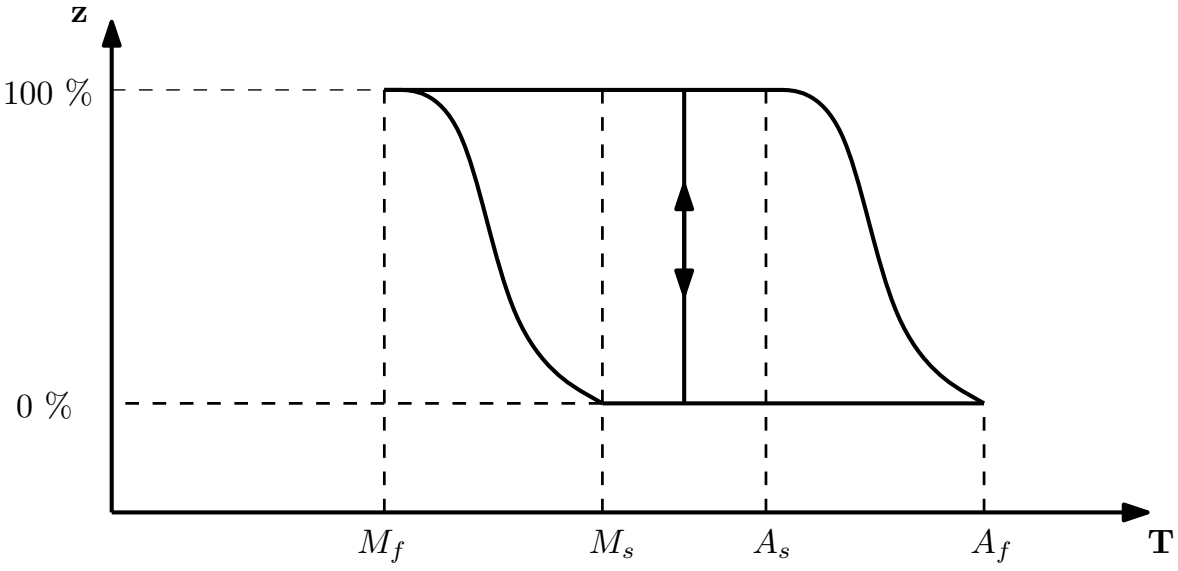


Figure 3.3. Martensite fraction vs. temperature curves in stress-free state [64].

$$z = \frac{1 - z_0}{2} \cos[a_M(T - M_f) + b_M\sigma] + \frac{1 + z_0}{2} \tag{3.12}$$

where, z_0 is the martensite fraction before the transformation (if fully austenite, z_0=0),

and, a_M and b_M are given as:

$$\begin{aligned} a_M &= \pi/(M_s - M_f) \\ b_M &= -a_M/C_M \end{aligned} \tag{3.13}$$

with C_M being the $\tan(\alpha)$ value taken from Figure 3.4.

Similarly for reverse transformation, the martensite fraction function takes the following form:

$$z = \frac{z_0}{2}\left\{\cos[a_A(T - A_s) + b_A\sigma] + 1\right\} \tag{3.14}$$

where, z_0 is again the current martensite fraction, and, a_A and b_A are given as:

$$\begin{aligned} a_A &= \pi/(A_f - A_s) \\ b_A &= -a_A/C_A \end{aligned} \tag{3.15}$$

with C_A being the $\tan(\beta)$ value taken from Figure 3.4 which shows the experimental critical phase transition stresses for different temperatures. Liang and Rogers assumed that α and β values are equivalent [12, 63].

From Equation 3.12 and 3.14, limit values for stresses are also derived. Since cosine function, can only take values between -1 and 1, the stress range during forward transformation is given as:

$$C_A(T - A_s) - \frac{\pi}{|b_A|} \leq \sigma \leq C_A(T - A_s) \tag{3.16}$$

and, for reverse transformation, it is given as:

$$C_M(T - M_f) - \frac{\pi}{|b_M|} \leq \sigma \leq C_M(T - M_f) \tag{3.17}$$

For the rest of the work, different cases for SMA wires or fibers are investigated. Stress-

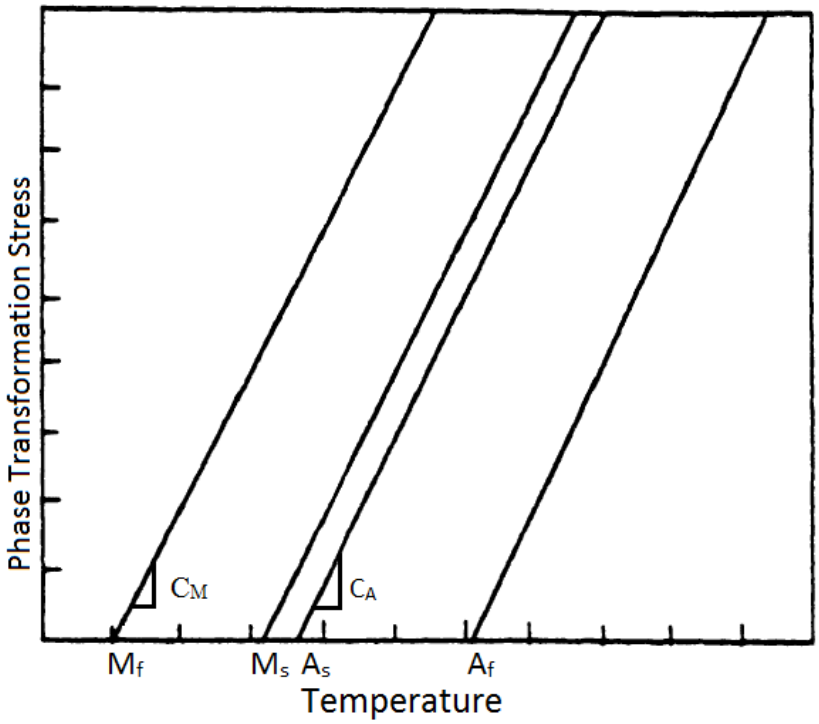


Figure 3.4. Evolutions of phase transition stresses with respect to temperature traced by Liang and Rogers using experimental data [12].

strain diagrams obeying SMA characteristics and fitting experimental data for copper based SMA are obtained. In conclusion, the claim of Liang and Rogers is that, their unified and thermomechanical constitutive model is, although based on Tanaka's work, has better accuracy in fitting the experimental data.

3.3. Brinson

Brinson, her work dated 1993 [65], takes on from the point where Tanaka [10, 11] and Liang [12, 63] had left. She uses the exact methodology, up to the point where martensite fraction enters. The novelty she brings is about martensite fraction which is divided to two parts as z_σ and z_T, stress induced martensite fraction and temperature induced martensite fraction respectively, where:

$$z = z_\sigma + z_T \tag{3.18}$$

She argues that, the Equation 3.11, derived by Liang and Rogers, in its current from, with only a single martensite fraction variable is not suitable for the cases where $T < M_f$. If an example case is taken with the initial conditions of $K_0 = L_0 = 0, z_0 = 1$ and temperature is held constant at $T = T_0$ the Equation 3.11 becomes:

$$K = EL + \Theta(1 - 1) + \Omega(1 - 1) = EL \tag{3.19}$$

which is the pure linear elastic stress-strain relation which cannot represent the SMA behavior. Brinson also uses another case with the Equation 3.11 to obtain the transformation tensor (a constant coefficient in this 1D case), using the initial conditions as $K_0 = L_0 = z_0 = 0$ and final conditions as $K = 0$, $L = e_L$, $z = 1$ with $T = T_0$ at $M_s < T < A_s$ where e_L, maximum transformation strain, is a material constant. Under this case, one obtains the following relationship:

$$\Omega = -e_L\, E \tag{3.20}$$

In addition to that, since stress is a function of three variables, namely, strain, temperature, and, martensite fraction, she differentiates stress:

$$dK = \frac{\partial K}{\partial L}dL + \frac{\partial K}{\partial z}dz + \frac{\partial K}{\partial T}dT \tag{3.21}$$

and combines Equation 3.18 with the Equation 3.21 to obtain:

$$dK = \frac{\partial K}{\partial L}dL + \frac{\partial K}{\partial z_\sigma}dz_\sigma + \frac{\partial K}{\partial z_T}dz_T + \frac{\partial K}{\partial T}dT \tag{3.22}$$

Integrating Equation 3.22 yields:

$$K - K_0 = E(L - L_0) + \Omega_\sigma(z_\sigma - z_{\sigma 0}) + \Omega_T(z_T - z_{T0}) + \Theta(T - T_0) \tag{3.23}$$

where $z_{\sigma 0}$ and z_{T0} are initial stress induced and temperature induced martensite fractions respectively. Now, applying the same conditions used to reach the Equation 3.19,

the following result is reached:

$$K = EL + \Omega_\sigma z_\sigma \tag{3.24}$$

which is suitable for the expected nonlinear behavior. Brinson also uses experimental results by others such as Dye [66] to improve the critical transformation stress curves already given by Liang and Rogers in Figure 3.4. The assumption made is that the critical stress values for temperatures below martensite start temperature, M_s, to be constant. The resulting curves are given by Brinson on Figure 3.5 where y-axis is the critical phase transformation stress labeled as K_{crit} and x-axis is the temperature axis labeled as T. Now, using the cruves in Figure 3.5, Brinson obtains new martensite

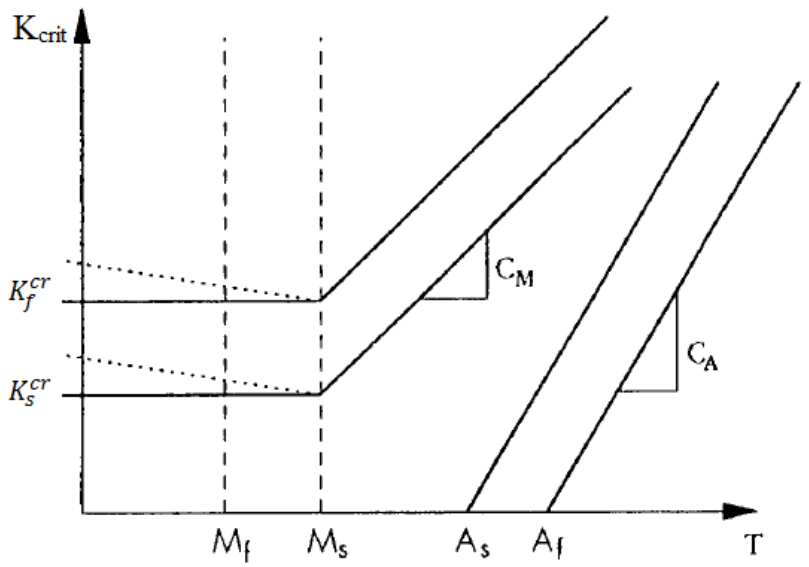


Figure 3.5. Evolutions of phase transition stresses with respect to temperature traced by Brinson using experimental data by Dye [65, 66].

fraction evolution equations for some special cases. First case for the conversion to detwinned martensite where K values are in the interval $K_s^{cr} + C_M(T - M_s) < K < K_f^{cr} + C_M(T - M_s)$ and T $> M_s$:

$$\begin{aligned} z_\sigma &= \frac{1 - z_{\sigma 0}}{2} \cos\left\{ \frac{\pi}{K_s^{cr} - K_f^{cr}} [K - K_f^{cr} - C_M(T - M_s)] \right\} + \frac{1 + z_{\sigma 0}}{2} \\ z_T &= z_{T0} - \frac{z_{T0}}{1 - z_{\sigma 0}} (z_\sigma - z_{\sigma 0}) \end{aligned} \tag{3.25}$$

where K_s^{cr} and K_f^{cr} values are taken from Figure 3.5 for the temperature values

For the other case of conversion to detwinned martensite where K values are in the interval $K_s^{cr} < K < K_f^{cr}$ and $T < M_s$:

$$\begin{aligned} z_\sigma &= \frac{1 - z_{\sigma 0}}{2} \cos\left\{ \frac{\pi}{K_s^{cr} - K_f^{cr}} (K - K_f^{cr}) \right\} + \frac{1 + z_{\sigma 0}}{2} \\ z_T &= z_{T0} - \frac{z_{T0}}{1 - z_{\sigma 0}} (z_\sigma - z_{\sigma 0}) + \Delta_{Tz} \end{aligned} \tag{3.26}$$

where, if $T < T_0$, $\Delta_{Tz} = 0$ and if $M_f < T < M_s$:

$$\Delta_{Tz} = \frac{1 - z_{T0}}{2} \left\{ \cos[a_M (T - M_f)] + 1 \right\} \tag{3.27}$$

For conversion to austenite where $T > A_s$ and $C_A(T - A_f) < K < C_A(T - A_s)$:

$$\begin{aligned} z &= \frac{z_0}{2} \left\{ \cos\left[a_A \left(T - A_s - \frac{K}{C_A} \right) \right] + 1 \right\} \\ z_\sigma &= z_{\sigma 0} - \frac{z_{\sigma 0}}{z_0} (z_0 - z) \\ z_T &= z_{T0} - \frac{z_{T0}}{z_0} (z_0 - z) \end{aligned} \tag{3.28}$$

Also, to obtain the final form of constitutive equations, Brinson takes up from the point where Tanaka left about the elastic modulus (Equation 3.2) as:

$$E(z) = E_A + (E_M - E_A) z \tag{3.29}$$

where the notation $E(z)$ is used to notify that E is a function of martensite fraction, z. From this point, the transformation tensor, Ω is obtained also as a function of martensite fraction by first expanding Ω in a Taylor Series about z_0 and by neglecting second order and higher order terms as:

$$\Omega(z) = \Omega(z_0) + (z - z_0) \Omega'(z_0) \tag{3.30}$$

When $z = z_0$ and remains constant, the results already obtained from constant E and constant Ω case, namely, the Equation 3.20 is obtained:

$$\Omega(z_0) = -e_L\, E(z_0) \tag{3.31}$$

Substituting it together with Equation 3.29 into Equation 3.30, the equation obtained is as follows:

$$\Omega(z) = -e_L\, E_A - e_L\, z\, (E_M - E_A) \tag{3.32}$$

She then assumes that $\Theta(e, z, T)$ will remains constant since it will have relatively small values and also, assumes that $\Omega_T \equiv 0$ with the derivation used in deriving Equation 3.24 from Equation 3.23. Hence, she rewrites Equation 3.22 as:

$$dK = E(z)dL + \Omega(z)dz_s + \Theta dT \tag{3.33}$$

and by partial integration, obtains:

$$K+c = E_A L+(E_M-E_A)\, zL+C(z)-e_L\, E_A\, z_\sigma-e_L(E_M-E_A)\left[\frac{z_\sigma^2}{2}+z_T\, z_\sigma\right]+\Theta\, T \tag{3.34}$$

where c is an arbitrary constant and C(z) is an arbitrary function of z. Since the expansion of D(z) multiplied by z_σ is:

$$E(z)z_\sigma = E_A\, z_\sigma + (E_M - E_A)z_\sigma^2 + (E_M - E_A)z_\sigma\, z_T \tag{3.35}$$

Equation 3.34 simplifies to:

$$K + c = E(z)L + \Omega(z)z_\sigma + \Theta\, T + e_L(E_M - E_A)\frac{z_\sigma^2}{2} + C(z) \tag{3.36}$$

and, to obtain the constant, c, when the initial conditions (K_0, e_0, z_0, T_0) are put into

Equation 3.36, c is found as:

$$c = E(z_0)L_0 + \Omega(z_0)z_{\sigma 0} + \Theta\, T_0 + e_L(E_M - E_A)\frac{z_{\sigma 0}^2}{2} + C(z_0) - K_0 \tag{3.37}$$

and when c is put back into Equation 3.36, it becomes:

$$K - K_0 = E(z)L - E(z_0)L_0 + \Omega(z)z_\sigma - \Omega(z_0)z_{\sigma 0} + \Theta(T - T_0) + e_L(E_M - E_A)\frac{z_\sigma^2 - z_{\sigma 0}^2}{2} + C(z) - C(z_0) \tag{3.38}$$

Now, the only remaining arbitrary parameter is $C(z)$, to find it, Brinson makes an assumption about the maximum transformation strain and current transformation strain as follows:

$$L^{tr} = e_L\, z_\sigma \tag{3.39}$$

which means that, current transformation strain is directly proportional to the value of martensite fraction created by loadings. Using Equation 3.39, the initial state of $K_0 = L_0 = z_{\sigma 0} = 0$, and the final state of $K = 0$, $L = L_{tr} = e_L z_\sigma$, z_σ under isothermal conditions ($T = T_0$), one obtains:

$$0 = E(z)e_L\, z_\sigma + \Omega(z)z_\sigma + e_L(E_M - E_A)\frac{z_\sigma^2}{2} + C(z) - C(0) \tag{3.40}$$

which by using Equation 3.31 reduces to:

$$C(z) = -e_L(E_M - E_A)\,\frac{z_\sigma^2}{2} \tag{3.41}$$

Finally, the ultimate constitutive equation of Brinson's work is reached as putting Equation 3.41 into Equation 3.38:

$$K - K_0 = E(z)L - E(z_0)L_0 + \Omega(z)z_\sigma - \Omega(z_0)z_{\sigma 0} + \Theta(T - T_0) \tag{3.42}$$

3.4. Lagoudas *et al.*

Lagoudas' works on constitutive modeling of SMA span over a long time period with many different coworkers [3, 14, 15, 56, 67–69]. One of the ideas that distinguish Lagoudas *et al.*'s work from others is the choice of the free energy function. Contrary to the literature, Lagoudas and coworkers use Gibbs free energy function instead of Helmholtz free energy. As explained in Chapter 2, Section 2.2 this choice of different energy makes stress a variable of the free energy function instead of strain inside. Also, in addition to the usage of martensite fraction, z, as a variable, Lagoudas considers transformation strain, ϵ^{tr}, also to be a variable an internal state variable. Also, a different form of Clausius-Duhem inequality given Equation 2.20 is used by Lagoudas with an assumption that the term $-q_i T_{,i}/T^2$ will always be greater than or equal to zero. The reduced inequality is then:

$$\rho\dot{s} - \frac{\theta}{T} + \frac{q_{i,i}}{T} \geq 0 \tag{3.43}$$

which is called Clausius-Planck inequality. Using this inequality and also using the relation between Gibbs free energy and internal energy as given in Equation 2.30:

$$G = u - Ts - \frac{1}{\rho}\sigma_{ij}\epsilon_{ij} \tag{3.44}$$

Similar to the procedure used in Section 2.2, combining the Equation 3.43 with the first law as given in Equation 2.12 gives:

$$\rho\dot{u} = \dot{\epsilon}_{ij}\sigma_{ij} + \theta - q_{i,i} \tag{3.45}$$

$$\rho\dot{s} - \frac{(\rho\dot{u} + q_{i,i} - \dot{\epsilon}_{ij}\sigma_{ij})}{T} + \frac{q_{i,i}}{T} \geq 0 \tag{3.46}$$

Now, similar to the procedure done with Helmholtz free energy in Equation 2.52, taking the time derivative of the internal energy given in Equation 3.44 gives:

$$\dot{u} = T\dot{s} + s\dot{T} + G_\sigma \dot{\sigma}_{ij} + G_T \dot{T} + G_z \dot{z} + G_{\epsilon^{tr}} \dot{\epsilon}^{tr}_{ij} + \frac{1}{\rho}\dot{\sigma}_{ij}\epsilon_{ij} + \frac{1}{\rho}\sigma_{ij}\dot{\epsilon}_{ij} \tag{3.47}$$

where G_σ, G_T, G_z, and, $G_{\epsilon^{tr}}$ are derivatives of Gibbs free energy with respect to stress, to temperature, to martensite fraction, and, to transformation strain respectively. Combining Equation 3.46 and 3.47 yields:

$$\frac{\rho(T\dot{s} - T\dot{s} - s\dot{T} - G_\sigma \dot{\sigma}_{ij} - G_T \dot{T} - G_z \dot{z} - G_{\epsilon^{tr}} \dot{\epsilon}^{tr}_{ij} - \frac{1}{\rho}\dot{\sigma}_{ij}\epsilon_{ij} - \frac{1}{\rho}\sigma_{ij}\dot{\epsilon}_{ij})}{T} - \frac{q_{i,i} - \dot{\epsilon}_{ij}\sigma_{ij} - q_{i,i}}{T} \geq 0 \tag{3.48}$$

which further simplifies to:

$$\frac{\rho(-s\dot{T} - G_\sigma \dot{\sigma}_{ij} - G_T \dot{T} - G_z \dot{z} - G_{\epsilon^{tr}} \dot{\epsilon}^{tr}_{ij} - \frac{1}{\rho}\dot{\sigma}_{ij}\epsilon_{ij})}{T} \geq 0 \tag{3.49}$$

which can be rewritten after multiplying both sides by T as:

$$-\rho\left[(G_T + s)\dot{T} + \left(G_\sigma + \frac{1}{\rho}\epsilon_{ij}\right)\dot{\sigma}_{ij} + G_z \dot{z} + G_{\epsilon^{tr}} \dot{\epsilon}^{tr}_{ij}\right] \geq 0 \tag{3.50}$$

from which, we obtain the following relations:

$$\begin{aligned} \epsilon_{ij} &= -\rho\, G_\sigma, \\ s &= -G_T, \end{aligned} \tag{3.51}$$

and the relation:

$$-\rho\, G_z \dot{z} - \rho\, G_{\epsilon^{tr}} \dot{\epsilon}^{tr}_{ij} \geq 0 \tag{3.52}$$

The Gibbs free energy function in quadratic polynomial form is taken as:

$$G(\sigma_{ij}, T, z, \epsilon_{ij}^{tr}) = -\frac{1}{2\rho}\sigma_{ij}C_{ijkl}\sigma_{kl} - \frac{1}{\rho}\sigma_{ij}\left[\alpha_{ij}(T - T_0) + \epsilon_{ij}^{tr}\right] + c\left[(T - T_0) - T\,ln\left(\frac{T}{T_0}\right)\right] - s_0\,T + u_0 + \frac{1}{\rho}f(z) \tag{3.53}$$

where C_{ijkl} is the compliance tensor, α_{ij} is the thermal expansion tensor, c is the specific heat, s is the specific entropy, u is the specific internal energy, and $f(z)$ is the transformation hardening function. It should be noted that, this work assumes strains to be infinitesimal, hence ϵ_{ij} is the infinitesimal strain tensor. Also, material properties are not constant with respect to martensite fraction, instead a rule of mixtures-like relation exists for the compliance tensor, the thermal expansion tensor, the specific heat, the specific entropy and the specific internal energy. For the compliance tensor, the relation is:

$$C_{ijkl}(z) = C_{ijkl}^{A} + z(C_{ijkl}^{M} - C_{ijkl}^{A}) \tag{3.54}$$

where C_{ijkl}^{A} is the austenite phase compliance tensor and C_{ijkl}^{M} is the martensite phase compliance tensor. For the other four material properties mentioned above, the same relation also exists. However, it is also noted by Lagoudas that, using micromechanical methods, these material properties can be more accurately approximated. From this point on, to obtain the infinitesimal strain tensor ϵ_{ij}, and, the entropy, s, the Equation 3.51 is used as:

$$s = -G_T = \frac{1}{\rho}\sigma_{ij}\alpha_{ij} + c\,ln\left(\frac{T}{T_0}\right) + s_0 \tag{3.55}$$

$$\epsilon_{ij} = -\rho G_\sigma = C_{ijkl}\sigma_{kl} + \alpha_{ij}(T - T_0) + \epsilon_{ij}^{tr} \tag{3.56}$$

Now, combining Equation 3.52 and 3.53 gives:

$$-\rho\,G_z\dot{z} + \sigma_{ij}\dot{\epsilon}_{ij}^{tr} \geq 0 \tag{3.57}$$

For the internal variables, martensite fraction, z, and transformation strain ϵ_{ij}^{tr}, rate-form equations, also called evolution equations are proposed. For these two variables, a concept mostly used in plasticity is employed and the relation between them is written as flow rule which normally relates plastic strain and the applied stress [70], in Lagoudas it is given as:

$$\dot{\epsilon}_{ij}^{tr} = \Lambda_{ij}\dot{z} \tag{3.58}$$

where Λ_{ij} is the transformation tensor which serves to determine the transformation strain direction. This tensor is assumed to be of the following form for forward transformation:

$$\Lambda_{ij} = \frac{3}{2}\epsilon_L \frac{\sigma_{ij}^{dev}}{\bar{\sigma}^{dev}} \tag{3.59}$$

where, ϵ_L is the maximum transformation strain, σ_{ij}^{dev} is the deviatoric stress and $\bar{\sigma}^{dev}$ is the von Mises stress. $\bar{\sigma}^{dev}$ is:

$$\bar{\sigma}^{dev} = \sqrt{\frac{3}{2}\sigma_{ij}^{dev}\sigma_{ij}^{dev}} \tag{3.60}$$

where σ_{ij}^{dev} is:

$$\sigma_{ij}^{dev} = \sigma_{ij} - \frac{\sigma_{kk}}{3}\delta_{ij} \tag{3.61}$$

where δ_{ij} is the Kroenecker delta. For reverse transformation, instead of Equation 3.59, the assumed form is:

$$\Lambda_{ij} = \epsilon_L \frac{\epsilon_{ij}^{tr-r}}{\bar{\epsilon}^{tr-r}} \tag{3.62}$$

where ϵ_{ij}^{tr-r} is the transformation strain at the phase transformation reversal and $\bar{\epsilon}^{tr-r}$ is the corresponding effective transformation strain given by:

$$\bar{\epsilon}^{tr-r} = \sqrt{\frac{2}{3}\epsilon_{ij}^{tr-r}\epsilon_{ij}^{tr-r}} \tag{3.63}$$

Combining Equation 3.57 and 3.58 gives:

$$(\sigma_{ij}\Lambda_{ij} - \rho\, G_z)\dot{z} = \pi\dot{z} \geq 0 \tag{3.64}$$

where π is defined as the general thermodynamic force conjugated to z. Combining Equation 3.53 and 3.64 gives π as:

$$\begin{aligned}\pi(\sigma_{ij}, T, z) = \sigma_{ij}\Lambda_{ij} + \frac{1}{2\rho}\sigma_{ij}(C_{ijkl}^{M} - C_{ijkl}^{A})\sigma_{kl} + \sigma_{ij}\left[(\alpha_{ij}^{M} - \alpha_{ij}^{A})(T - T_0)\right] - \\ \rho(c^{M} - c^{A})\left[(T - T_0) - T\, ln\left(\frac{T}{T_0}\right)\right] + \rho(s_0^{M} - s_0^{A})\, T - \\ \rho(u_0^{M} - u_0^{A}) - f_z(z)\end{aligned} \tag{3.65}$$

where $f_z(z)$ is the derivative of hardening function with respect to martensite fraction. It should also be noted that the presence of the terms $(C_{ijkl}^{M} - C_{ijkl}^{A})$, $(\alpha_{ij}^{M} - \alpha_{ij}^{A})$, $(c^{M} - c^{A})$, $(s_0^{M} - s_0^{A})$, and, $(u_0^{M} - u_0^{A})$ arise from the fact that the material properties are not constant and they vary with changing martensite fraction z as given in Equation 3.54 for C_{ijkl}. Also, since in Equation 3.58 the dependence of transformation strain and martensite fraction is established, the transformation strain no longer exists as a variable of the function π. From this point on, the two important scalars are the thermodynamic force, π and martensite fraction change rate, $\dot{z}$ as shown in the final form of Clausius-Planck inequality shown in Equation 3.64. This inequality is always satisfied when there is no phase transformation since $\dot{z} = 0$ when no transformation occurs. In the case of forward transformation, where, $\dot{z} > 0$, π has to have a positive value, and in the case of reverse transformation, where, $\dot{z} < 0$, π has to have a negative value. This value which is equal to π during phase transformation is represented by Y. Y is found experimentally by imposing different state conditions on the material and

using experimentally obtained phase transformation start and finish temperatures, and, stress influence coefficient. Finally, as for the transformation hardening function, which is first introduced in Equation 3.53, Lagoudas proposes a second-order polynomial form as follows:

$$f(z) = \begin{cases} \frac{1}{2}\rho b^M z^2 + (\mu_1 + \mu_2)z & \text{if } \dot{z} > 0 \\ \frac{1}{2}\rho b^A z^2 + (\mu_1 - \mu_2)z & \text{if } \dot{z} < 0 \end{cases} \tag{3.66}$$

where, ρb^M, ρb^A, μ_1, and μ_2 are coefficients determined by the imposing of five different state conditions and the usage of experimental data as done in finding Y. Hence, having laid out the thermodynamical foundations and the usage of Gibbs free energy, and having given a transformation hardening function, Lagoudas' constitutive model is implemented numerically to for finite elements modeling of SMA [68, 71]. This constitutive model is used in Chapter 4 in FE fracture problem solutions [72].

3.5. Leclercq and Lexcellent

Leclerq and Lexcellent, provides a general thermomechanical model of shape memory alloy behavior [16]. Two internal variables, volume fraction of self-accommodating (pure thermal effect) and oriented (stress-induced) product-phase are taken into account. A specific free energy, valid in the total range of phase transition is defined with particular attention to the interaction term. Kinetic equations for internal variables are written in order to comply with the second law of thermodynamics. Five yield functions (each related to one process) are given. This work is able to model complete thermomechanical loadings, including non-isothermal ones. The volume fraction of self-accommodating martensite is given as z_σ and the oriented volume fraction as z_T. The interactions between different phases are given in Figure 3.6.

Here, it can be seen that, while by pure thermal effects, the self-accommodating martensite phase can be obtained, by applying stress, one obtains the oriented martensite. Also, from self-accommodating martensite, by applying stress, oriented martensite phase can be obtained too. For both phases, the free energy is the same and

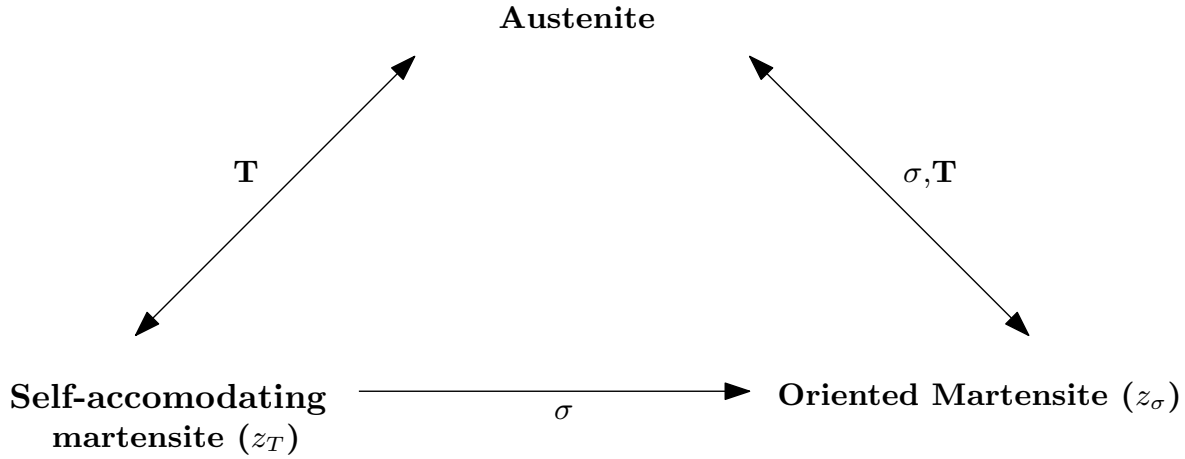


Figure 3.6. Different phases and their relations [16].

they can both exist simultaneously in a sample. It can be said that; in an isothermal mechanical loading, the only type of martensite created is the oriented martensite, whose, the volume fraction is specified as z_σ. In thermal loading, namely cooling, the only type of martensite obtained is the self-accommodating martensite, of which, the volumetric fraction is given as z_T; and in the case of thermomechanical loading, both self-accommodating martensite and oriented martensite can be created and can coexist. Also, the strain is decomposed into two parts as

$$\epsilon = \epsilon^e + \epsilon^{tr} \tag{3.67}$$

where ϵ^e is the elastic strain, and ϵ^{tr} is the transformation strain. Although it is accepted that strain amounts can go up to 8%, small strains assumption is made. In addition to that, thermal dilation is not taken into account since it is negligible compared to the elastic and transformation strains. The only source of transformation strain is seen as the oriented martensite phase. Hence, when named as ϵ_1, ϵ_2, and ϵ_3 for the average strains corresponding respectively to austenite, self-accommodating martensite, and oriented martensite; the relation between transformation strain and the different phases can be given as:

$$\begin{aligned} \epsilon_1^{tr} &= \epsilon_2^{tr} = 0 \\ \epsilon_3^{tr} &= \epsilon^{tr} \end{aligned} \tag{3.68}$$

The following relation establishes the relation between the volume fraction of martensite and the transformation strain:

$$\begin{aligned} \dot{\epsilon}^{tr} &= \kappa \dot{z}_{\sigma} \\ \kappa &= \frac{3}{2}\gamma \frac{\text{dev } \sigma}{\bar{\sigma}} \end{aligned} \tag{3.69}$$

where $\bar{\sigma}$ is the Von Mises equivalent stress and γ is the total pseudoelastic uniaxial strain. For the thermodynamical principles, the method of choosing a potential and combining it with the Clausius-Duhem equation in order to obtain constitutive relations is followed as explained in Chapter 2. The chosen potential energy is the Helmholtz free energy and it is written as a sum of three distinct Helmholtz free energies each one for a different phase multiplied by their respective volume fractions.

$$\psi = (1 - z)\psi^1 + z_T\psi^2 + z_{\sigma}\psi^3 + \Delta\psi \tag{3.70}$$

Where ψ is the term for Helmholtz free energy, z is the total martensite volume fraction, z_T is the self-accommodating martensite volume fraction, z_{σ} is the oriented martensite volume fraction, ψ^{α} are their respective free energies and $\Delta\psi$ is the interaction energy. Also another term exists which is the configurational energy term, which exists in order to account for the interactions between the different phases. From the combination of Clasius-Duhem and the Equation 3.69, two thermodynamic forces are obtained, namely, π^f_{σ} which is the thermodynamic force associated to volumetric oriented martensite fraction and π^f_T which is the thermodynamic force associated to volumetric self-accommodating martensite fraction.

3.6. Auricchio *et al.*

Auricchio and Sacco, in 1997, published an article on a 1D model able to simulate the superelastic behavior of shape memory alloys [41]. In order to obtain this model, the scalar internal variable martensite fraction is utilized and for martensite fraction, evolutionary equations in rate form are proposed. For the evolution of elastic modulus,

E, different methodologies are proposed and compared. These are; Voigt scheme;

$$E = zE_M + (1-z)E_A \tag{3.71}$$

where z is the martensite fraction and, E_M and E_A are martensitic and austenitic elastic moduli respectively. Reuss scheme;

$$E = \frac{E_A}{1 + \left(\frac{E_A}{E_M} - 1\right)z} \tag{3.72}$$

where z is the martensite fraction and, E_M and E_A are martensitic and austenitic elastic moduli respectively. and Mori-Tanaka scheme with elliptical or spherical inclusions;

$$E = \frac{E_A E_M}{2}\left[\frac{(1-z) + z\,A^{MA}}{E_M(1-z) + z\,A^{MA}E_A} + \frac{(1-z)A^{AM} + z}{E_M(1-z)A^{AM} + z\,E_A}\right] \tag{3.73}$$

where z is the martensite fraction and, E_M and E_A are martensitic and austenitic elastic moduli respectively, and A^{MA} and A^{AM} are;

$$A^{MA} = \frac{E_M}{E_A + p(E_M - E_A)}, \quad A^{AM} = \frac{E_A}{E_M + p(E_A - E_M)} \tag{3.74}$$

where z is the martensite fraction and, E_M and E_A are martensitic and austenitic elastic moduli respectively, and p is the geometry factor of the inclusion. If the inclusion is spherical, p is given as;

$$p = \frac{(4-5\nu)}{15(1-\nu)} \tag{3.75}$$

where ν is the Poisson ratio. If the inclusion is elliptical, then p is 1/2. Uniting those four cases in an Elastic Modulus vs. Volume fraction of martensite graph; the trends resulting from each of these schemes can be seen in Figure 3.7. From this point on, Reuss and Mori-Tanaka schemes are chosen, since experimentally Reuss scheme is the most valid and since Mori-Tanaka scheme represents a feasible upper bound.

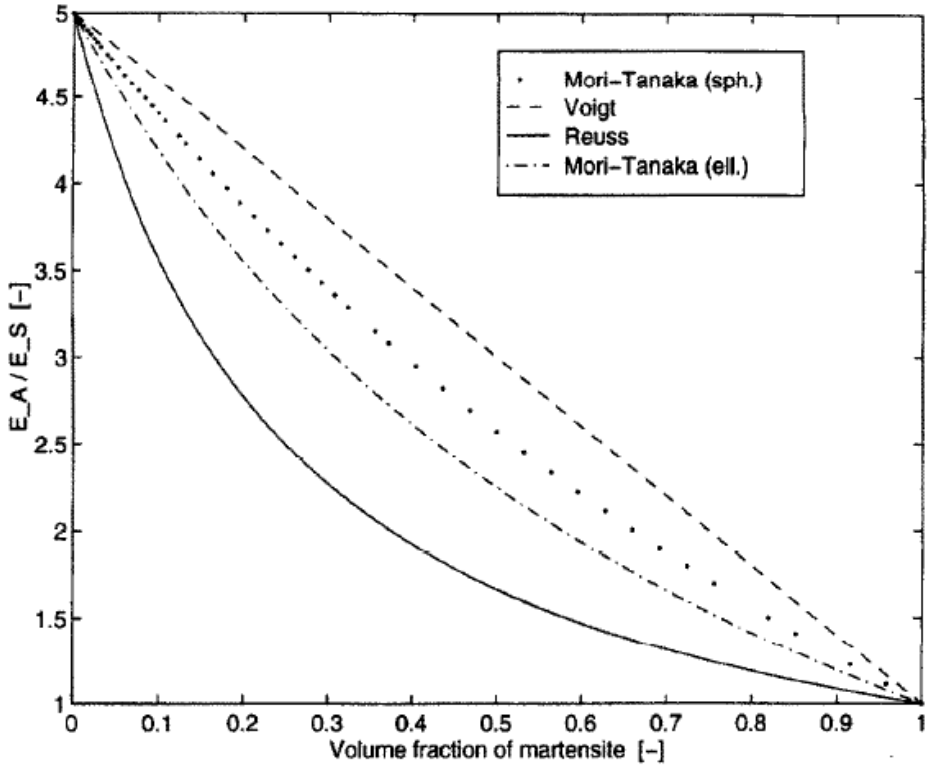


Figure 3.7. Comparison of different schemes for the evolution of elastic modulus [41].

In proceeding from elastic moduli, in order to devise uniaxial stress-strain behavior, 1D plasticity methods are employed. Results obtained from 1D uniaxial tension test using Ni-Ti properties given in the paper and MATLAB can be seen in Figure 3.8.

Auricchio *et al.*'s two other studies (1997) are [42, 43] also very important in the constitutive modeling of SMAs. The constitutive models resulting from these studies are the ones directly implemented into ABAQUS as Auricchio's model. For the conversion of austenite into martensite, in this work, following loading function form is assumed:

$$F^{AM} = \sqrt{K_{ij}^{dev} K_{ij}^{dev}} + 3\alpha_p p - C^{AM} T \tag{3.76}$$

where, K^{dev} is the deviatoric second Piola-Kirchoff stress, α_p is a material parameter called pressure sensitivity, p is the pressure, C^{AM} is a material parameter called stress temperature coefficient, and T is the temperature. This loading function is a function

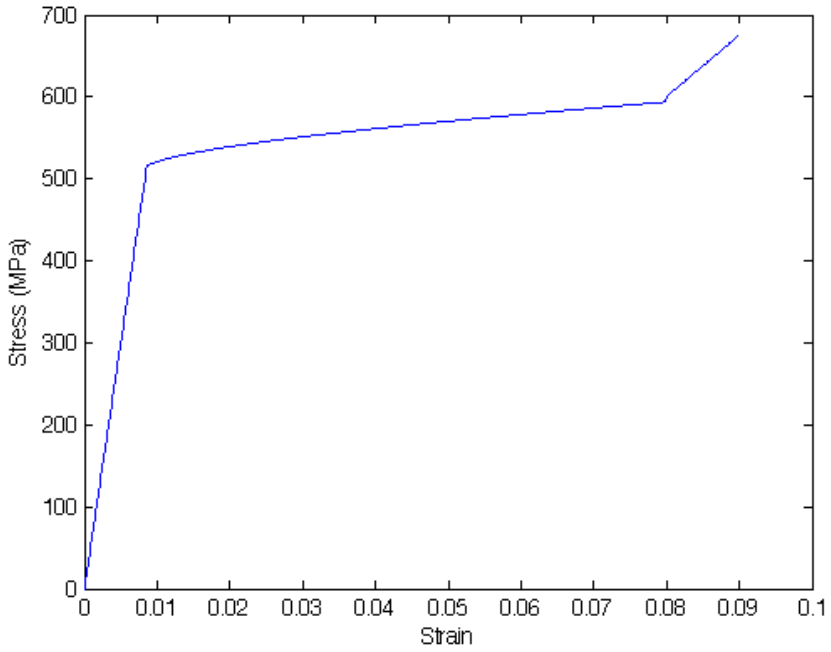


Figure 3.8. 1D Uniaxial Tension Test.

of the following transformation functions:

$$F_s^{AM} = F^{AM} - R_s^{AM} \tag{3.77}$$

$$F_f^{AM} = F^{AM} - R_f^{AM} \tag{3.78}$$

where, R_s^{AM}, and, R_f^{AM} are:

$$R_s^{AM} = \left[\sigma_{Ms}\left(\sqrt{\frac{2}{3}} + \alpha_p\right)\right] - C^{AM} M_s$$

$$R_f^{AM} = \left[\sigma_{Mf}\left(\sqrt{\frac{2}{3}} + \alpha_p\right)\right] - C^{AM} M_f$$

where, σ_{Ms} and σ_{Mf} are material parameters called martensite start stress and martensite finish stress respectively, and M_s, and M_f are material parameters called martensite start temperature and martensite finish temperature respectively.

With these transformation and loading functions at hand, the conditions for forward

transformation (transformation from austenite to martensite) are as follows:

$$F_s^{AM} > 0, \qquad F_f^{AM} < 0, \qquad \dot{F}^{AM} > 0 \tag{3.79}$$

For the martensite fraction under forward transformation, the relation is given in rate form as:

$$\dot{z} = H^{AM}\beta^{AM}(1-z)\frac{\dot{F}^{MA}}{(\dot{F}_f^{MA})^2} \tag{3.80}$$

where β^{AM} is a material parameter, and H^{AM} is given as:

$$H^{AM} = \begin{cases} 1 & \text{if } F_s^{AM} > 0,\ F_f^{AM} < 0,\ \dot{F}^{AM} > 0 \\ 0 & \text{otherwise} \end{cases} \tag{3.81}$$

For the conversion of martensite into austenite (reverse transformation), following loading function form is assumed:

$$F^{MA} = \sqrt{K_{ij}^{dev}K_{ij}^{dev}} + 3\alpha p - C^{MA}T \tag{3.82}$$

where this loading function is a function of the following transformation functions:

$$F_s^{MA} = F^{MA} - R_s^{MA} \tag{3.83}$$

$$F_f^{MA} = F^{MA} - R_f^{MA} \tag{3.84}$$

with R_s^{MA} and R_f^{MA}:

$$R_s^{MA} = \left[\sigma_{As}\left(\sqrt{\frac{2}{3}} + \alpha_p\right)\right] - C^{MA}A_s \tag{3.85}$$

$$R_f^{MA} = \left[\sigma_{Af}\left(\sqrt{\frac{2}{3}} + \alpha_p\right)\right] - C^{MA}A_f \tag{3.86}$$

where, σ_{As} and σ_{Af} are material parameters called austenite start stress and austenite

finish stress respectively, and A_s, and A_f are material parameters called austenite start temperature and austenite finish temperature respectively.

With these transformation and loading functions at hand, the conditions for reverse transformation to occur are as follows:

$$F_s^{MA} < 0, \qquad F_f^{MA} > 0, \qquad \dot{F}^{MA} < 0 \tag{3.87}$$

For the martensite fraction under reverse transformation, the relation is given in rate form as:

$$\dot{z} = H^{MA}\beta^{MA} z \frac{\dot{F}^{MA}}{(\dot{F}_f^{MA})^2} \tag{3.88}$$

where β^{MA} is a material parameter, and H^{MA} is given as:

$$H^{MA} = \begin{cases} 1 & \text{if } F_s^{MA} < 0,\ F_f^{MA} > 0,\ \dot{F}^{MA} < 0 \\ 0 & \text{otherwise} \end{cases} \tag{3.89}$$

4. COMPUTATIONAL ANALYSIS OF EDGE CRACKED SMA SPECIMEN

In literature, although there are extensive studies on uniaxial and multiaxial tests of uncracked specimens; in general, fracture behavior of SMA's has not been studied as much. In this work, Mode-I and Mixed-Mode fracture of an edge cracked SMA specimen is studied. In Table 4.1, material properties, taken from Lagoudas [73, 74], and, from Qidwai and Lagoudas [68], are tabulated.

Table 4.1. Nitinol properties.

Property	Value	Property	Value
E_A (GPa)	55	E_M (GPa)	46
ν_A	0.33	ν_M	0.33
ϵ_L	0.056	$(\partial\sigma/\partial T)_L$ (MPa/K)	7.4
$(\partial\sigma/\partial T)_U$ (MPa/K)	7.4	σ_{Ms} (MPa)	380
σ_{Mf} (MPa)	460	σ_{As} (MPa)	190
σ_{Af} (MPa)	120	T_0 (°C)	25
ϵ_L^V	0.056	α_A (K^{-1})	22×10^{-6}
α_M (K^{-1})	22×10^{-6}	M_s (°C)	-28
M_f (°C)	-43	A_s (°C)	-3
A_f (°C)	7	$\rho\Delta s^A$ (MPa/K)	-0.35
$\rho\Delta s^M$ (MPa/K)	-0.35		

The geometry of the edge-cracked specimen under Mode-I loading is shown in Figure 4.1. In finite element analysis, because symmetry boundary conditions are employed, only half of the original geometry is simulated. The model used in finite elements is shown in Figure 4.2. The edge-cracked specimen under mixed-mode loading is given in Figure 4.3.

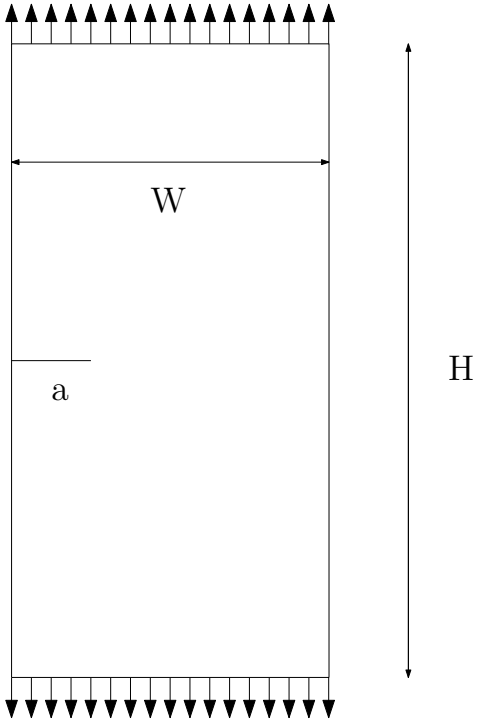


Figure 4.1. Mode-I loaded edge-cracked specimen (W = 100 mm, H = 200 mm, a = 25 mm).

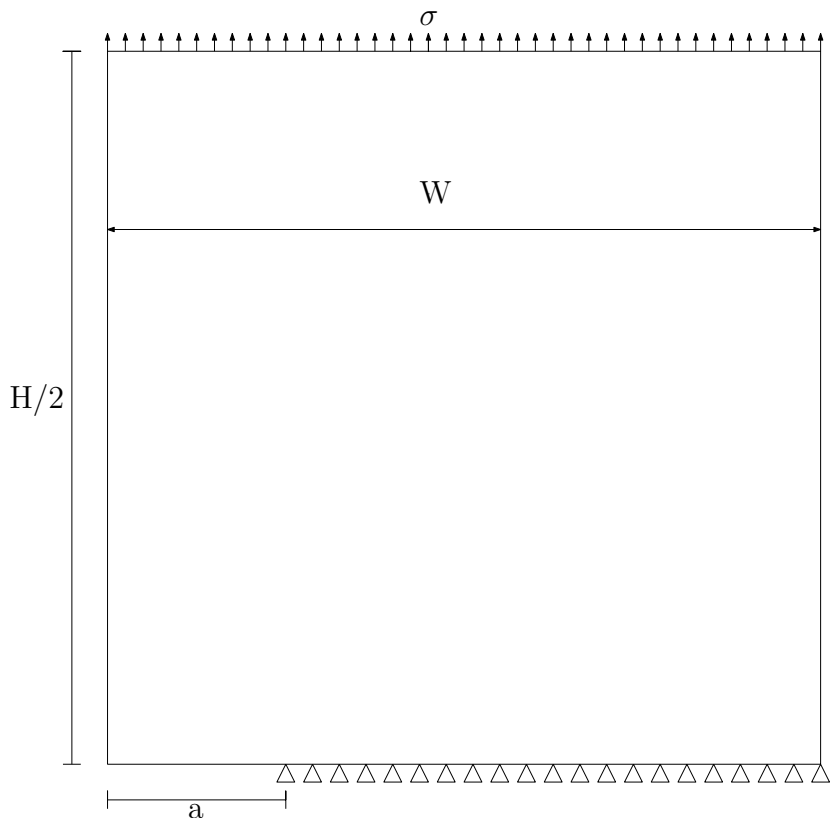


Figure 4.2. Symmetry simplification of edge-cracked specimen.

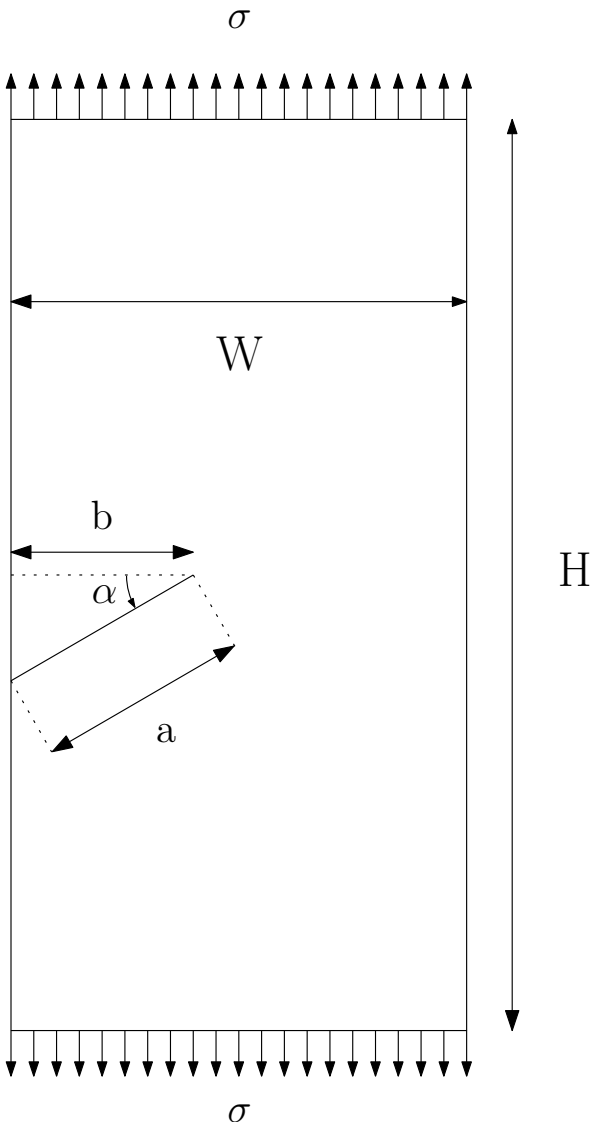


Figure 4.3. Mixed-mode loaded specimen (W = 100 mm, H = 200 mm, a = 46.2 mm, b = 40 mm, $\alpha = 30^{\circ}$).

The details of the mesh used is given in Figure 4.4. Around the crack tip mesh is refined to 1/64th of the coarsest mesh size in the model.

Abaqus has its own SMA model built in and it can be used directly [75]. For a different model, Abaqus' UMAT interface is used to implement Lagoudas' UMAT model [72,76]. Lagoudas' scheme is modified using three different phase transformation models. Namely, Tanaka's [10, 11], Liang and Rogers' [12, 13, 63], and, Boyd and Lagoudas' [3, 14, 15] phase transformation models. As explained in Chapters 2 and 3,

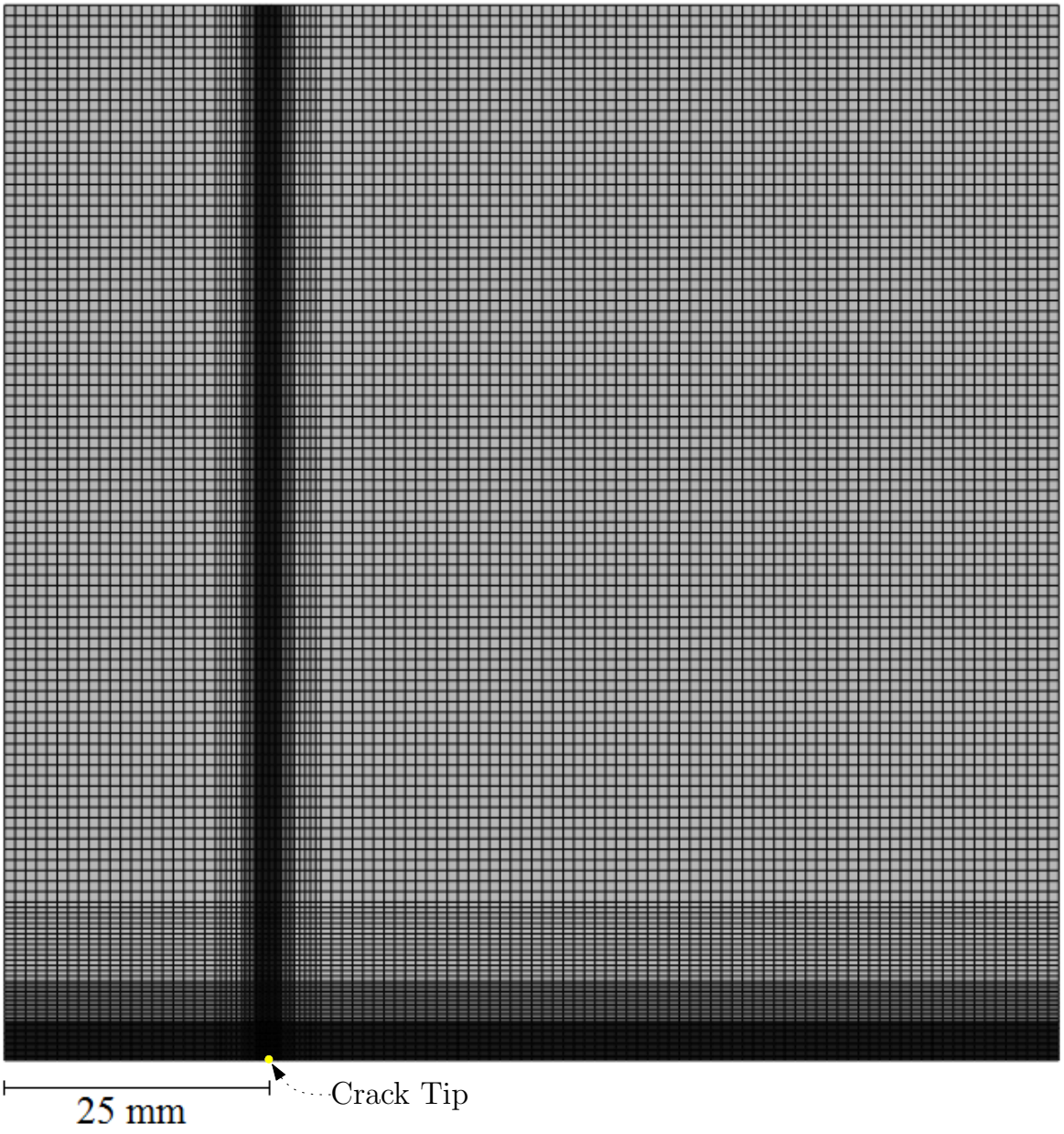


Figure 4.4. Mesh configuration of the edge-cracked specimen with the crack 25mm away from the edge.

these models share a common thermodynamic approach with different transformation models.

For Mode-I crack, four different crack sizes and three different loadings are applied. Hence, a total of 12 cases are modeled, and with 4 different constitutive models, a total of 48 different cases are studied.

Before starting to compare and study the results of different loading conditions, in order to have a better visualization of the models run, a uniaxial test has been done to show their loading-unloading behavior. The resulting stress-strain diagram with a uniaxial stress of 800 MPa is shown in Figure 4.5. As already mentioned previously, these models have different phase transformation models, affecting the characteristic of the martensitic fraction evolution during phase transformation. Auricchio's model, that uses an exponential behavior, stays at higher stresses during transformation and from this, it can be inferred that, for the same stress levels, there will be less transformation strain in Auricchio's model, resulting in lesser martensite presence in transformation zones, and, resulting in a smaller martensite zone. Likewise, Tanaka's model has also exponential character, but with the current parameters, it is the lower boundary in the stress-strain curve. Hence, martensite fraction in Tanaka's model results may be expected to be higher compared to the others. One other thing to note is the transition of stress-strain curves between Lagoudas' and Liang & Rogers' models. This is resulting from the fact that, Lagoudas' results in a straight transformation curve, while Liang & Rogers' model's hardening function is cosine, and it results in a wave-like shape, first having higher stress values at the same strain compared to Lagoudas, than after the midpoint of transformation, having lower stress values at the same strains compared to Lagoudas. Thus, while very close, it can be expected that fully transformed martensitic zone will be slightly bigger for Liang & Rogers' model. But, for transformation zones, where martensite and austenite is mixed, it will be slightly bigger for Lagoudas' model.

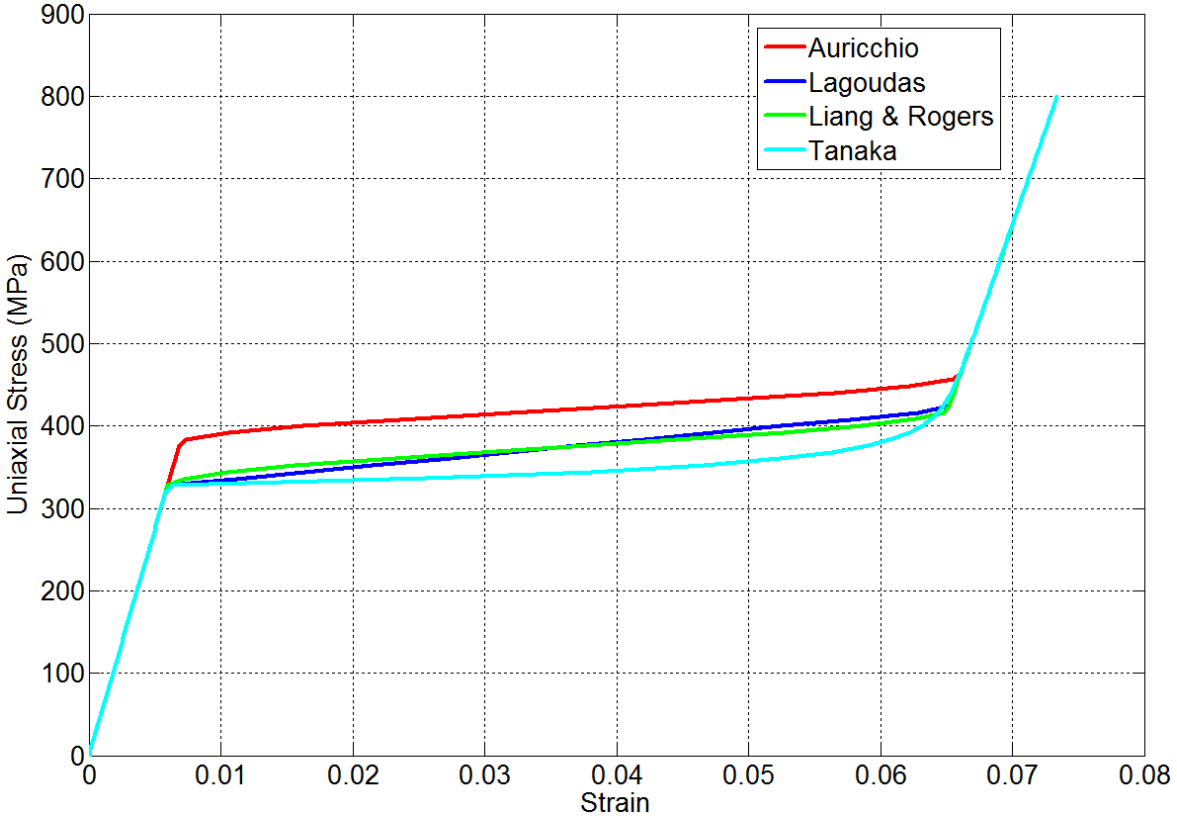


Figure 4.5. Comparison of uniaxial stress vs. strain diagrams of four different constitutive models used.

In the rest of the results part, the distribution of σ_{yy} under Mode-I loading are studied in detail and, the plots obtained using different models are compared. Martensite fraction distributions for both mode-I and mixed-mode loadings are plotted and compared. For a better comparison of differences of the two cases, a Mode-I loading case and a Mixed-Mode loading case with same loading and same crack-tip distance away from the edge are superposed on the same contour plot and the resulting martensite fraction zones are compared.

4.1. Stress Distributions for Mode-I Loading

In this section, σ_{yy}, along $y = 0$ line, with respect to the distance from the crack tip, are calculated. For the case where a/W = 0.25 and the applied load, $\sigma =$ 100 MPa, results are plotted in Figure 4.6. Details of Figure 4.6 are given in Figure 4.7a and 4.7b. In Figure 4.6, 4.7a, and 4.7b, it can clearly be seen that Auricchio's

and Tanaka's constitutive models [10, 11, 41–43] are the stress limits. Both of these models use exponential transformation rules. On the other hand, while Tanaka derives his model from thermodynamical foundations similar to Lagoudas, and Liang and Rogers, Auricchio's model is phase diagram based on micromechanical foundations as explained in Section 3.6. Since Tanaka's and Auriccho's are the limiting cases, for the same geometry a/W = 0.25 and same UMAT models, different loading schemes are applied to see the affect of loading on stress distribution in y-direction. Results from Auricchio's model with a/W = 0.25 can be seen in Figure 4.8. Results from Tanaka's model, also with a/W = 0.25 can be seen in Figure 4.9. A similar scheme, when applied to a crack with a/W = 0.35, yields the results seen in Figure 4.10.

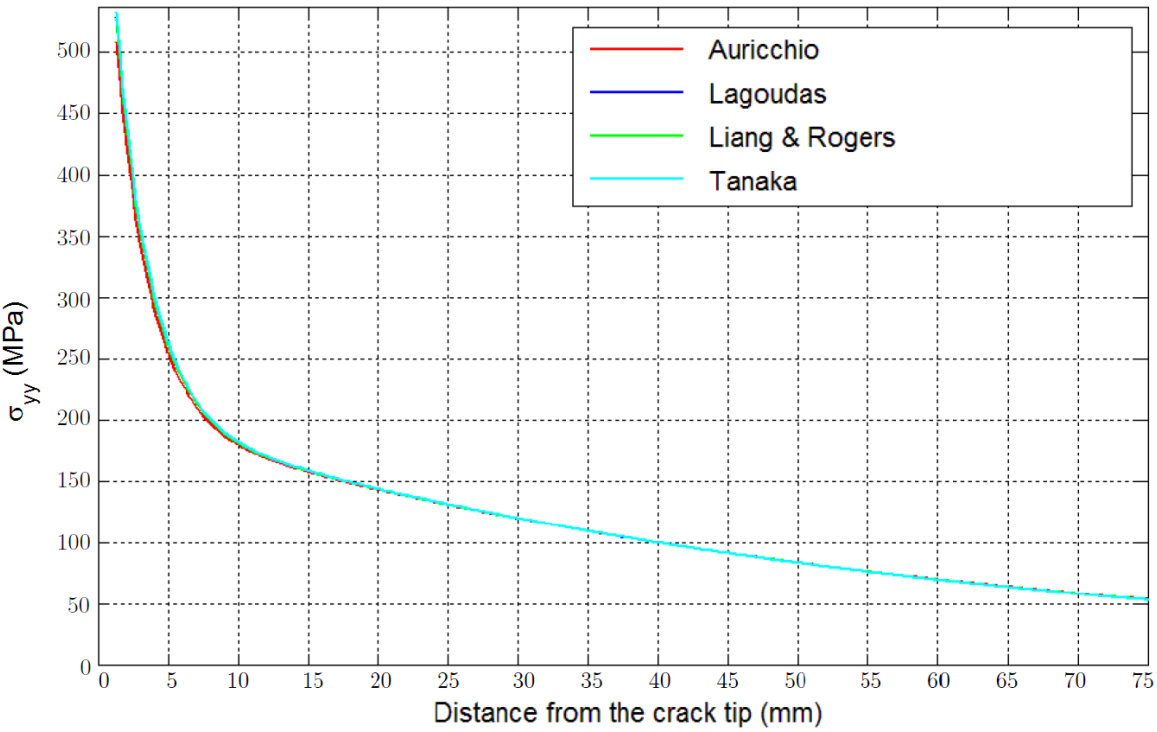
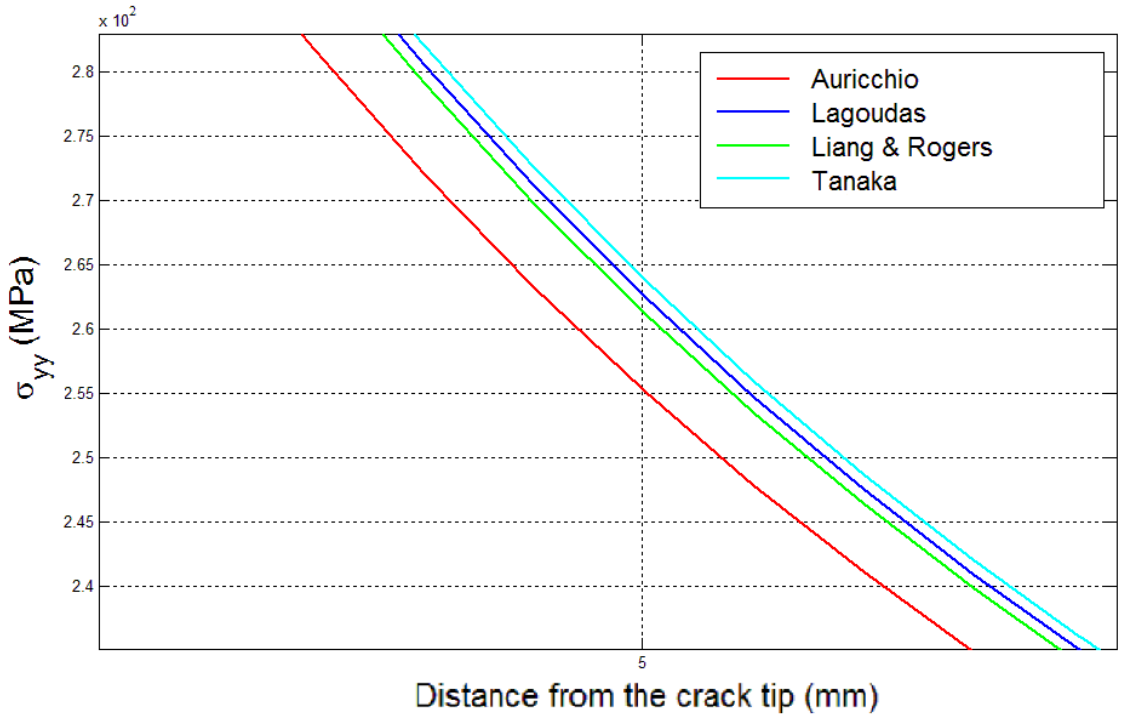
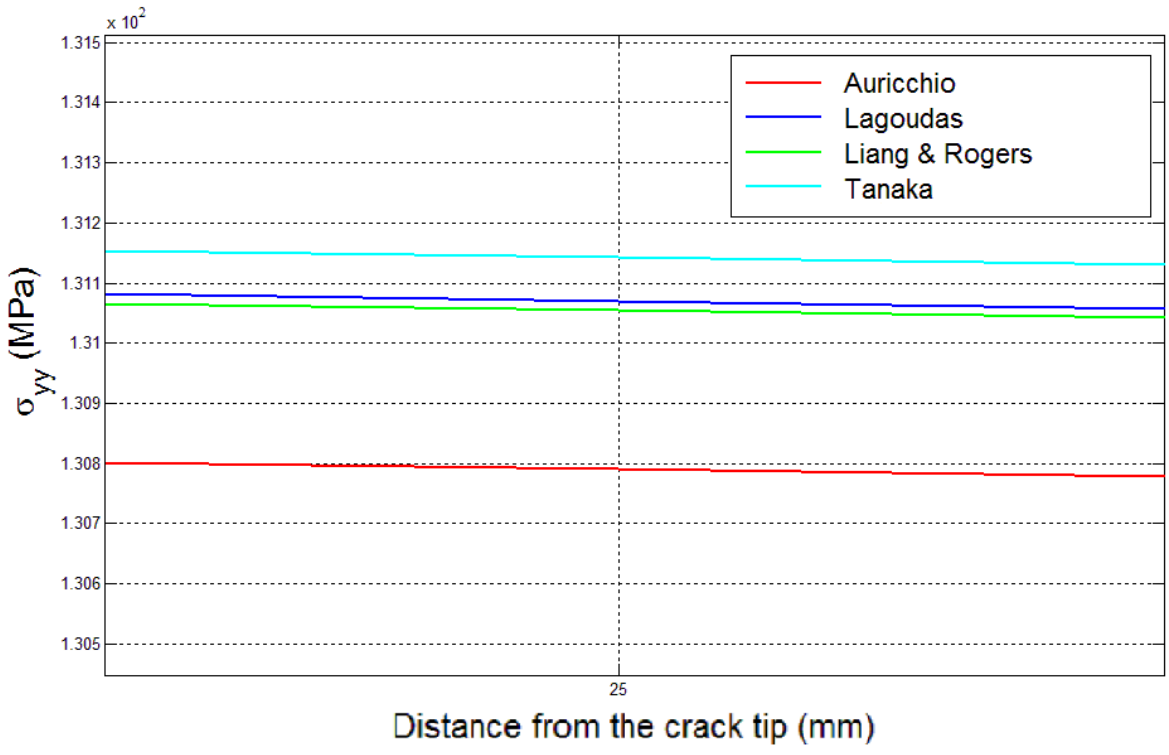


Figure 4.6. σ_{yy} vs. distance from crack tip, a/W = 0.25, σ = 100 MPa.



(a) Details of Figure 4.6 about 5 mm away from the crack.



(b) Details of Figure 4.6 about 25 mm away from the crack.

Figure 4.7. σ_{yy} vs. distance from crack tip, a/W = 0.25 and σ = 100 MPa with close-ups at about (a) 5 mm (b) 25 mm away from the crack.

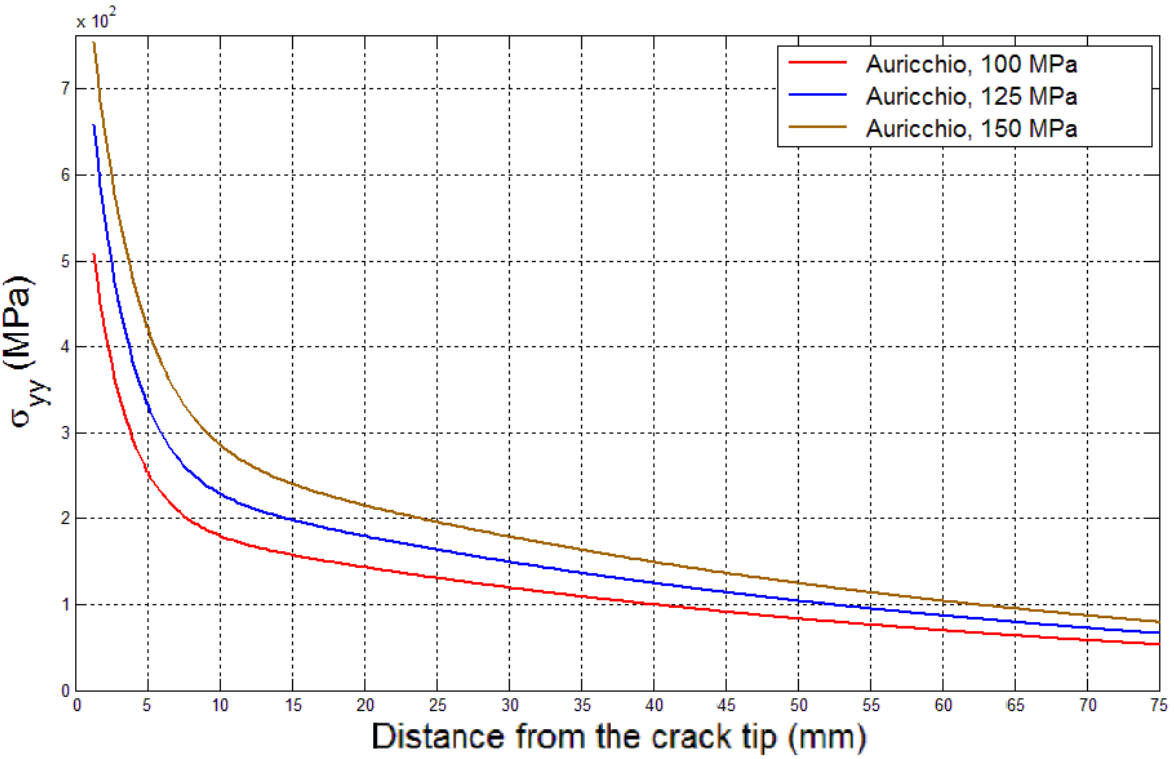


Figure 4.8. σ_{yy} vs. distance from crack tip for different applied loads, σ, using Auricchio's model.

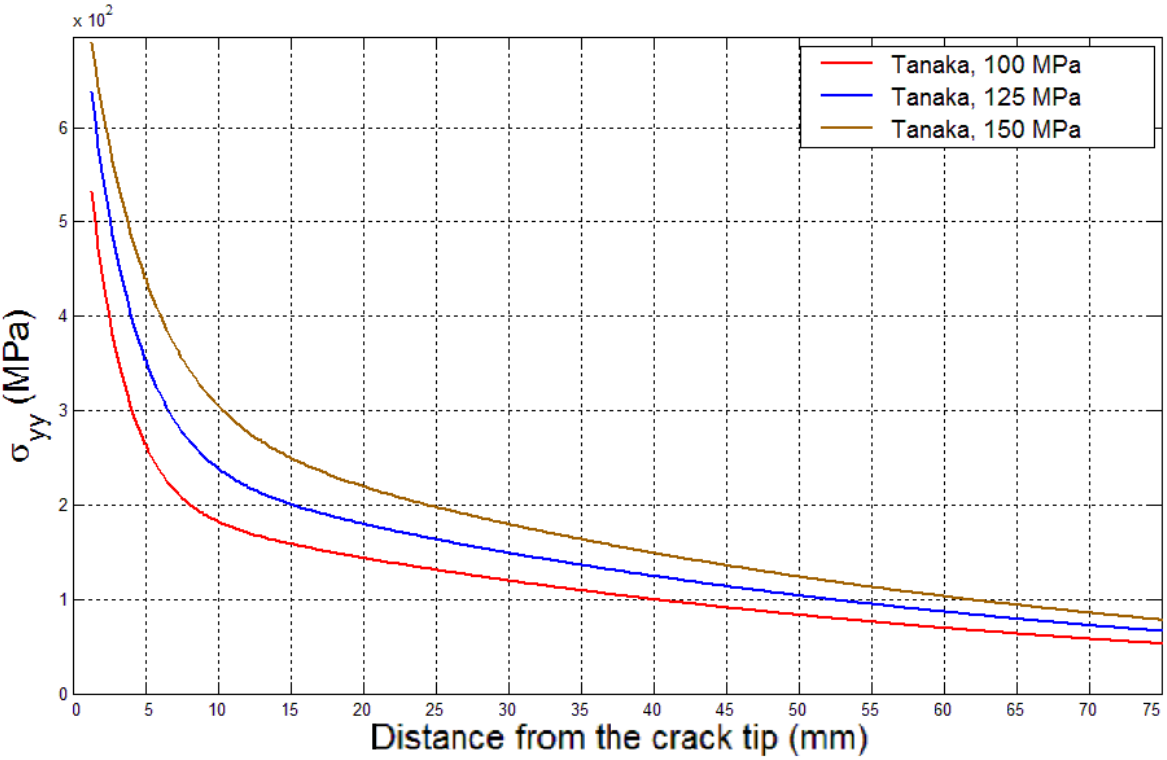


Figure 4.9. σ_{yy} vs. distance from crack tip for different applied loads, σ, using Tanaka's model.

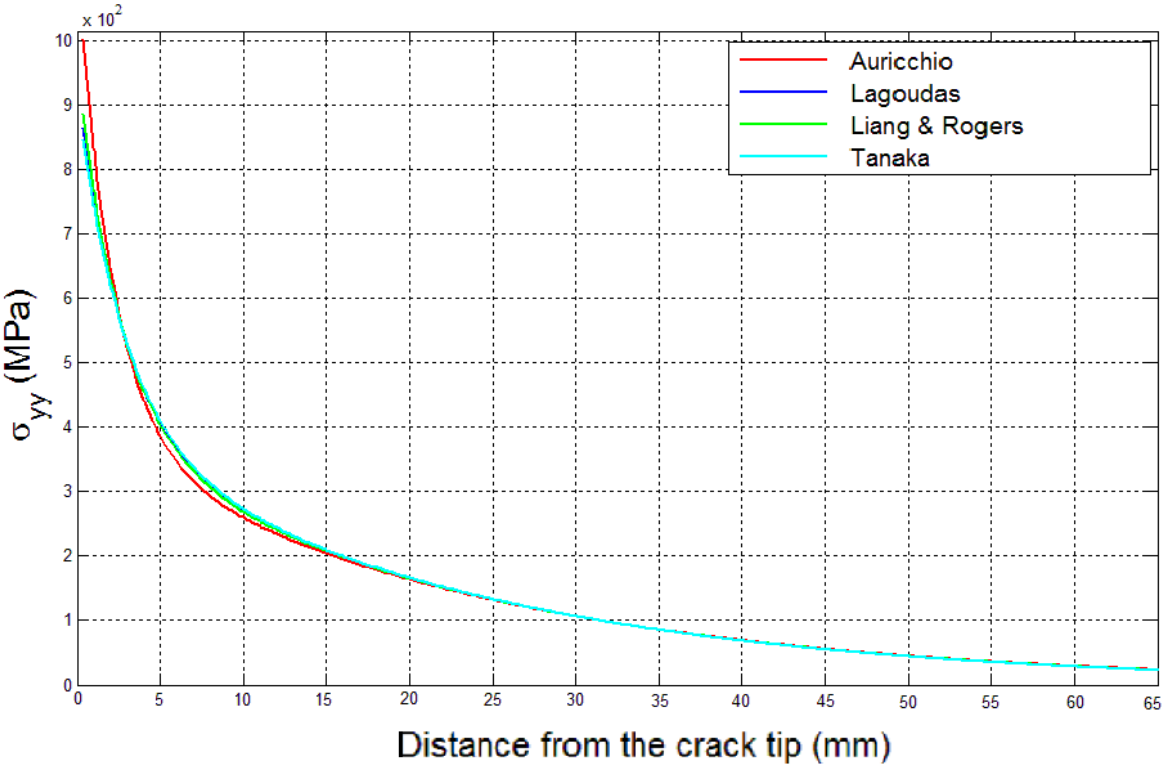


Figure 4.10. σ_{yy} vs. distance from crack tip, a/W = 0.35 and σ = 100 MPa.

4.2. Mode-I Crack Martensite Fraction

Martensite fraction is an important parameter to study in the case of fracture behavior of shape memory alloys. Because properties of the material change with the change of phase, the distribution of phases especially around the crack tip is very important. Throughout this work, when a single case is presented in a figure, to describe the martensite fraction in a particular zone of the specimen, three different colors are used. For fully austenitic zone (more than 99% austenitic), the color used is blue, for the fully martensitic zone (more than 99% martensitic) the color used is red, and, for the zones in between the two, which is also described as the transformation zone, the color used is green. In Figure 4.11 where transformation zones are plotted, Auricchio's model is used. In Figure 4.12 similar results are plotted using Tanaka's model. Also, when multiple cases are presented, to describe the zones clearly, contour lines are used. Similar to the approach used in single case figures, for contour lines separating fully austenitic and transformation zones, the color used is blue, and for contour lines separating fully martensitic and transformation zones, the color used

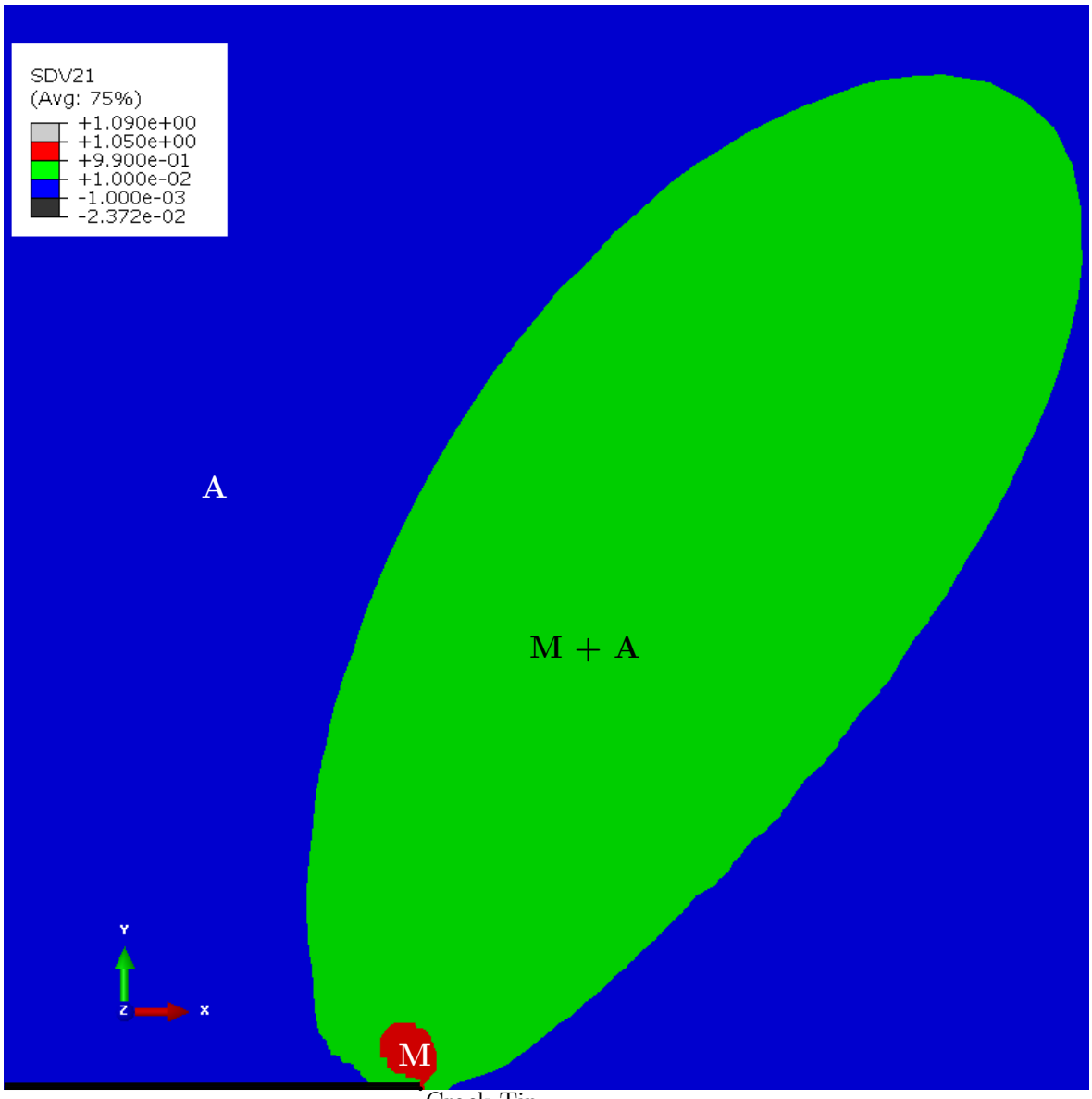


Figure 4.11. Martensite fraction distribution, a/W = 0.4 and σ = 150 MPa Auricchio's model used (M signifying the fully martensitic zone, M+A signifying the transformation zone, A signifying the fully austenitic zones).

is red. Different models' results are plotted in Figure 4.13-16. Following a similar approach used in Section 4.1, to see the effect of loading, Figure 4.17 and 4.18 are plotted.

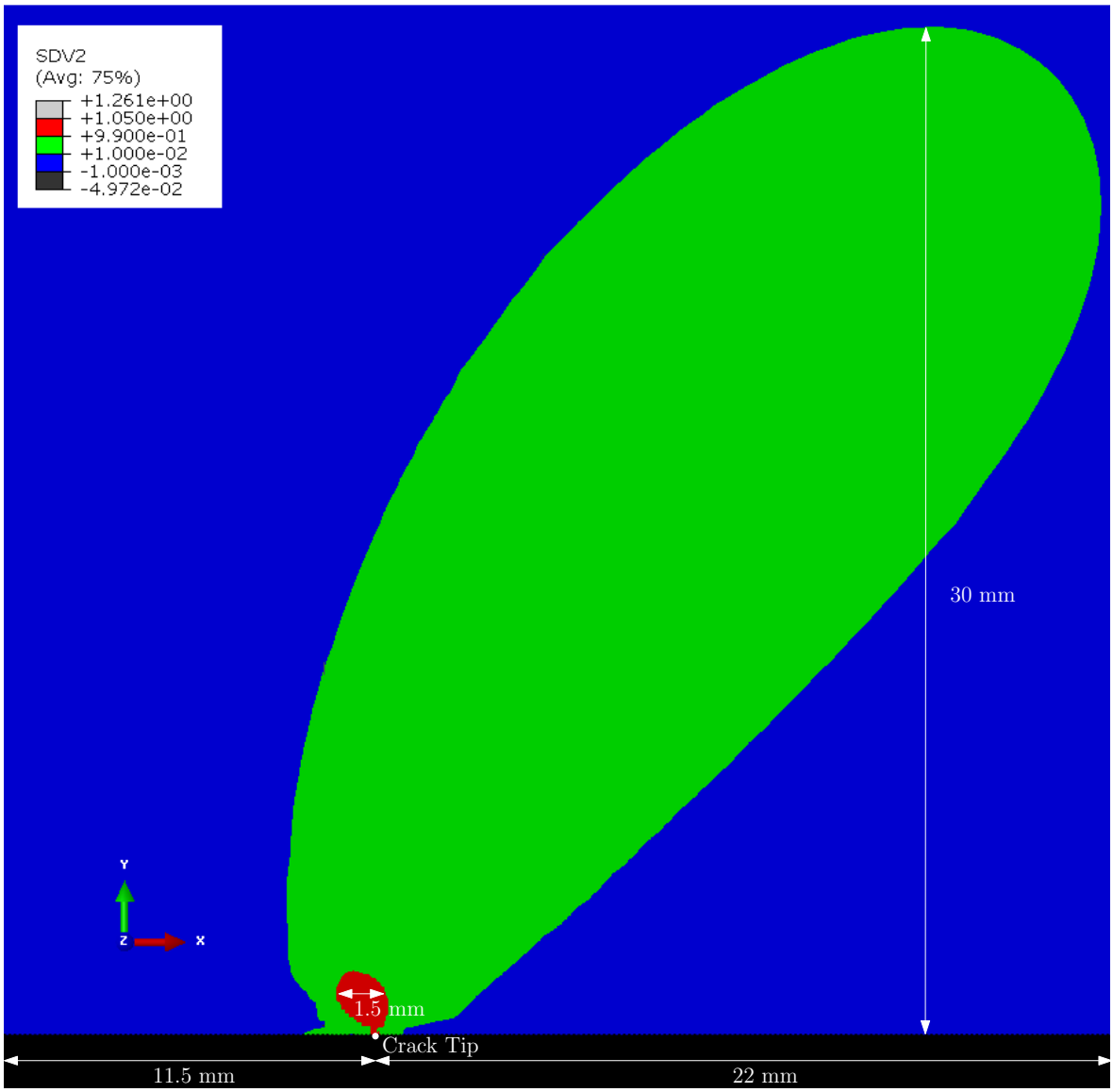


Figure 4.12. Martensite fraction distribution of specimen with a/W = 0.4 and σ = 150 MPa using Tanaka's model.

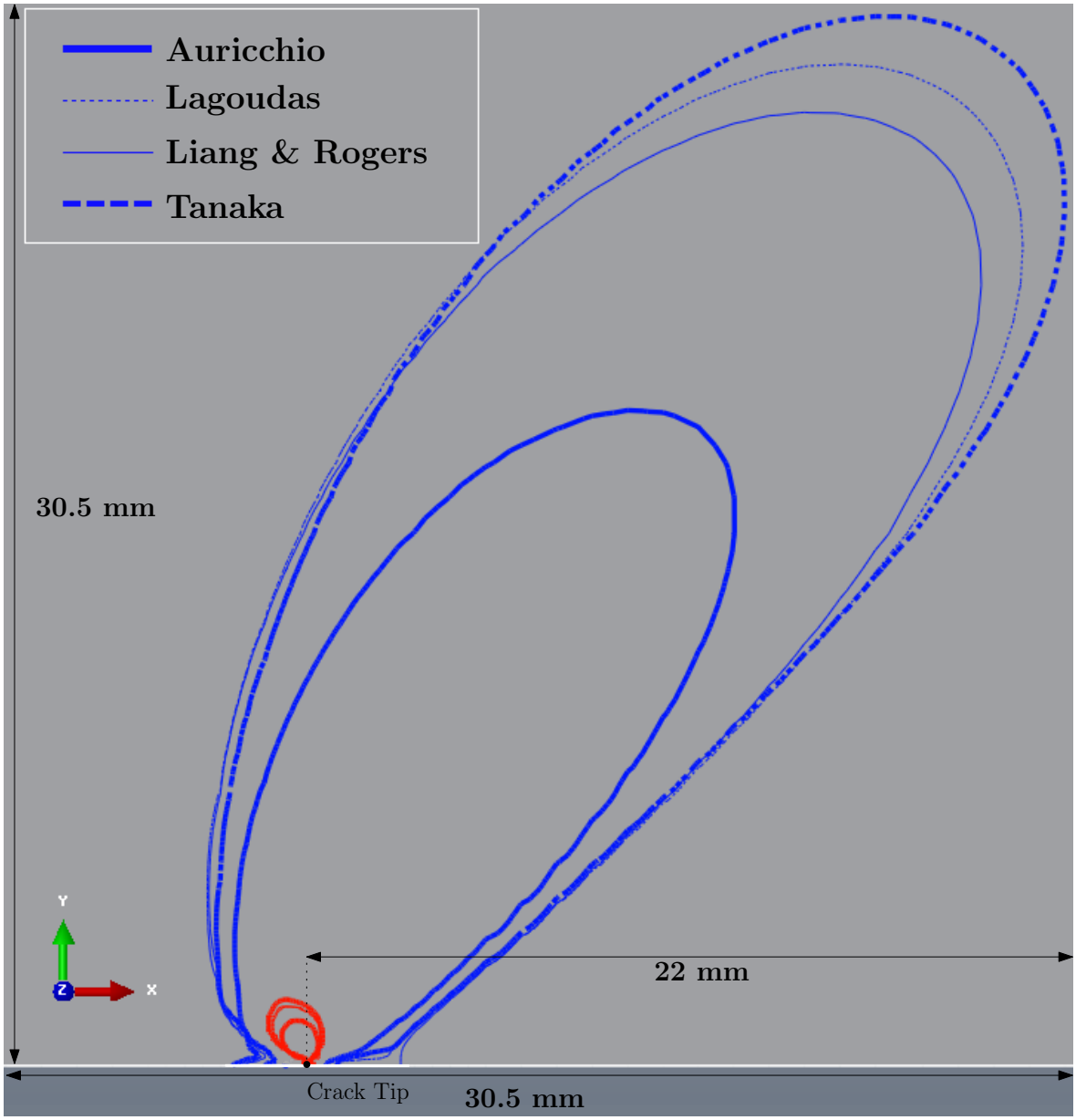


Figure 4.13. Martensite fraction contours obtained using four different models, a/W = 0.4 and σ =150 MPa (Fully martensite inside the red contours, fully austenite outside the blue contours).

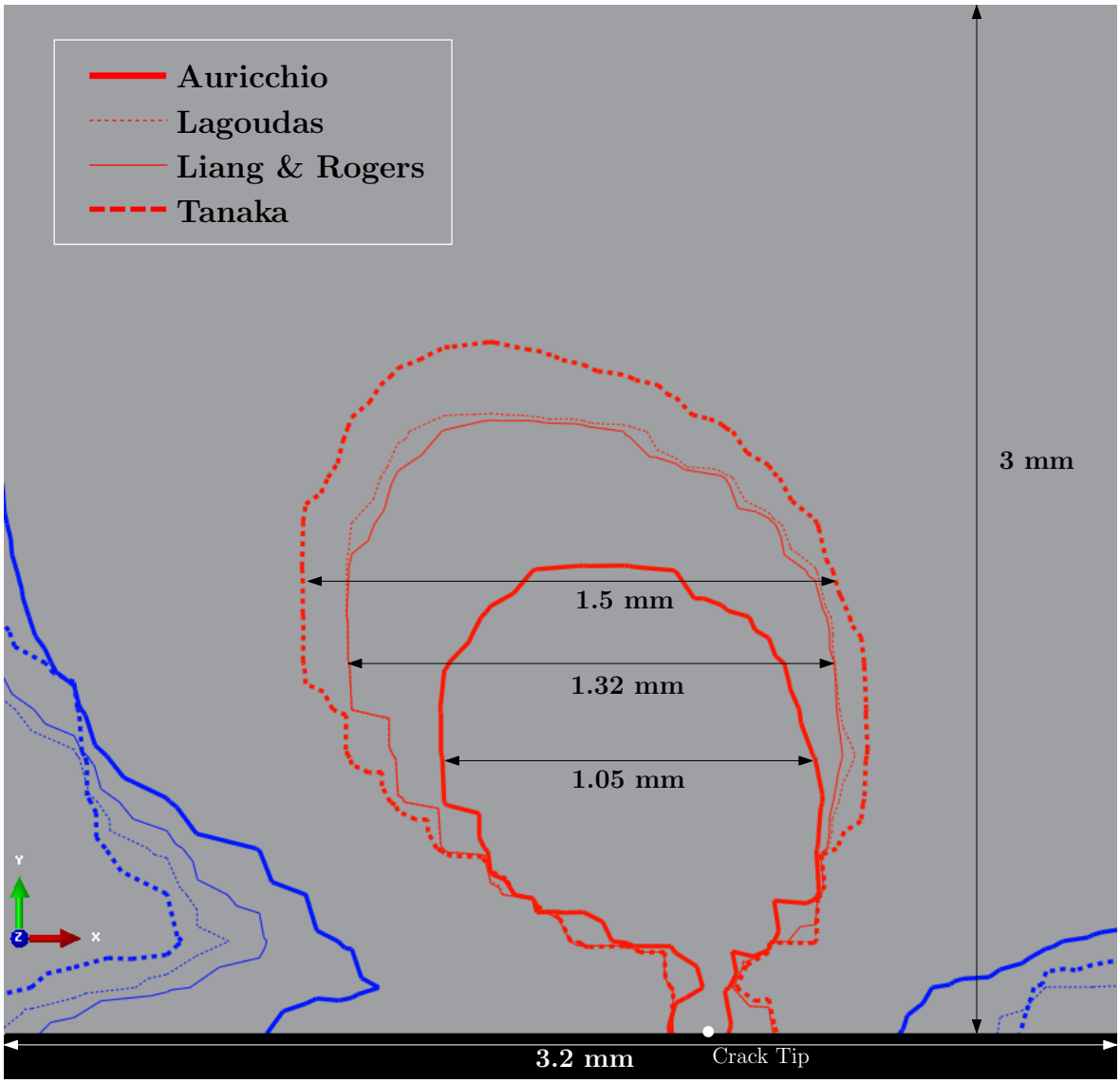


Figure 4.14. Close-up of martensite fraction contours for four different models shown in Figure 4.13 (Fully martensite inside the red contours).

Table 4.2. Comparison of approximate martensite areas, a/W = 0.4.

Model	σ_{yy}	Martensite Area
Auricchio	100 MPa	0.04688 mm^2
Liang & Rogers	100 MPa	0.09375 mm^2
Lagoudas	100 MPa	0.08594 mm^2
Tanaka	100 MPa	0.10938 mm^2
Auricchio	125 MPa	0.28125 mm^2
Liang & Rogers	125 MPa	0.45313 mm^2
Lagoudas	125 MPa	0.42188 mm^2
Tanaka	125 MPa	0.59375 mm^2
Auricchio	150 MPa	0.84375 mm^2
Liang & Rogers	150 MPa	1.57813 mm^2
Lagoudas	150 MPa	1.48438 mm^2
Tanaka	150 MPa	1.85938 mm^2

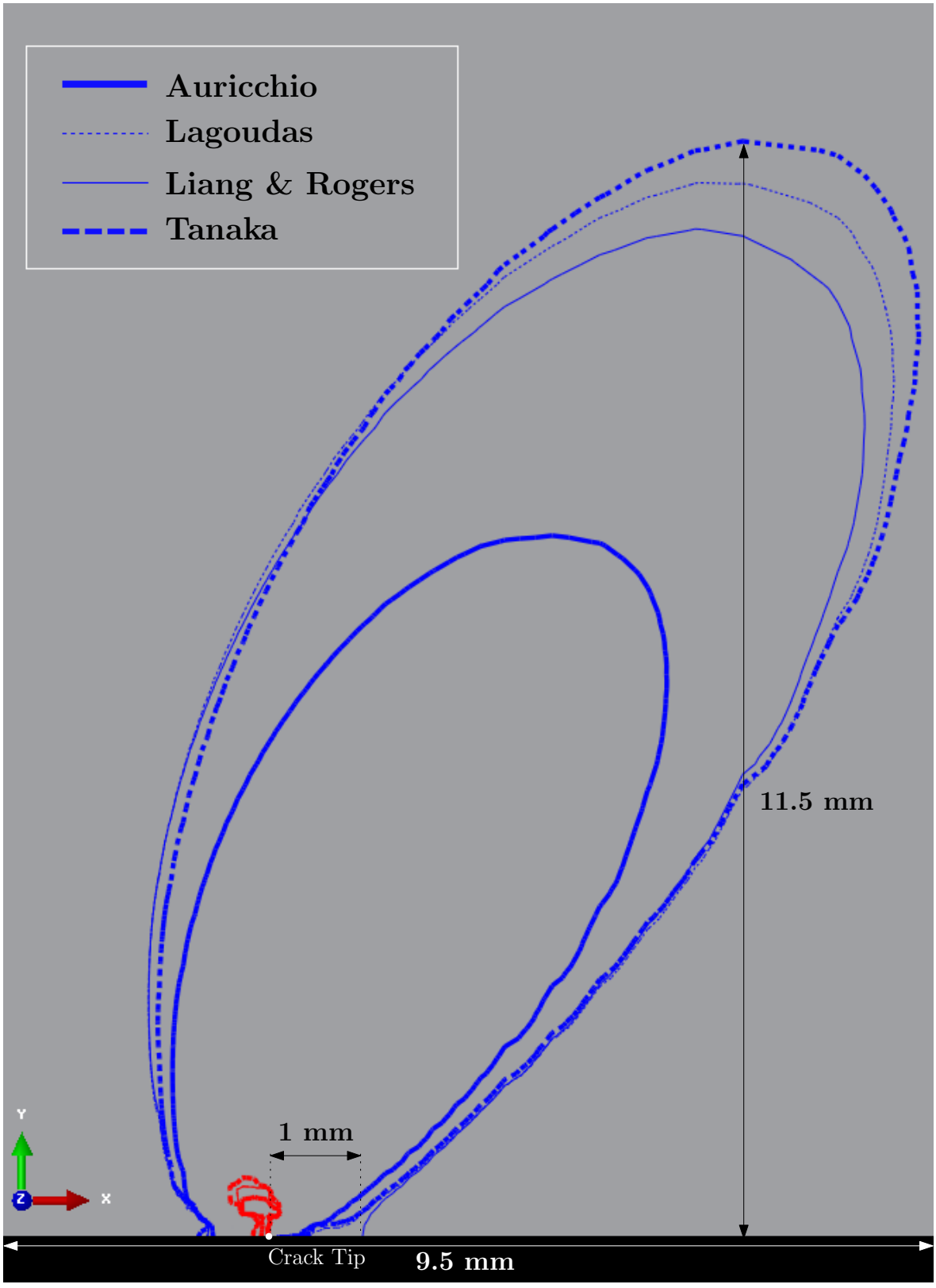


Figure 4.15. Martensite fraction contours of four different models, a/W = 0.35 and σ = 125 MPa (Fully martensite inside the red contours, fully austenite outside the blue contours).

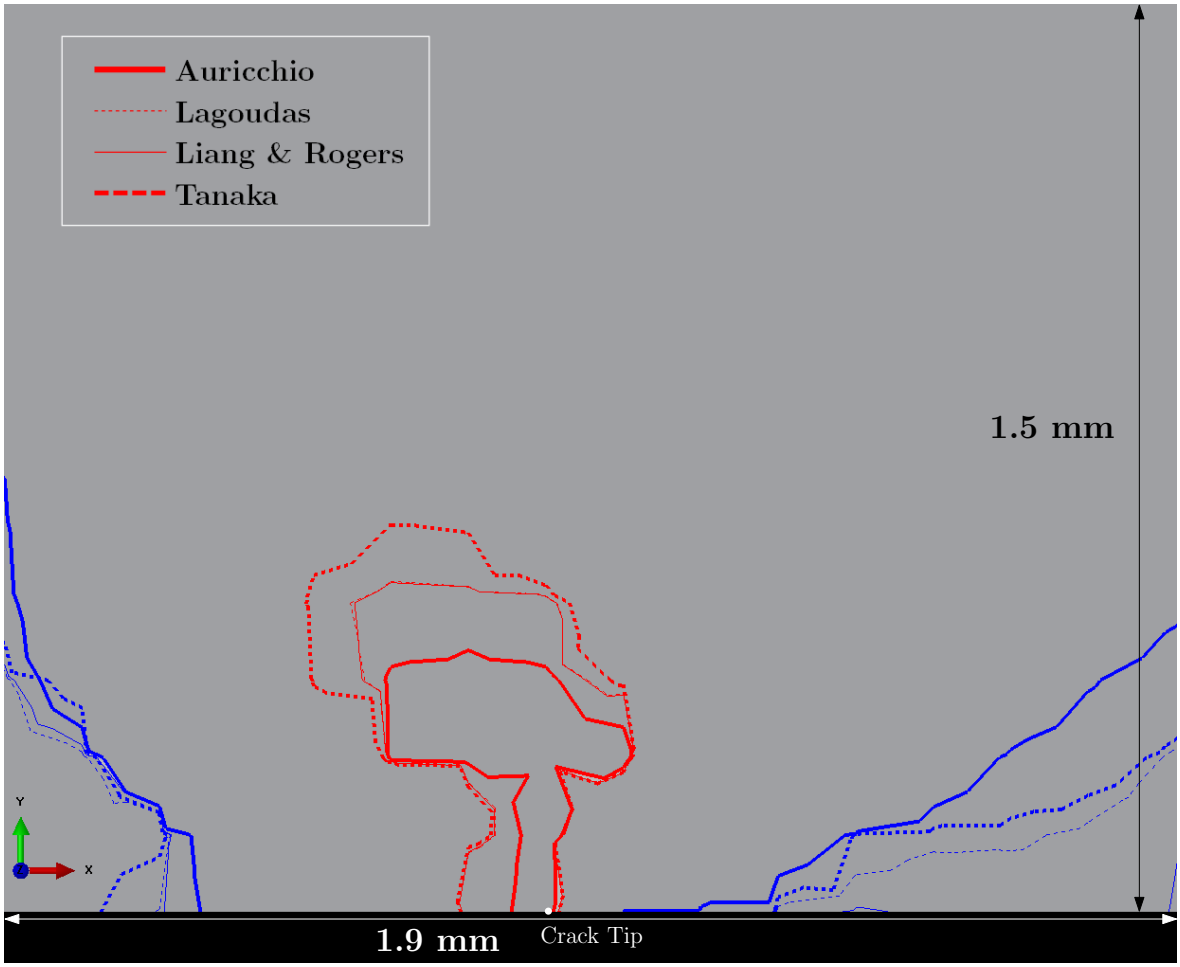


Figure 4.16. Close-up of superimposed martensite fraction contours for four different models shown in Figure 4.15 (Fully martensite inside the red contours).

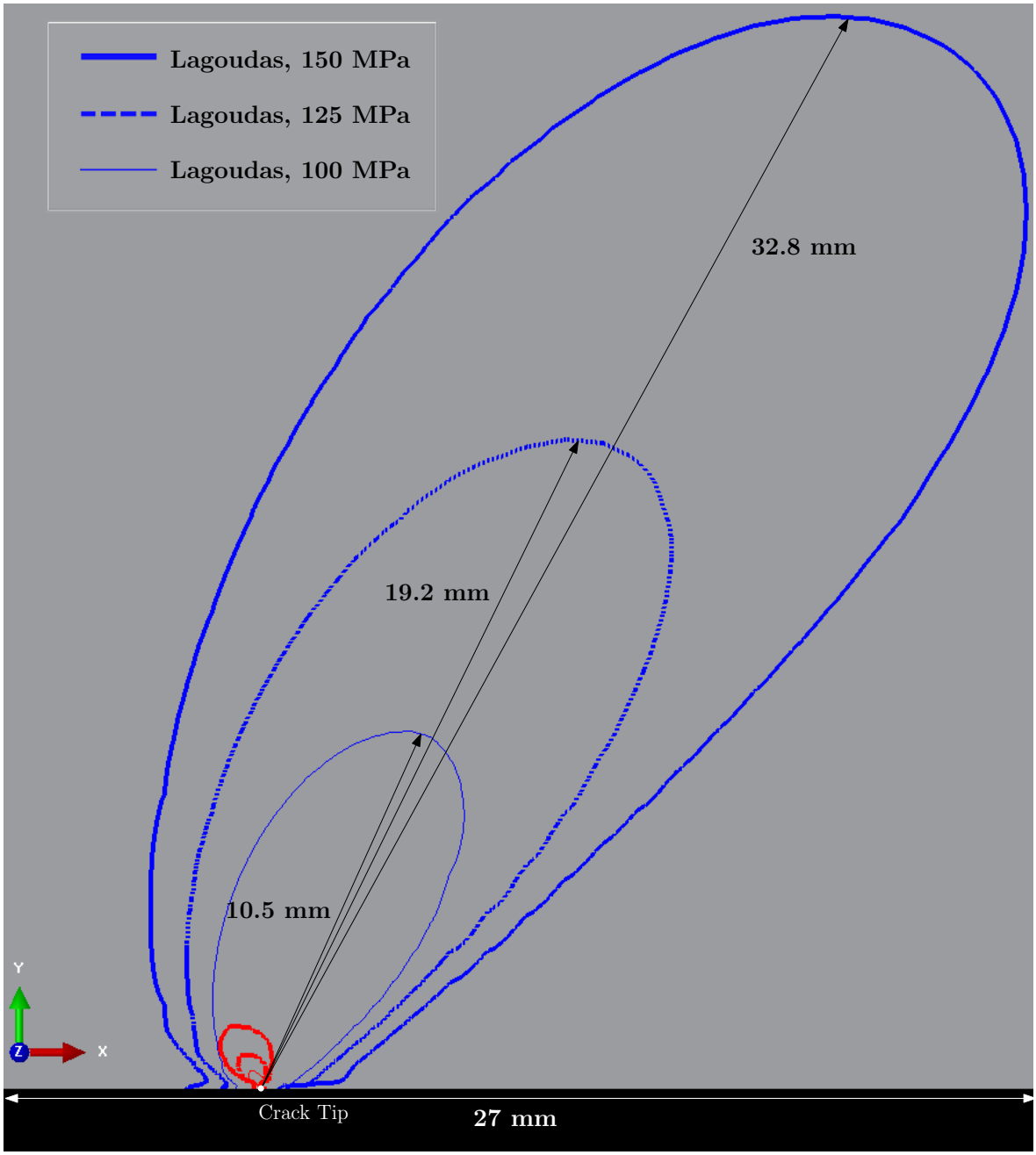


Figure 4.17. Martensite fraction contours using Lagoudas' model with a/W = 0.4 and three different loadings (Fully martensite inside the red contours, fully austenite outside the blue contours).

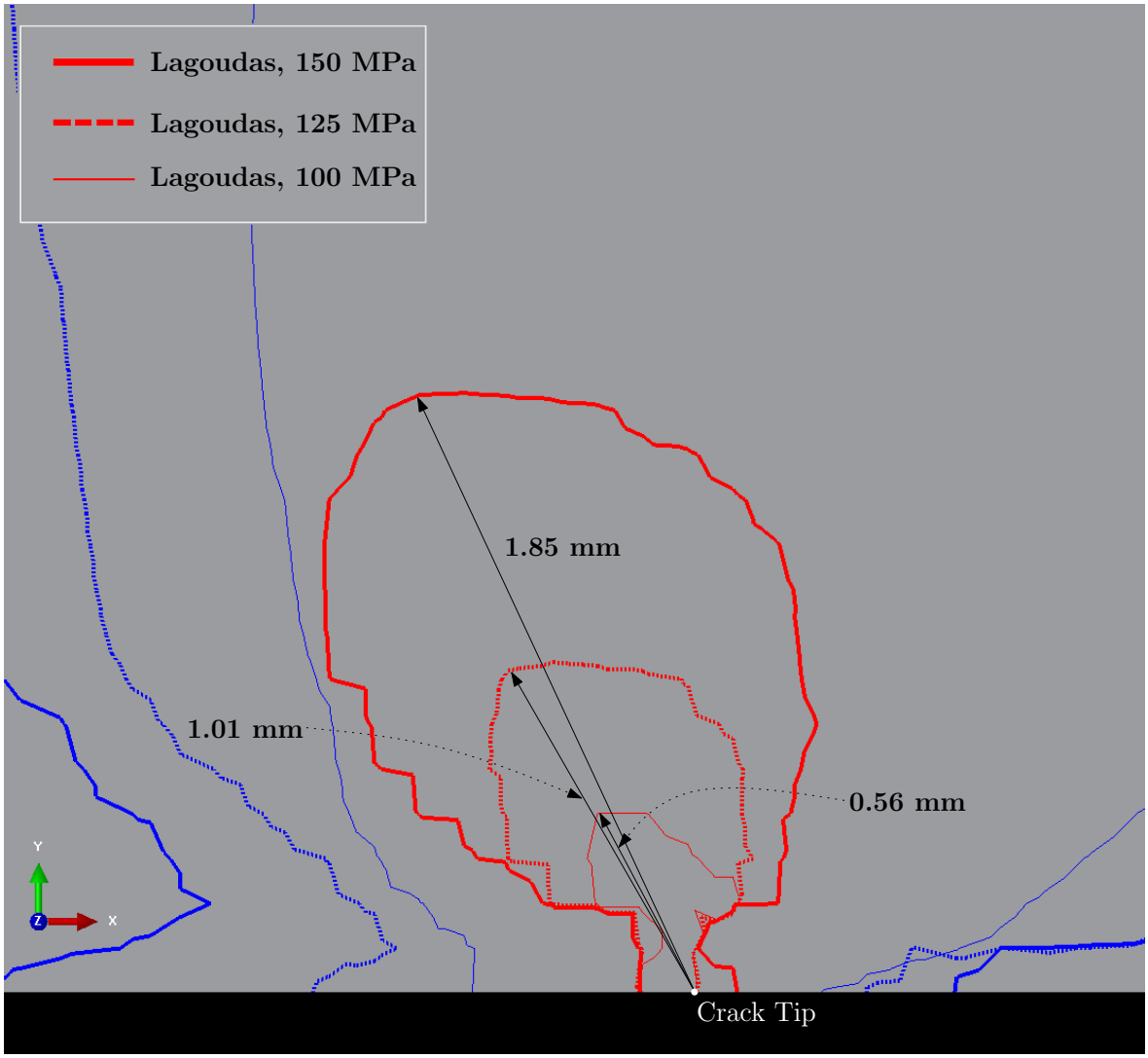


Figure 4.18. Close-up of martensite fraction contours shown in figure 4.17 (Fully martensite inside the red contours).

4.3. Mixed-mode Loading

For mixed-mode loading, an angled crack with crack angle $\alpha = 30^\circ$ a = 46.2 mm, and b = 40 mm, with H = 200 mm and W = 100 mm is simulated with four different constitutive models; resulting martensite fractions are plotted in Figure 4.19 and 4.20. Also, von Mises stress distributions under mixed-mode loading are studied. The loading, σ, is 190 MPa, and the crack angle is 30 degrees. In Figure 4.21 the results of this simulation are shown. Finally, an angled crack with crack angle $\alpha = 45^\circ$, a = 56.6 mm, and, b = 40 mm, with H = 200 mm and W = 100 mm is simulated with

Auricchio's model and compared to a Mode-I loading with a/W = 0.4, both having crack tips 40 mm away from the edge, giving the occasion to compare the two different loadings, the applied load, σ, is 300 MPa, and the results are given in Figure 4.22.

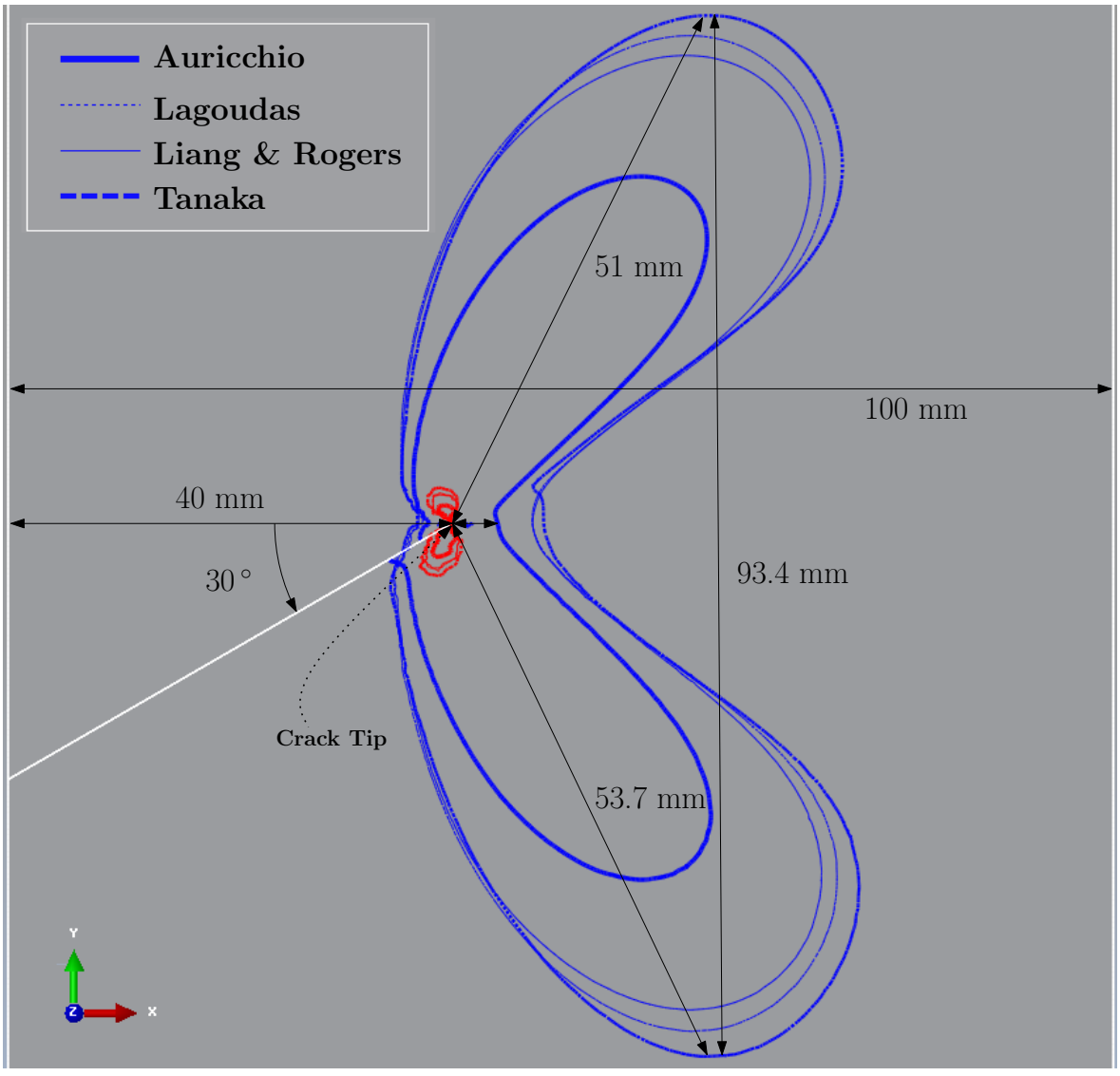


Figure 4.19. The extent of martensite transformation zones under mixed-mode loading, σ = 190 MPa (Fully austenite outside blue contours).

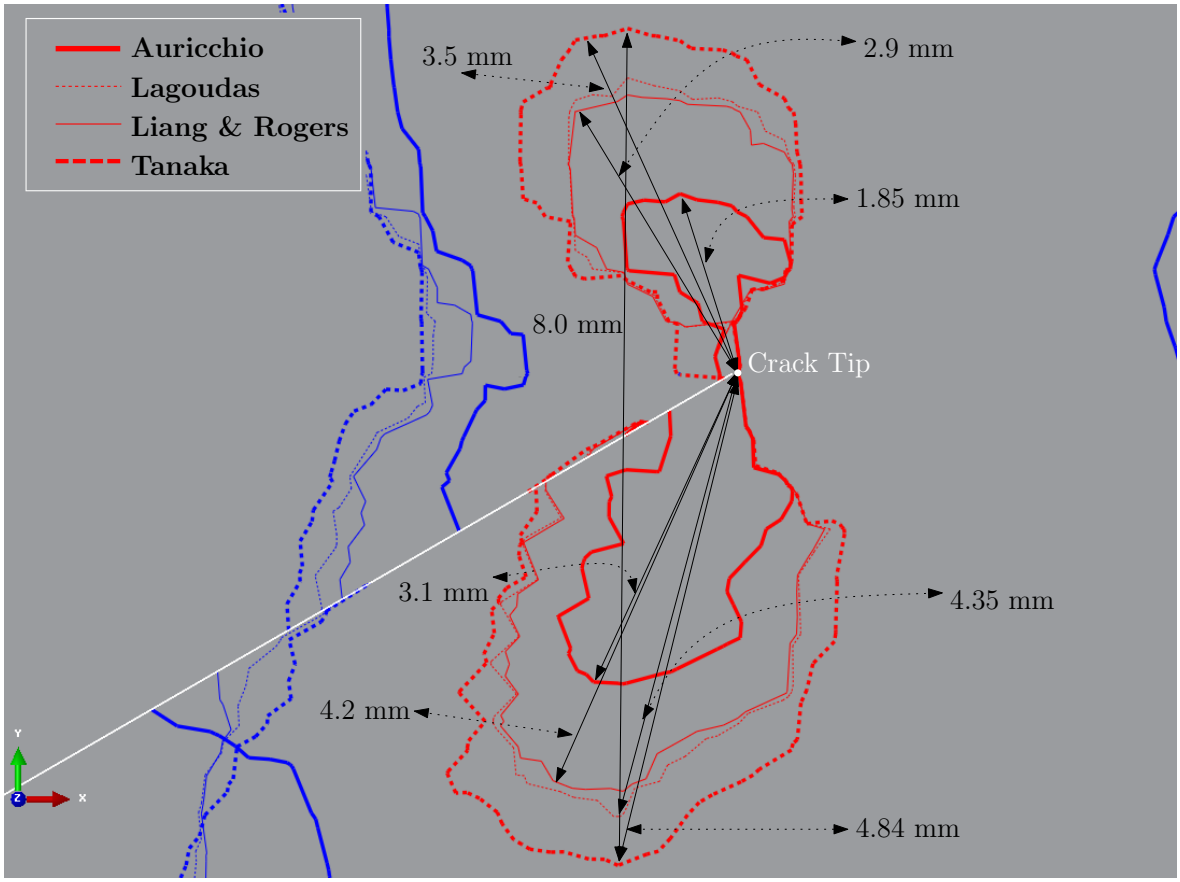


Figure 4.20. Close-up of superimposed martensite fraction contours shown in Figure 4.19 (Fully martensite inside red contours).

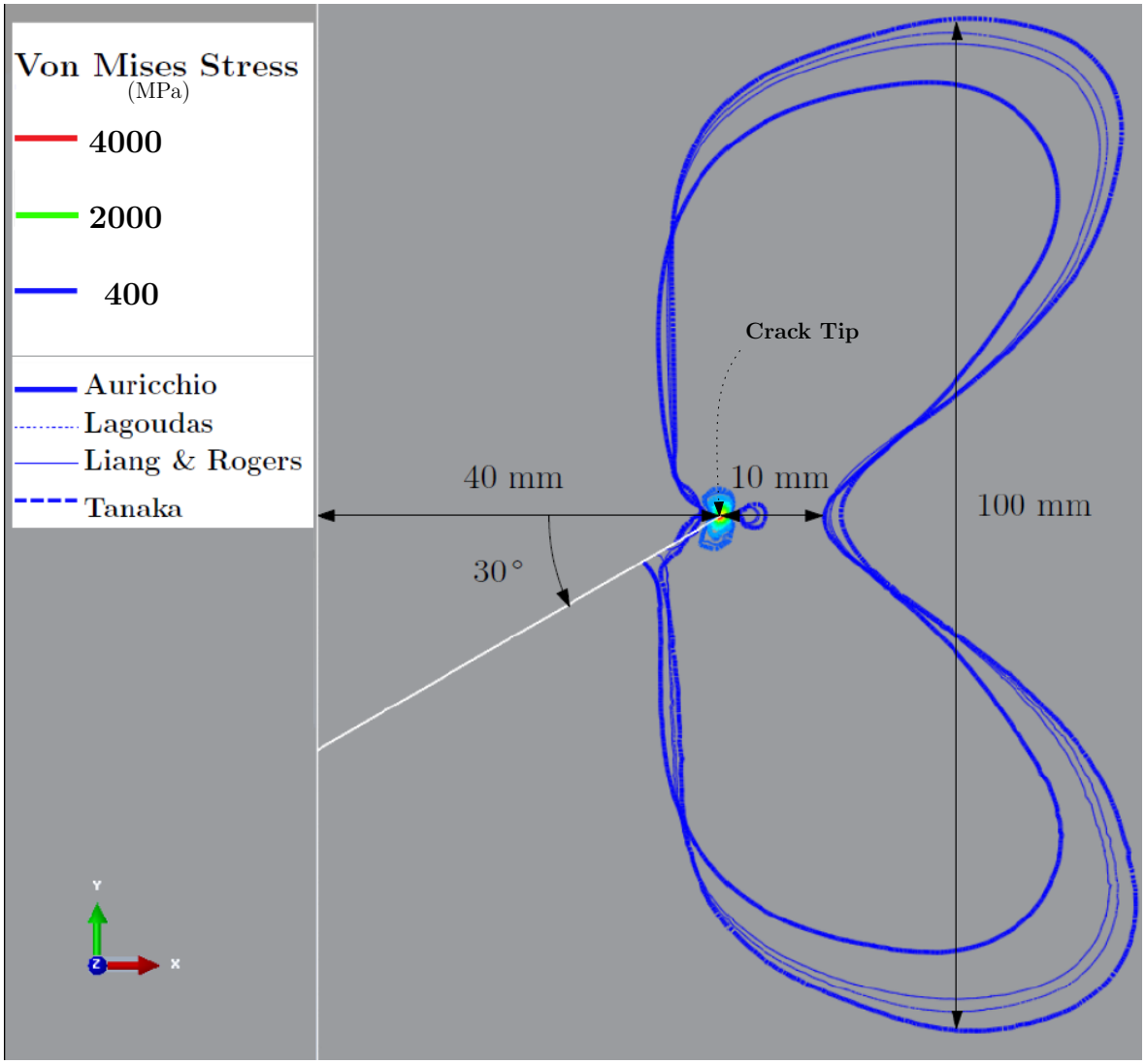


Figure 4.21. Von Mises stress distribution around the crack tip under mixed-mode loading.

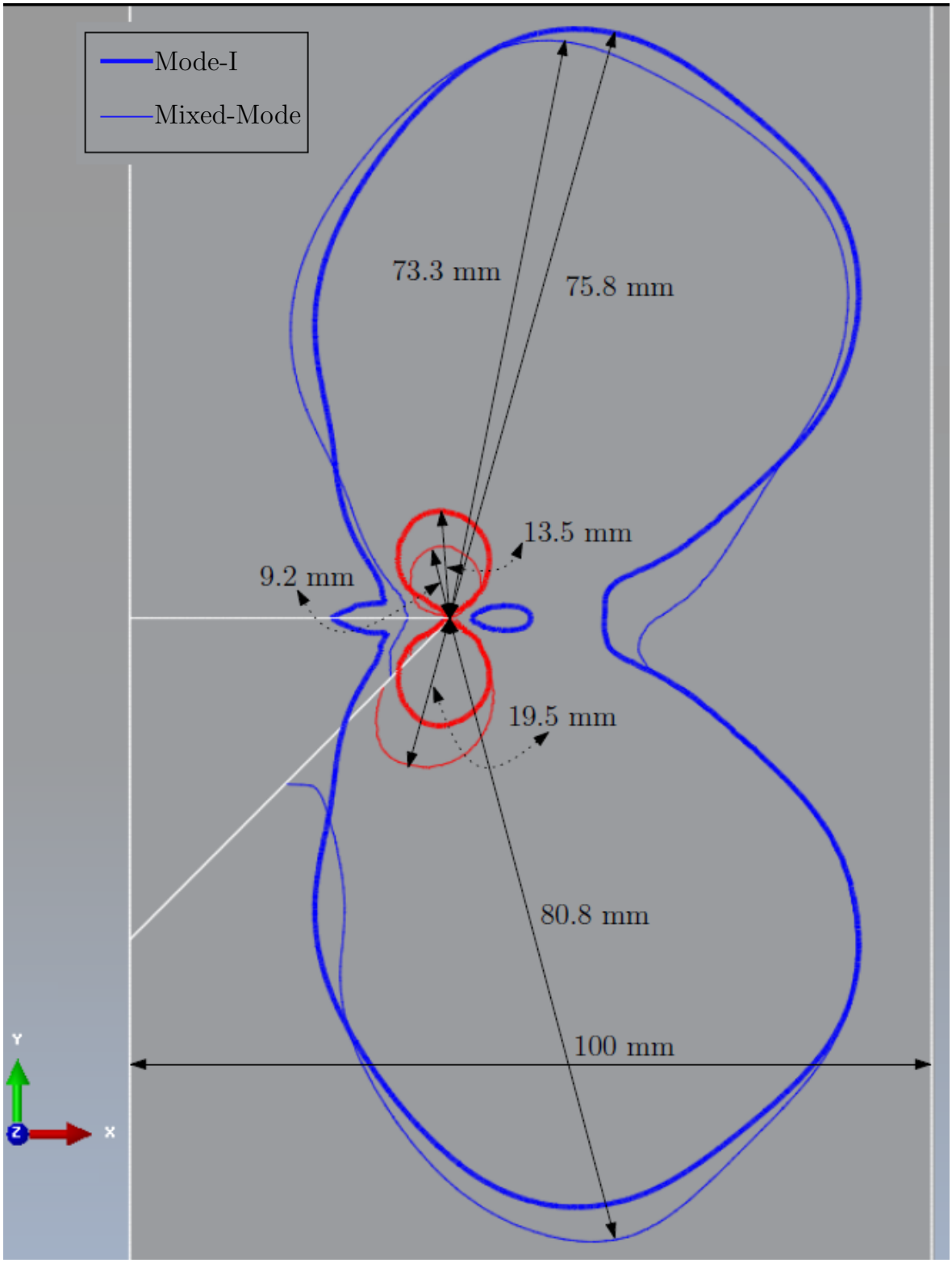


Figure 4.22. Martensite fraction distributions, a/W = 0.4 and b/W = 0.4 for mode-I and mixed-mode loadings respectively.

4.4. Fracture Toughness in Mode-I

Simsek tried to use linear elastic fracture mechanics in determining fracture parameters of SMAs but faced problems [6]. Therefore, to find stress intensity factors (SIF), energy release rates can be used. The relation between energy release rate is as follows [6, 77]:

$$G = \frac{K_I^2}{E'} \tag{4.1}$$

where, G is the energy release rate, K_I is the mode-I stress intensity factor, and E' is the effective elastic modulus given by:

$$E' = \begin{cases} E & \text{in plane stress} \\ E/(1-\nu^2) & \text{in plane strain} \end{cases} \tag{4.2}$$

For the energy release rates, the following is assumed:

$$G \approx \frac{\Delta U}{\Delta A} \tag{4.3}$$

by using the assumption in the Equation 4.3, for four different constitutive models and for four different crack widths in mode-I loading the energy release rates have been calculated. This calculation is done by node releasing in Abaqus. Node releasing is accomplished by running two consecutive simulations in which the first simulation is done with the crack at distance x_1 from the edge. For this distance, the potential energy available for crack growth is output as U_1. Similarly, when the adjacent node is released, the crack is now at distance x_2 from the edge and the available potential energy is output as U_2. The difference of U_2 and U_1 is then found and divded to the area calculated by multiplying $x_2 - x_1$ by unit thickness. The node release scheme is illustrated in Figure 4.23. The results obtained are shown in Table 4.3.

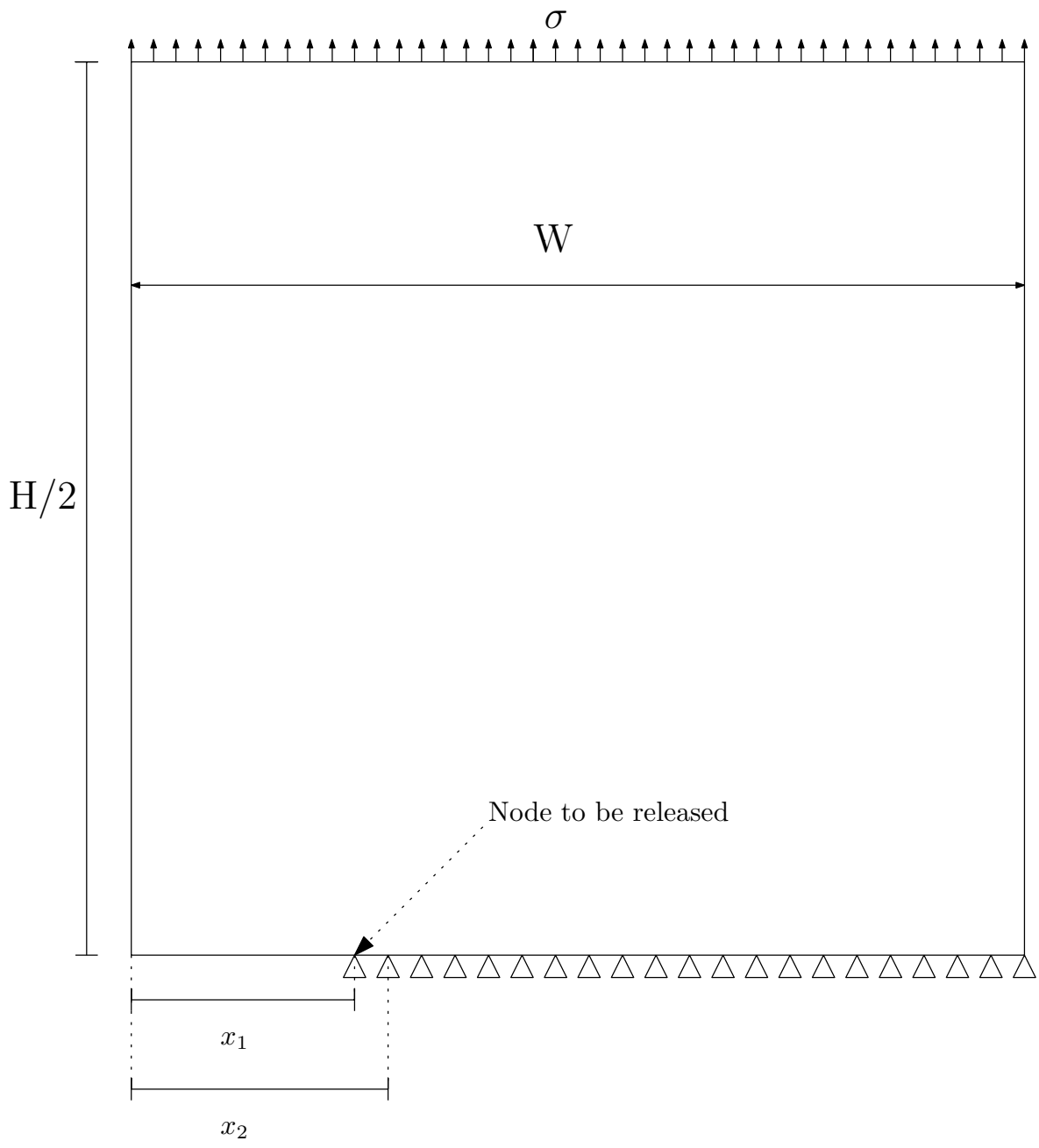


Figure 4.23. Node release scheme.

Table 4.3. Comparison of energy release rates.

Model	a/W	G (J/m^2)
Auricchio	0.25	38080
Liang & Rogers	0.25	41120
Lagoudas	0.25	41840
Tanaka	0.25	42400
Auricchio	0.30	60800
Liang & Rogers	0.30	69120
Lagoudas	0.30	70960
Tanaka	0.30	73280
Auricchio	0.35	102800
Liang & Rogers	0.35	126720
Lagoudas	0.35	131920
Tanaka	0.35	139120
Auricchio	0.40	191440
Liang & Rogers	0.40	261440
Lagoudas	0.40	283760
Tanaka	0.40	304640

Using Equation 4.1 with plane strain case in Equation 4.2 and putting in energy release rate values as tabulated in Table 4.3, obtained stress intensity factor values are shown in Table 4.4:

Table 4.4. Comparison of stress intensity factors.

Model	a/W	K_I $(MPa\sqrt{m})$
Auricchio	0.25	44.34
Liang & Rogers	0.25	46.07
Lagoudas	0.25	46.47
Tanaka	0.25	46.78
Auricchio	0.30	56.02
Liang & Rogers	0.30	59.73
Lagoudas	0.30	60.52
Tanaka	0.30	61.50
Auricchio	0.35	72.85
Liang & Rogers	0.35	80.88
Lagoudas	0.35	82.52
Tanaka	0.35	84.74
Auricchio	0.40	99.41
Liang & Rogers	0.40	116.17
Lagoudas	0.40	121.03
Tanaka	0.40	125.40

5. CONCLUSIONS

The aim of this work was to study existing constitutive macro-models of SMAs and to implement them to study an edge cracked specimen using finite elements.

As explained in Chapter 1, SMAs exhibit shape-memory effect (SME) and superelasticity (SE). Out of these two, in this study, the focus was given to superelasticity, and, especially in the finite elements (FE), the main area of interest was the phenomenological behavior of the SMA specimen during forward transformation under applied stress.

In Chapter 1, to basically introduce the phenomenon of SMA, history and applications of SMAs has been summarized. Also, to familiarize the reader with the phenomenon, although it is not the main topic of this thesis, an introduction to origins of SMAs have been given. The modeling efforts and a chronological literature survey starting from 70s and ending in the 2000s have been provided.

Having put aside the history and the basics of SMAs, Chapter 2 is on the thermodynamical fundamentals and the use of these fundamentals in modeling of SMAs.

To verify and to show characteristics of models employed in FE as explained in Chapter 3, a uniaxial tension test scheme has been employed and the results have been plotted on a single figure for a better comparison. From this point on, a 2D edge cracked SMA plate with plane strain and half-crack (by the usage of symmetry boundary conditions) assumptions has been modeled in ABAQUS, and it has been run with different a/W ratios and different loading magnitudes under mode-I loading. It should be noted that, in plane strain assumption, z-direction stress, namely, σ_{zz} is non-zero, and, due to this, von Mises stress gives different results compared to plane stress assumption, leading to a different shape in martensite fraction distributions. This procedure has been repeated for different constitutive models and it is observed that with the change of transformation characteristics, transformation zones changed.

Also with the increase of loading, transformation zones grew keeping the same trend between different constitutive models.

The distribution of y-direction stresses along the line extending in the x-direction from the crack-tip for different constitutive models have been compared and the results are provided. Consistent results expected from constitutive model characteristics have been obtained in those comparisons. These results also fit the expected behavior near the crack-tip.

Mixed-mode loading, which is the combination of mode-I and mode-II loadings has been simulated by employing an angled full-crack model. This full-crack model has been compared to another full-crack model with mode-I loading only and the resulting martensite fractions, for Auricchio's model have been compared to distinguish between the symmetric distribution in mode-I crack and non-symmetric distribution in mixed-mode crack. The asymmetry arising in mixed-mode loading has been observed.

Von Mises stress distribution under mixed-mode loading has been compared for four different models and results paralleling but non identical to martensite fraction distributions have been obtained.

For the fracture behavior of edge-cracked SMA plates under mode-I loading, energy release rates under different a/W ratios and different constitutive models have been tabulated and by linear elastic fracture mechanics' assumptions, stress intensity factors have been obtained

As for the future work, an open source UMAT code can be developed and improved in order to have full control over the parameters of FE analyses. With some influence from computational plasticity and return mapping algorithms, and, with the theory at hand, a UMAT code may be written to satisfy those needs. As for the theoretical background, although the thermodynamical part has less improvement space, new and more complex hardening functions which are able to simulate empirical data more accurately may be developed. In addition to that, to obtain the thermoelastic

moduli and other materials properties during the transformation more accurately, micromechanical factors may be taken into account in the future work. Effect of different variants of martensite may be considered and each variant of martensite may be added as an internal state variable in the developed constitutive models. Finally, applications, especially control applications benefiting from the current level of SMA constitutive model knowledge and finite elements may be researched and developed.

APPENDIX A: SOME BACKGROUND FORMULATIONS

A.1. The equality of $\dot{u}_{i,j}\sigma_{ij}$ and $\dot{\epsilon}_{ij}\sigma_{ij}$

In Chapter 2, Section 2.1, the fact that $\dot{u}_{i,j}\sigma_{ij} = \dot{\epsilon}_{ij}\sigma_{ij}$ is perennial in the derivation of the local form of the first law of thermodynamics. It can be proved by first decomposing the velocity gradient tensor into symmetric and anti-symmetric parts:

$$u_{i,j} = \frac{1}{2}\left(\frac{\partial u_i}{\partial x_j} + \frac{\partial u_j}{\partial x_i}\right) + \frac{1}{2}\left(\frac{\partial u_i}{\partial x_j} - \frac{\partial u_j}{\partial x_i}\right) \tag{A.1}$$

taking the time differential of it yields to

$$\dot{u}_{i,j} = \frac{1}{2}\left(\frac{\partial \dot{u}_i}{\partial x_j} + \frac{\partial \dot{u}_j}{\partial x_i}\right) + \frac{1}{2}\left(\frac{\partial \dot{u}_i}{\partial x_j} - \frac{\partial \dot{u}_j}{\partial x_i}\right) \tag{A.2}$$

where, the symmetric part,

$$D_{ij} = \frac{1}{2}\left(\frac{\partial \dot{u}_i}{\partial x_j} + \frac{\partial \dot{u}_j}{\partial x_i}\right) \tag{A.3}$$

is named *rate of deformation tensor* and the anti-symmetric part,

$$V_{ij} = \frac{1}{2}\left(\frac{\partial \dot{u}_i}{\partial x_j} - \frac{\partial \dot{u}_j}{\partial x_i}\right) \tag{A.4}$$

is named *vorticity*.

By combining Equaton A.2-4, the double-dot product between $\dot{u}_{i,j}$ and σ_{ij} becomes

$$\dot{u}_{i,j}\sigma_{ij} = D_{ij}\sigma_{ij} + V_{ij}\sigma_{ij} \tag{A.5}$$

Since the stress tensor is symmetric and the vorticity tensor is antisymmetric, their

double-dot product is zero, and Equation A.5 becomes

$$\dot{u}_{i,j}\sigma_{ij} = D_{ij}\sigma_{ij} \tag{A.6}$$

Since

$$\dot{\epsilon}_{ij} = \frac{1}{2}\left(\frac{\partial \dot{u}_i}{\partial x_j} + \frac{\partial \dot{u}_j}{\partial x_i}\right) = D_{ij} \tag{A.7}$$

Equation A.6, finally, becomes:

$$\dot{u}_{i,j}\sigma_{ij} = \dot{\epsilon}_{ij}\sigma_{ij} \tag{A.8}$$

Which is the required identity in the derivations mentioned above.

REFERENCES

1. Auricchio, F., L. Faravelli, G. Mogonette and V. Torra, "Considerations on the Constitutive Modeling of Shape-Memory Alloys", *Shape Memory Alloys: Advances in Modelling and Applications*, pp. 125–187, CIMNE, Barcelona, 2001.

2. Kumar, S. and S. M. Sivakumar, "Numerical Simulation of Shape Memory Effect and Superelasticity in SMA Wires and Beams", *Proceedings of SPIE*, Vol. 5062, pp. 936–943, 2003.

3. Lagoudas, D. C., *Shape Memory Alloys: Modeling and Engineering Applications*, Springer Verlag, College Station, Texas, 2008.

4. Goldstein, D., *A Source Manual for Information on NITINOL and NiTi*, Naval Surface Weapons Center, Silver Spring, Maryland, February 1980.

5. Otsuka, K. and C. M. Wayman, *Shape Memory Materials*, Cambridge University Press, Cambrdige, UK, 1999.

6. Simsek, M., *Fracture Mechanics Analysis of Shape Memory Alloys Using Finite Elements*, M.S. Thesis, Bogazici University, 2009.

7. Rahman, M. A., "Patents on Superelastic Shape Memory Alloy", *Recent Patents on Mechanical Engineering*, Vol. 1, pp. 65–67, 2008.

8. Mok, K. S., *Shape-Memory Alloys: Stress-Inducted Phase Transformation, Constitutive Model, and Nonlinear Finite-Element Formulation*, Ph.D. Thesis, University of Florida, 2003.

9. Pavia University Computational Mechanics and Advanced Materials Group, *SMA Modeling: A Review on Phenomenological Shape Memory Alloy Constitutive Modeling Approaches*, 2010,

http://www-2.unipv.it/compmech/Slides-SMA/appendix_sma_modeling.pdf, accessed at June 2010.

10. Tanaka, K. and S. Nagaki, "A Thermomechanical Description of Materials with Internal Variables in the Process of Phase Transitions", *Archive of Applied Mechanics*, Vol. 51, No. 5, pp. 287–299, 1982.

11. Tanaka, K., S. Kobayashi and Y. Sato, "Thermomechanics of Transformation Pseudoelasticity and Shape Memory Effect in Alloys", *International Journal of Plasticity*, Vol. 2, No. 1, pp. 59–72, 1986.

12. Liang, C. and C. Rogers, "One-Dimensional Thermomechanical Constitutive Relations for Shape Memory Materials", *Journal of Intelligent Material Systems and Structures*, Vol. 1, No. 2, pp. 207–234, 1990.

13. Liang, C. and C. A. Rogers, "A Multi-Dimensional Constitutive Model for Shape Memory Alloys", *Journal of Engineering Mathematics*, Vol. 26, No. 3, pp. 429–443, 1992.

14. Boyd, J. G. and D. C. Lagoudas, "A Thermodynamical Constitutive Model for Shape Memory Materials. Part I. The Monolithic Shape Memory Alloy", *International Journal of Plasticity*, Vol. 12, No. 6, pp. 805–842, 1996.

15. Boyd, J. G. and D. C. Lagoudas, "A Thermodynamical Constitutive Model for Shape Memory Materials. Part II. The SMA Composite Material", *International Journal of Plasticity*, Vol. 12, No. 7, pp. 843–873, 1996.

16. Leclercq, S. and C. Lexcellent, "A General Macroscopic Description of the Thermomechanical Behavior of Shape Memory Alloys", *Journal of the Mechanics and Physics of Solids*, Vol. 44, No. 6, pp. 953–957, 1996.

17. Souza, A., E. Mamiya and N. Zouain, "Three-Dimensional Model for Solids Undergoing Stress-Induced Phase Transformations", *European Journal of Mechanics*

- *A/Solids*, Vol. 17, No. 5, pp. 789–806, 1998.

18. Delaey, L., R. V. Krishnan, H. Tas and H. Warlimont, "Thermoelasticity, Pseudoelasticity and the Memory Effects Associated with Martensitic Transformations Part I: Structural and Microstructural Changes Associated with the Transformations", *Journal of Materials Science*, Vol. 9, No. 9, pp. 1521–1535, 1974.

19. Krishnan, R. V., L. Delaey, H. Tas and H. Warlimont, "Thermoelasticity, Pseudoelasticity and the Memory Effects Associated with Martensitic Transformations Part II: The Macroscopic Mechanical Behaviour", *Journal of Materials Science*, Vol. 9, No. 9, pp. 1536–1544, 1974.

20. Warlimont, H., L. Delaey, R. V. Krishnan and H. Tas, "Thermoelasticity, Pseudoelasticity and the Memory Effects Associated with Martensitic Transformations Part III: Thermodynamics and Kinetics", *Journal of Materials Science*, Vol. 9, No. 9, pp. 1545–1555, 1974.

21. Muller, I., "A Model for a Body with Shape-Memory", *Archive for Rational Mechanics and Analysis*, Vol. 70, No. 1, pp. 61–77, 1979.

22. Falk, F., "Model Free Energy, Mechanics, and Thermodynamics of Shape Memory Alloys", *Acta Metallurgica*, Vol. 28, No. 12, pp. 1773–1780, 1980.

23. Falk, F., "Martensitic Domain Boundaries in Shape-Memory Alloys as Solitary Waves", *Le Journal de Physique*, Vol. 43, No. C4, pp. 203–208, 1982.

24. Cross, M. C., *Landau Theory of Second Order Phase Transitions*, 2006, `http://www.pma.caltech.edu/~mcc/Ph127/b/Lecture6.pdf`, accessed at February 2011.

25. Achenbach, M. and I. Muller, "A Model for Shape Memory", *Le Journal de Physique*, Vol. 43, No. C4, pp. 163–167, 1982.

26. Achenbach, M., T. Atanackovic and I. Muller, "A Model for Memory Alloys in Plane Strain", *International Journal of Solids and Structures*, Vol. 22, No. 2, pp. 171–193, 1986.

27. Patoor, E., A. Eberhardt and M. Berveiller, "Potentiel Pseudoelastique et Plasticite de Transformation Martensitique Dans les Monoet Polycristaux Metalliques", *Acta Metallurgica*, Vol. 35, No. 11, pp. 2779–2789, 1987.

28. Patoor, E., A. Eberhardt and M. Berveiller, "Thermomechanical Behavior of Shape Memory Alloys", *ESOMAT 1989-Ist European Symposium on Martensitic Transformations in Science and Technology*, pp. 133–140, 1989.

29. Falk, F. and P. Konopka, "Three-Dimensional Landau Theory Describing the Martensitic Phase Transformation of Shape-Memory Alloys", *Journal of Physics: Condensed Matter*, Vol. 2, p. 61, 1990.

30. Berveiller, M., E. Patoor and M. Buisson, "Thermomechanical Constitutive Equations for Shape Memory Alloys", *Journal de Physique IV*, Vol. 1, No. C4, pp. 387–396, 1991.

31. Abeyaratne, R. and J. Knowles, "A Continuum Model of a Thermoelastic Solid Capable of Undergoing Phase Transitions", *Journal of the Mechanics and Physics of Solids*, Vol. 41, No. 3, pp. 541–571, 1993.

32. Lindgard, P. A., "Theory and Modeling of the Martensitic Transformation", *Le Journal de Physique IV*, Vol. 1, No. C4, pp. 3–12, 1991.

33. Raniecki, B., C. Lexcellent and K. Tanaka, "Thermodynamic Models of Pseudoelastic Behaviour of Shape Memory Alloys", *Archives Mechanics Archiwum Mechaniki Stosowanej*, Vol. 44, pp. 261–284, 1992.

34. Sun, Q. P. and K. C. Hwang, "Micromechanics Modelling for the Constitutive Behavior of Polycrystalline Shape Memory Alloys–I. Derivation of General Rela-

tions", *Journal of the Mechanics and Physics of Solids*, Vol. 41, No. 1, pp. 1–17, 1993.

35. Sun, Q. P. and K. C. Hwang, "Micromechanics Modelling for the Constitutive Behavior of Polycrystalline Shape Memory Alloys–II. Study of the Individual Phenomena", *Journal of the Mechanics and Physics of Solids*, Vol. 41, No. 1, pp. 19–33, 1993.

36. Raniecki, B. and C. Lexcellent, "RL-Models of Pseudoelasticity and Their Specification for Some Shape Memory Solids", *European Journal of Mechanics - A/Solids*, Vol. 13, No. 1, pp. 21–50, 1994.

37. Entemeyer, D., E. Patoor, A. Eberhardt and M. Berveiller, "Micromechanical Modelling of the Superthermoelastic Behavior of Materials Undergoing Thermoelastic Phase Transition", *Le Journal de Physique IV*, Vol. 5, No. C8, pp. 233–238, 1995.

38. Patoor, E., A. Eberhardt and M. Berveiller, "Micromechanical Modelling of Superelasticity in Shape Memory Alloys", *Le Journal de Physique IV*, Vol. 6, No. C1, pp. 277–292, 1996.

39. Goo, B. and C. Lexcellent, "Micromechanics-Based Modeling of Two-Way Memory Effect of a Single Crystalline Shape-Memory Alloy", *Acta Materialia*, Vol. 45, No. 2, pp. 727–737, 1997.

40. Huang, M. and L. Brinson, "A Multivariant Model for Single Crystal Shape Memory Alloy Behavior", *Journal of the Mechanics and Physics of Solids*, Vol. 46, No. 8, pp. 1379–1409, 1998.

41. Auricchio, F. and E. Sacco, "A One-Dimensional Model for Superelastic Shape-Memory Alloys with Different Elastic Properties Between Austenite and Martensite", *International Journal of Non-Linear Mechanics*, Vol. 32, No. 6, pp. 1101–1114, 1997.

42. Auricchio, F. and R. Taylor, "Shape-Memory Alloys: Modelling and Numerical Simulations of the Finite-Strain Superelastic Behavior", *Computer Methods in Applied Mechanics and Engineering*, Vol. 143, No. 1-2, pp. 175–194, 1997.

43. Auricchio, F., R. Taylor and J. Lubliner, "Shape-memory Alloys: Macromodelling and Numerical Simulations of the Superelastic Behavior", *Computer Methods in Applied Mechanics and Engineering*, Vol. 146, No. 3-4, pp. 281–312, 1997.

44. Bernardini, D., "On the Macroscopic Free Energy Functions for Shape Memory Alloys", *Journal of the Mechanics and Physics of Solids*, Vol. 49, No. 4, pp. 813–838, 2001.

45. Govindjee, S. and C. Miehe, "A Multi-Variant Martensitic Phase Transformation Model: Formulation and Numerical Implementation", *Computer Methods in Applied Mechanics and Engineering*, Vol. 191, No. 3-5, pp. 215–238, 2001.

46. Brocca, M., L. C. Brinson and Z. P. Bazant, "Three-Dimensional Constitutive Model for Shape Memory Alloys Based on Microplane Model", *Journal of the Mechanics and Physics of Solids*, Vol. 50, No. 5, pp. 1051–1077, 2002.

47. Hall, G. J. and S. Govindjee, "Application of a Partially Relaxed Shape Memory Free Energy Function to Estimate the Phase Diagram and Predict Global Microstructure Evolution", *Journal of the Mechanics and Physics of Solids*, Vol. 50, No. 3, pp. 501–530, 2002.

48. Levitas, V. and D. Preston, "Three-Dimensional Landau Theory for Multivariant Stress-Induced Martensitic Phase Transformations. I. Austenite-Martensite", *Physical Review B*, Vol. 66, No. 13, pp. 1–9, 2002.

49. Nae, F. A., Y. Matsuzaki and T. Ikeda, "Micromechanical Modeling of Polycrystalline Shape-Memory Alloys Including Thermo-Mechanical Coupling", *Smart Materials and Structures*, Vol. 12, pp. 6–17, 2003.

50. Ikeda, T., F. A. Nae, H. Naito and Y. Matsuzaki, "Constitutive Model of Shape Memory Alloys for Unidirectional Loading Considering Inner Hysteresis Loops", *Smart Materials and Structures*, Vol. 13, pp. 916–925, 2004.

51. Jung, Y., P. Papadopoulos and R. O. Ritchie, "Constitutive Modelling and Numerical Simulation of Multivariant Phase Transformation in Superelastic Shape-Memory Alloys", *International Journal for Numerical Methods in Engineering*, Vol. 60, No. 2, pp. 429–460, 2004.

52. Idesman, A., V. Levitas, D. Preston and J. Cho, "Finite Element Simulations of Martensitic Phase Transitions and Microstructures Based on a Strain Softening Model", *Journal of the Mechanics and Physics of Solids*, Vol. 53, No. 3, pp. 495–523, 2005.

53. Patoor, E., D. C. Lagoudas, P. B. Entchev, L. C. Brinson and X. Gao, "Shape Memory Alloys, Part I: General Properties and Modeling of Single Crystals", *Mechanics of Materials*, Vol. 38, No. 5-6, pp. 391–429, 2006.

54. Ottosen, N. S. and M. Ristinmaa, *The Mechanics of Constitutive Modeling*, Elsevier, Oxford, UK, 2005.

55. Holzapfel, G. A., *Nonlinear Solid Mechanics: A Continuum Approach for Engineering*, John Wiley & Sons Limited, Chichester, UK, 2000.

56. Machado, L. G., *Shape Memory Alloys for Vibration Isolation and Damping*, Ph.D. Thesis, Texas A&M University, 2007.

57. Nelson, K. A. and M. Bawendi, *Massachussetts Institute of Technology – 5.60 Thermodynamics and Kinetics Course*, 2008, `http://ocw.mit.edu/courses/chemistry/5-60-thermodynamics-kinetics-spring-2008/`, accessed at February 2011.

58. Kovalenko, A. D., *Thermoelasticity: Basic Theory and Applications*, Wolters-

Noordhoff Publishing Groningen, Netherlands, 1969.

59. Coleman, B. D. and M. E. Gurtin, "Thermodynamics with Internal State Variables", *The Journal of Chemical Physics*, Vol. 47, pp. 597–613, 1967.

60. Rice, J., "Inelastic Constitutive Relations for Solids: An Internal-Variable Theory and Its Application to Metal Plasticity", *Journal of the Mechanics and Physics of Solids*, Vol. 19, No. 6, pp. 433–455, 1971.

61. Koistinen, D. P. and R. E. Marburger, "A General Equation Prescribing the Extent of the Austenite-Martensite Transformation in Pure Iron-Carbon Alloys and Plain Carbon Steels", *Acta Metallurgica*, Vol. 7, No. 1, pp. 59–60, 1959.

62. Yu, H., "A New Model for the Volume Fraction of Martensitic Transformations", *Metallurgical and Materials Transactions A*, Vol. 28, No. 12, pp. 2499–2506, 1997.

63. Liang, C., *The Constitutive Modeling of Shape Memory Alloys*, Ph.D. Thesis, Virginia Polytechnic Institute, Blacksburg, Virginia, 1990.

64. Saadat, S., J. Salichs, M. Noori, Z. Hou, H. Davoodi, I. Bar-On, Y. Suzuki and A. Masuda, "An Overview of Vibration and Seismic Applications of NiTi Shape Memory Alloy", *Smart Materials and Structures*, Vol. 11, pp. 218–229, 2002.

65. Brinson, L., "One-Dimensional Constitutive Behavior of Shape Memory Alloys: Thermomechanical Derivation with Non-Constant Material Functions and Redefined Martensite Internal Variable", *Journal of Intelligent Material Systems and Structures*, Vol. 4, No. 2, pp. 229–242, 1993.

66. Dye, T., *An Experimental Investigation of the Behavior of Nitinol*, M.S. Thesis, Virginia Polytechnic Institute, Blacksburg, Virginia, 1990.

67. Lagoudas, D. C., Z. Bo and M. A. Qidwai, "A Unified Thermodynamic Constitutive Model for SMA and Finite Element Analysis of Active Metal Matrix Composites",

Mechanics of Advanced Materials and Structures, Vol. 3, No. 2, pp. 153–179, 1996.

68. Qidwai, M. A. and D. C. Lagoudas, "Numerical Implementation of a Shape Memory Alloy Thermomechanical Constitutive Model Using Return Mapping Algorithms", *International Journal for Numerical Methods in Engineering*, Vol. 47, No. 6, pp. 1123–1168, 2000.

69. Boyd, J. and D. Lagoudas, "Thermomechanical Response of Shape Memory Composites", *Journal of Intelligent Material Systems and Structures*, Vol. 5, No. 3, p. 333, 1994.

70. Simo, J. C. and T. J. R. Hughes, *Computational Inelasticity*, Springer Verlag, New York, USA, 1998.

71. Qidwai, M. A., P. B. Entchev, D. C. Lagoudas and V. G. DeGiorgi, "Modeling of the Thermomechanical Behavior of Porous Shape Memory Alloys", *International Journal of Solids and Structures*, Vol. 38, No. 48-49, pp. 8653–8671, 2001.

72. Lagoudas, D. C., Z. Bo, M. A. Qidwai and P. B. Entchev, *SMA UM: User Material Subroutine for Thermomechanical Constitutive Model of Shape Memory Alloys*, Texas A&M University, College Station, Texas, March 2003.

73. Lagoudas, D. C., *Shape Memory Alloys: Modeling and Engineering Applications*, chap. 2, pp. 91–92, Springer Verlag, College Station, Texas, 2008.

74. Lagoudas, D. C., *Shape Memory Alloys: Modeling and Engineering Applications*, chap. 3, pp. 140–141, Springer Verlag, College Station, Texas, 2008.

75. Dassault, *Abaqus User Subroutines Reference Manual*, Dassault Systems, Velizy-Villacoublay, France, 2010.

76. Lagoudas, D. C., Z. Bo, M. A. Qidwai and P. B. Entchev, *SMA UM: User Material Subroutine for Thermomechanical Constitutive Model of Shape Memory*

Alloys, 2003, http://smart.tamu.edu/SMAText/SMA_UM_Manual.pdf, accessed at July 2010.

77. Anderson, T. L., *Fracture Mechanics: Fundamentals and Applications*, CRC Press, Florida, USA, 1995.